technische universität dortmund

In vitro–in vivo extrapolation of hepatotoxicity for food-relevant compounds in the rat

Dissertation zur Erlangung des akademischen Grades

des Doktors der Naturwissenschaften (Dr. rer. nat.)

vorgelegt von Lisa Gründler, M.Sc.

Erstgutachter: Prof. Dr. med. Jan G. Hengstler

Zweitgutachter: Prof. Dr. rer. nat. Jörg Rahnenführer

May 2025

Veröffentlicht als Dissertationsschrift zur Erlangung des akademischen Grades des Doktors der Naturwissenschaften (Dr. rer. nat.) an der Fakultät für Chemie und chemische Biologie der TU Dortmund.

Promotionsort und Jahr: Dortmund 2025

Table of contents

Summary

Hepatotoxicity of food-relevant compounds poses a significant public health risk, ranging from mild elevations in liver enzymes to severe liver failure. Particular concern arises from contaminants such as mycotoxins (e.g., aflatoxin B1), environmental pollutants including per- and polyfluoroalkyl substances (PFAS), pesticides, and pharmaceuticals found in drinking water. Chemical safety assessments still largely rely on animal studies, in which repeated-dose toxicity is evaluated based on the administered dose.

To refine the assessment of organ-specific toxicity, a novel approach methodology (NAM), following Albrecht et al. (2019), was applied. This integrated *in vitro* and *in silico* methods to compare *in vitro* effective concentrations with the simulated peak plasma concentration in the portal vein at the oral dose corresponding to the lowest observed adverse effect level (LOAEL). Specifically, a species-internal *in vitro*–in vivo extrapolation (IVIVE) strategy employing physiologically based pharmacokinetic (PBPK) modeling was used to convert oral hepatotoxic LOAELs from repeated-dose animal studies into estimated portal vein plasma concentrations. Unlike in humans, for rats there is dose-dependent data on liver-specific adverse effects from repeated-dose studies, making them a suitable reference. The aim was to compare these modeled C_{max} concentrations at the LOAEL with effective concentrations measured in *in vitro* assays.

A total of 40 food-relevant compounds—including PFAS, polychlorinated biphenyls (PCBs), pharmaceuticals, pesticides, and plant constituents—were evaluated. Hepatotoxic doses were systematically extracted from published rat studies using a novel scoring system (Score of Significance, SOS), which provides a measure of study quality and enables comparison of adverse effect severity across compounds. To derive *in vitro* effective concentrations, three rat hepatocyte-based models were employed: two hepatoma cell lines (H4IIE, Zajdela) and cultured primary rat hepatocytes. A test battery covering three endpoints—cytotoxicity, lipid droplet accumulation, and nuclear enumeration via Hoechst staining—was used to determine effective concentrations (EC_{10}, EC_{20}, EC_{50}) for each compound, cell system, and endpoint.

Comparison of *in vitro* effective concentrations with modeled *in vivo* C_{max} values at the LOAEL was performed to identify the most predictive assay and cell system. This was achieved using a custom performance metric, the Toxicity Iso-concentration Index (TII), which quantifies the deviation from the iso-concentration line in either direction in a $\log_{10}$-scaled scatterplot for each *in vitro*–in vivo pair.

The results showed that the hepatoma cell lines outperformed primary rat hepatocytes across all assays (TII > 0.8 vs. TII < 0.8). Among the assays, cytotoxicity exhibited the best predictive performance and yielded the highest number of positive test results. Aggregating the results

of all three assays into a single lowest observed effect concentration (LOEC) per cell system did not lead to an improvement in the TII. In the best-performing setup—cytotoxicity testing in H4IIE cells—50 % of the compounds matched in vivo concentrations within a 3.16-fold deviation, another 25 % within a 3.16–10-fold range, 21 % between 10–100-fold, and only 3.4 % deviated by more than 100-fold. According to PBPK modeling standards in drug development, 75 % of compounds falling within a 10-fold deviation are considered good to acceptable, and the remainder warrant further investigation. Therefore, this approach enables a quantitative estimation of the *in vivo* C_{max} in the portal vein at the LOAEL, with a geometric mean fold error of 5.3 and a geometric standard deviation of 5.5.

The resulting dataset provides species- and organ-specific concentration–effect relationships and has potential utility for regulatory databases such as ECHA, PubChem, or the CompTox Chemicals Dashboard. Furthermore, it may serve as a training set for machine learning algorithms to predict the hepatotoxicity of untested substances, thereby contributing to more efficient, animal-free chemical safety assessment strategies.

Zusammenfassung

Die Hepatotoxizität lebensmittelrelevanter Substanzen stellt ein erhebliches Risiko für die öffentliche Gesundheit dar – mit einem Spektrum, das von leichten Erhöhungen der Leberenzyme bis hin zu schwerem Leberversagen reicht. Besonders besorgniserregend sind Kontaminanten wie Mykotoxine (z. B. Aflatoxin B1), Umweltkontaminanten wie per- und polyfluorierte Alkylsubstanzen (PFAS), Pestizide sowie Arzneimittelrückstände im Trinkwasser. Die chemische Sicherheitsbewertung basiert bislang weitgehend auf Tierversuchen, in denen die Toxizität über die verabreichte Dosis nach mehrfacherer Verabreichung beurteilt wird.

Zur Verfeinerung der organspezifischen Risikobewertung wurde eine neue Methodenstrategie (novel approach methodology, NAM) nach Albrecht et al. (2019) angewandt. Diese kombiniert *in vitro*- und *in silico*-Verfahren zum Vergleich von *in vitro* effektiven Konzentrationen und modellierten maximalen Plasmakonzentration (C_{max}) in der Pfortader, die beim oralen Erreichen der niedrigsten beobachteten, lebertoxischen Dosis (LOAEL – lowest observed adverse effect level) auftritt. Dabei wurde eine Spezies-interne *in vitro–in vivo*-Extrapolationsstrategie (IVIVE) mit physiologisch basierter Pharmakokinetikmodellierung (PBPK) genutzt, um LOAEL-Dosen aus Tierstudien in maximale Plasmakonzentrationen in der Pfortader umzuwandeln. Im Gegensatz zum Menschen liegen für Ratten dosisabhängige Daten zu leberspezifischen Effekten aus Toxizitätsstudien vor, was sie zu einer geeigneten Referenz macht. Ziel war es, diese modellierten *in vivo*-C_{max}-Werte mit den in *in vitro*-Assays gemessenen effektiven Konzentrationen zu vergleichen.

Untersucht wurden insgesamt 40 lebensmittelrelevante Substanzen – darunter PFAS, polychlorierte Biphenyle (PCB), Arzneimittel, Pestizide und Pflanzeninhaltsstoffe. Die lebertoxischen Dosen wurden systematisch aus Publikationen von Toxizitätsmessungen in der Ratte mit Hilfe eines neuen Bewertungssystems (Score of Significance, SOS) abgeleitet, das die Studienqualität bewertet und den Schweregrad der adversen Effekte vergleichbar macht. Zur Ermittlung effektiver *in vitro*-Konzentrationen wurden drei auf Rattenhepatozyten basierende Zellmodelle verwendet: zwei Hepatoma-Zelllinien (H4IIE, Zajdela) sowie kultivierte primäre Rattenhepatozyten. Eine Testbatterie mit drei Endpunkten – Zytotoxizität, Lipidtropfen Ansammlung und Zellkernauszählung mittels Hoechst-Färbung – wurde eingesetzt, um effektive Konzentrationen (EC_{10}, EC_{20}, EC_{50}) für jede Substanz, jedes Zellmodell und wenn möglich für jeden Endpunkt zu bestimmen.

Der Vergleich der *in vitro*-Effektkonzentrationen mit den modellierten *in vivo*-C_{max}-Werten am LOAEL erfolgte mit dem Ziel, das prädiktivste Testsystem zu identifizieren. Hierzu wurde ein spezieller Leistungsindikator, der Toxicity Iso-concentration Index (TII), entwickelt, der die

Abweichung von der Iso-Konzentrationslinie in einem logarithmisch skalierten Scatterplot quantifiziert.

Die Ergebnisse zeigten, dass die Hepatoma-Zelllinien den primären Rattenhepatozyten in allen Assays überlegen waren (TII > 0,8 vs. TII < 0,8). Unter den Assays zeigte sich der Zytotoxizitätstest als am prädiktivsten und lieferte zudem die meisten positiven Testergebnisse. Die Aggregation der Ergebnisse aller drei Assays zu einer gemeinsamen niedrigsten beobachteten Effektkonzentration (LOEC – lowest observed effect concentration) pro Zellsystem führte zu keiner Verbesserung des TII.

Im leistungsstärksten Setup – dem Zytotoxizitätstest in H4IIE-Zellen – stimmten bei 50 % der Substanzen die *in vitro*-Effektkonzentrationen mit den *in vivo*-C_{max}-Werten innerhalb eines Faktors von 3,16 überein. Weitere 25 % lagen innerhalb eines 3,16–10-fachen Bereichs, 21 % im Bereich von 10–100, und nur 3,4 % wichen um mehr als das 100-Fache ab. Laut PBPK-Modellierungsstandards in der Arzneimittelentwicklung gelten 75 % der Substanzen mit einer Abweichung von weniger als dem 10-fachen als gut bis akzeptabel, die übrigen bedürfen einer genaueren Analyse.

Daraus ergibt sich, dass dieser *in vitro–in silico*-Ansatz eine quantitative Abschätzung der *in vivo*-C_{max} in der Pfortader auf LOAEL-Basis ermöglicht – mit einem geometrischen mittleren Abweichungsfaktor von 5,3 und einer geometrischen Standardabweichung von 5,5.

Der entstandene Datensatz liefert artspezifische und organspezifische Konzentrations-Wirkungs-Beziehungen und eignet sich potenziell für regulatorische Datenbanken wie ECHA, PubChem oder das CompTox Chemicals Dashboard. Darüber hinaus könnte er als Trainingsdatensatz für maschinelles Lernen zur Vorhersage der Hepatotoxizität bislang ungetesteter Substanzen dienen – und so zu effizienteren, tierversuchsfreien Strategien in der chemischen Sicherheitsbewertung beitragen

Abbreviations

Abbreviation	Description
3R	Replace, Reduce, Refine; ethical use of animals in research
AC50	Concentration at 50 % maximal activity
AFB1	Aflatoxin B1
AI	Artificial intelligence
ALP	Alkaline phosphatase
ALT	Alanine aminotransferase
APAP	Acetaminophen
AS	Arsenic
AST	Aspartate aminotransferase
ATSDR	Agency for Toxic Substances and Disease Registry
AUC	Area under the curve
BHT	Butylated hydroxytoluene
BPA	Bisphenol A
BUN	Blood urea nitrogen
CBD	Cannabidiol
CBZ	Carbamazepine
CHOL	Cholesterol
C_{max}	Peak concentration
CMFDA	5-Chloromethylfluorescein
CO_2	Carbon dioxide
COU	Coumarin
CREA	Creatinine
CRY	Chrysin
CTB	Cell Titre Blue
CU	Copper
CYP1A1	Cytochrome P450, family 1, subfamily A, polypeptide 1
DBA	Dibromoacetic acid
Dbili	Direct bilirubin
DEHP	Di(2-ethylhexyl)phthalate
DINP	Di-isononylphthalate
DIX	1,4-Dioxane
DMEM	Dulbecco’s Modified Eagle’s Medium
DMSO	Dimethyl sulfoxide
EC	Effective concentration
ECHA	European Chemicals Agency
EFSA	European Food Safety Authority
EGTA	Ethylene glycol-bis(β-aminoethyl ether)-N,N,N′,N′-tetraacetic acid
EMO	Emodin
ETOH	Ethanol
f	Female
F344	Fisher 344 rats
FBS	Fetal bovine serum
FFA	Free fatty acids
FRC	Food-relevant compounds
FTOH	8-2 Fluorotelomer Alcohol
g	Gram

GA	Gallic acid
GENX	2,3,3,3-tetrafluoro-2-(heptafluoropropoxy)propanoate
GFME	Geometric mean fold error
GFM	Gemifloxacin mesylate
GGT	Gamma-glutamyltransferase
GOF	Goodness of fit
GSD	Geometric standard deviation
GSH	Glutathione
GST	Genistein
IEG	Isoeugenol
IMI	Imidacloprid
IVIVE	*In vitro–in vivo* extrapolation
kg	Kilogram
LIN	Lindane
LOEC	Lowest observed effective concentration
LOAEL	Lowest observed adverse effect level
LogP	Logarithm (base 10) of the partition coefficient between n-octanol and water
m	Male
M	Molar concentration, mol/L
mM	Millimolar concentration, mmol/L
MEG	Methyleugenol
MET	Methanol
MOR	Morin
mg	Milligram
mL	Milliliter
N.A.	Not available
NAM	Novel Approach Methodology
nm	Nanometer
NOAEL	No observed adverse effect level
NR	Nile red
NTP	National Toxicology Program
OAEL	Observed adverse effect level
OECD	Organisation for Economic Co-operation and Development
ORES	Oxyresveratrol
PBPK	Physiologically based pharmacokinetics
PBS	Phosphate-buffered saline
PCB	Polychlorinated biphenyls
PCB118	2,3’,4,4’,5-pentachlorobiphenyl
PCB126	3,3',4,4',5-pentachlorobiphenyl
PFAS	Per- and polyfluoroalkyl substances
PFBA	Perfluorobutanoic acid
PFBS	Perfluorobutane sulfonic acid
PFHxA	Perfluorohexanoic acid
PFOA	Perfluorooctanoic acid
PFOS	Perfluorooctane sulfonic acid
POP	Persistent organic pollutant
PRH	Primary rat hepatocytes
PYR	Pyridine

ROF	Rule of five
rpm	Revolutions per minute
SD	Sprague-Dawley rats
SDH	Succinate dehydrogenase
SOS	Score of Significance
SBA	Serum bile acids
TAG	Triacylglyceride
TCAB	3,3,4,4-Tetrachloroazobenzene
Tbili	Total bilirubin
TEI	Toxicity Estimation Index
THIA	Thiabendazole
TII	Toxicity Iso-concentration Index
Tmax	Time at peak concentration
TRI	Triticonazole
TRL	Toxicity Research Laboratories
TSN	Triclosan
US EPA	United States Environmental Protection Agency
w/o	Without
w/	With
µL	Microliter
µM	Micromolar concentration, µmol/L

1 Introduction

1.1 Hepatotoxicity

In humans and other higher organisms, the liver plays a pivotal role in vital functions including xenobiotic metabolism, the processing of food, and protein synthesis, among numerous others. However, due to its role in metabolism, which involves the processing, detoxification, and excretion of chemicals, liver cells are exposed to elevated concentrations of endogenous and exogenous substances and their metabolites. This exposure can potentially result in liver dysfunction (Devarbhavi et al. 2018; Roth et al. 2019). To maintain the homeostasis of the internal milieu of chemicals, the liver has a special position in the circulatory system. It is situated between the intestinal tract and the systemic circulation. Nutrient-rich blood from the organs of the gastrointestinal tract flows into the portal vein and then passes through the liver before entering the systemic circulation. Consequently, the liver is the initial organ that encounters a diverse set of substances, which are ingested through food such as nutrients, drugs, environmental toxins and bacterial byproducts - (Gu and Manautou 2012; Roth et al. 2019).

Exposure to potentially hepatotoxic substances can lead to a spectrum of pathological reactions, collectively known as "Drug-Induced Liver Injury" (DILI) (Allison et al. 2023). DILI can be classified into two main forms: a dose-dependent and predictable form, and an idiosyncratic form, which is also dose-dependent but may be allergic, immune-mediated, or non-allergic and non-immune-mediated (Kolaric et al. 2021). While idiosyncratic reactions pose a significant challenge in clinical toxicology, this study focuses on the mechanistically tractable, dose-dependent forms of liver injury, which can be recapitulated in experimental systems and are thus suitable for quantitative risk assessment.

The liver’s response to toxicants can manifest in various histopathological and biochemical patterns, such as hepatocellular necrosis, cholestasis, steatosis, inflammation or fibrosis. These injury patterns are associated with specific molecular and cellular mechanisms, including oxidative stress, mitochondrial dysfunction, endoplasmic reticulum stress, and the activation of inflammatory pathways (Gómez-Lechón et al. 2016; McGill and Jaeschke 2019). Understanding and predicting such dose-dependent hepatic injury has become a central goal of modern toxicology, particularly as regulatory frameworks begin to shift toward animal-free testing strategies.

Driven by the European Commission’s “Roadmap Towards Phasing-Out Animal Testing for Chemical Safety Assessments” (European Commission 2023), which aims to eliminate regulatory animal tests by 2030, efforts to implement alternative testing strategies have

intensified. The adoption of novel approach methodologies (NAMs) in hepatotoxicity assessment has accelerated through the integration of *in vitro* liver assays, *in silico* physiologically based pharmacokinetic (PBPK) modeling, machine learning techniques, and access to large-scale toxicological databases, enabling more predictive, quantitative approaches to hazard characterization. To enhance both the translational relevance and mechanistic specificity of such approaches, the incorporation of species- and organ-specific testing systems is crucial. Although recent NAM-based approaches have advanced hepatotoxicity prediction in rats, limitations remain due to the exclusive use of primary rat hepatocytes, and the absence of systematic derivation of liver-specific lowest observed adverse effect levels (LOAELs) (Papa et al. 2018; Shah et al. 2021; Pannala et al. 2025).

1.2 Food-relevant compounds (FRCs)

Food-related compounds can be defined as chemical components or contaminants in food and feed that can enter the food chain through various pathways including agricultural practices, food processing, contact materials, environmental pollution, or naturally occurring substances (EFSA 2024). These FRCs can be further categorized into: a) substances that are unintentionally present in ingredients, such as phytotoxins, mycotoxins, (heavy) metals, and persistent organic pollutants (POPs); b) substances that arise during food preparation, including processing aids, process-related contaminants, and food contact materials, and c) substances intentionally used to manage productivity or acceptability of supply chains, such as pesticides and veterinary drugs. Additionally, human pharmaceuticals may enter the environment via wastewater and contaminate the surface or even drinking water, posing a potential route of indirect exposure through the food chain (aus der Beek et al. 2016; Rietjens et al. 2025).

Chronic exposure to certain FRCs can exert a wide range of toxic effects on the human body, including e.g., neurotoxicity, cardiotoxicity, gastrointestinal disturbances, and carcinogenicity, with the liver being particularly susceptible due to its central role in xenobiotic metabolism. Aflatoxin B1, a naturally occurring mycotoxin, exemplifies this risk by inducing both acute liver toxicity and hepatocellular carcinoma through mechanisms involving oxidative stress, DNA adduct formation, and disruption of hepatic enzyme function (Wild and Gong 2010; Schrenk et al. 2020). As awareness of these contaminants increases, regulatory agencies have begun to prioritize their assessment within risk frameworks such as EFSA’s emerging risk program (Donohoe et al. 2018). Given their widespread occurrence and potential toxicological impact, FRCs represent a relevant compound class for developing predictive approaches in hepatotoxicity assessment.

1.3 Aim of this work

The aim of this study was to determine whether it is possible to simulate peak concentrations in the portal vein at the lowest observed adverse effect level (LOAEL) using *in vitro* methods. Hepatotoxic LOAELs were systematically derived from regulatory *in vivo* toxicity studies. These values were then translated into peak concentrations (C_{max}) in the portal vein using physiologically based pharmacokinetic (PBPK) modeling.

This approach represents a novel approach methodology (NAM) for chemical risk assessment by integrating *in vitro* data with PBPK modeling. It aims to generate concentration–effect data for hepatotoxic substances that are relevant for regulatory public databases, such as the European Chemicals Agency (ECHA). Moreover, this strategy supports the refinement and potential reduction of animal testing in regulatory toxicology, aligning with the 3R principles (Russel and Burch 1959).

To investigate the relationship between effective *in vitro* concentrations and *in vivo* concentrations following hepatotoxic exposure (LOAEL), a set of 40 hepatotoxic compounds with well-defined LOAELs was evaluated using an *in vitro* test battery and three different hepatocyte models. The test battery included three distinct readouts capturing different modes of cell damage: cytotoxicity, lipid droplet accumulation, and nuclear enumeration. A central objective of the study is to identify the most predictive combination of cell system and readout to optimize the *in vitro* testing strategy.

A novel scoring system ("Score of Significance") was developed to enable a systematic derivation of the LOAEL from repeated-dose toxicity studies in rats. Additionally, a performance metric was implemented (“Toxicity Iso-concentration Index”) to evaluate and optimize the predictive quality of the *in vitro–in silico* approach. Finally, the effective concentrations at 10 % response change (EC_{10}) were compared with the simulated peak concentrations (C_{max}) in the portal vein at the LOAEL, which serves as an indirect reference to literature-based *in vivo* data.

2 Material & Methods

2.1 *In vitro* materials

2.1.1 Instruments

Table 1 List of instruments used in the laboratory

Instrument	Company
Autoclave Systec VX-150	Systec
Autoclave 5075 ELV	Tuttenauer
Bright Field Microscope	Vert.A1 Zeiss Axio cam 305 color
Bright Field Microscope	Primo Vert Zeiss Axio cam icc1
Centrifuge	VWR Megastar 1.6R
Centrifuge with cooling function	Hettich Rotina 35
Fumehood	Electronics FAZ 2, Waldner
Fumehood	Kötermann
Incubators	CO2 Incubator C150 R Hinge 230, Binder
Infinite M200 Pro Plate Reader	Tecan
Laminar Flow Hood	CLEAN AIR SYSTEMS
Laminar Flow Hood	Heraeus HERASAFE
Laminar Flow Hood	Heraeus LaminAir HBB 2472
Magnetic stirrer	IKAMAG RCT, IKA
Multichannel pipette manual	Gilson Pipetman
Multichannel pipette	Research Eppendorf
Multichannel pipette	Research Plus, Eppendorf
Multichannel pipette	Research Pro, Eppendorf
Multichannel pipette	Xplorer, Eppendorf
Perfusion pump	Fresenius medical care, Type D0132
pH Meter	CG 842, Schott
Pipetteboy	Integra
Pipettes	ErgoOne, Starlab
Pipettes	Pipetman, Gibson
Pipettes	Research, Eppendorf
Pipettes	Research Plus, Eppendorf
Pipettes	Reference, Eppendorf
Precision balance	Kern ALJ 200 5DA
Precision balance	Mettler AE240
Reagent reservoir	Dual solution, Heathrow scientific
Reagent reservoir	StarTub PP Reagent Reservoir for Multichannel pipettes
Sonification bath	Labson 200 Bender & Hobein
Vaccuum pump	BVC professional vacuumbrand
Vortex	Vortex-genie 2, Bender & Hobein
Water purification system	Maxima Ultra-Pure Water, ELGA
Water purification system	Milli- Q® Integral 15 System, Merck
Waterbath	GFL 1083, Gesellschaft für Labortechnik
Waterbath	Precision GP28 Thermo Scientific

2.1.2 Consumables

Table 2 List of consumables used in the laboratory

Consumable	Company	Catalog number
Cell culture microtiter plate black, 96 well	Greiner Bio-One, Kremsmünster, Austria	655986
Centrifugation tube, 15 mL	Sarstedt, Numbrecht, Germany	62.554.512
Centrifugation tube, 50 mL	Sarstedt, Numbrecht, Germany	62.547.254
Filtropur S 0.2syringe filter	Sarstedt, Numbrecht, Germany	83.1826.001
Omnifix yringe, 10 mL	B.Braun, Melsungen, Germany	1616103V
Parafilm Wrap	Cole-Parmer, Kehl/Rhein, Germany	PM-992
Pasteur pipette, glass, 150 mm	Carl Roth, Karlsruhe, Germany	4518.1
Pipette Tips, 5000 µL	Eppendorf, Hamburg, Germany	22492080
Pipette Tips, 1250 µL, long	Sarstedt Numbrecht, Germany	70.1186
Pipette Tips, 1000 µL	Sarstedt Numbrecht, Germany	70.762
Pipette Tips, 200 µL	Sarstedt Numbrecht, Germany	70.760.002
Pipette Tips, 20 µL	Sarstedt Numbrecht, Germany	70.1116
SafeSeal 5 mL microtube	Sarstedt Numbrecht, Germany	72.701
SafeSeal 2 mL microtube	Sarstedt Numbrecht, Germany	72.695.500
SafeSeal 1.5 mL microtube	Sarstedt Numbrecht, Germany	72.706
SafeSeal 0.5 mL microtube	Sarstedt Numbrecht, Germany	72.699
Seal alu	Thermo Fisher Scientific, Waltham, MA, USA	232698
Serological Pipette, 50 mL	Sarstedt Numbrecht, Germany	86.1256.001
Serological Pipette, 25 mL	Sarstedt Numbrecht, Germany	86.1685.001
Serological Pipette, 10 mL	Sarstedt Numbrecht, Germany	86.1254.001
Serological Pipette, 5 mL	Sarstedt Numbrecht, Germany	86.1253.001
Tissue Culture Plat Flat-Bottom 96 well Plate	Sarstedt Numbrecht, Germany	83.3924
Tissue Culture Flask T25	Sarstedt Numbrecht, Germany	83.3910.002
Tissue Culture Flask T75	Sarstedt Numbrecht, Germany	83.3911.002
Vacuum Filtration Unit, 0.22 µm	Sarstedt Numbrecht, Germany	83.1822.001
Weighing tray	Sarstedt Numbrecht, Germany	719923211

2.1.3 Chemicals

Table 3 List of chemicals

Chemical	Company	Catalog number
Acetaminophen	Merck KGaA, Darmstadt, Germany	A7085
AdipoRed™ Assay Reagent	Lonza, Basel, Switzerland	PT-7009
Aflatoxin B1	Merck KGaA, Darmstadt, Germany	A6636
Bisphenol A	Merck KGaA, Darmstadt, Germany	239658
Butylatedhydroxy tolune	Merck KGaA, Darmstadt, Germany	47168
Cannabidiol	Biomol GmbH, Hamburg, Germany	Cay90080
Carbamazepine	Merck KGaA, Darmstadt, Germany	C4024
Cell Titer Blue	Promega	G8081
Chrysin	Biomol GmbH, Hamburg, Germany	Cay17402-5
Copper II sulfate	Merck KGaA, Darmstadt, Germany	908940
Coumarin	Merck KGaA, Darmstadt, Germany	C4261
Dibromo acetic acid	Merck KGaA, Darmstadt, Germany	242357
Dimethyl sulfoxide	PanReac Applichem	A36720050
1,4-Dioxane	Merck KGaA, Darmstadt, Germany	589591
Di(2-Ethylhexyl) Phthalate	Merck KGaA, Darmstadt, Germany	36735
Di-isononylphthalate	Merck KGaA, Darmstadt, Germany	49568
Emodin	Biomol GmbH, Hamburg, Germany	Cay13109
Ethanol	VWR Chemicals, Germany	20821.2
8-2 fluorotelomer alcohol (FTOH)	Merck KGaA, Darmstadt, Germany	532789-5G
Gallic acid	Merck KGaA, Darmstadt, Germany	8.42649
Gemifloxacin mesylate	Biomol GmbH, Hamburg, Germany	TGM-T1492-10mg
Genistein	Biomol GmbH, Hamburg, Germany	TGM-T1737-50mg
Glucose	Merck KGaA, Darmstadt, Germany	67021

Table 3 (continued) List of chemicals

Chemical	Company	Catalog number
Hoechst 33342	Thermo Fisher Scientific, Waltham, MA, USA	H1399
Imidacloprid	Merck KGaA, Darmstadt, Germany	37894
Isoeugenol	Merck KGaA, Darmstadt, Germany	34038-5ML-R
Lindane	Merck KGaA, Darmstadt, Germany	45548
Methanol	Carl Roth, Karlsruhe, Germany	8388.6
Methyleugenol	Merck KGaA, Darmstadt, Germany	284424
Morin hydrate	Merck KGaA, Darmstadt, Germany	M4008
Oxyresveratol	Biomol GmbH, Hamburg, Germany	TGM-T3S1068-100m
2,3',4,4',5-pentachlorobiphenyl (PCB118)	Carl Roth, Karlsruhe, Germany	1TYA.1
3,3',4,4',5-pentachlorobiphenyl (PCB126)	LGC Standards, Teddington, England	ERM-AC821
Perfluorobutanoic acid	Merck KGaA, Darmstadt, Germany	164194-5G
Perfluorobutane sulfonic acid	Merck KGaA, Darmstadt, Germany	562629-5G
Perfluorohexanoic acid	Merck KGaA, Darmstadt, Germany	29226-5ML
Perfluorooctanoic acid	Merck KGaA, Darmstadt, Germany	1809678
Perfluorooctane sulfonic acid	Biomol GmbH, Hamburg, Germany	Cay37233-25
Pyridine	Merck KGaA, Darmstadt, Germany	1097280100
3,3',4,4'-Tetrachloroazobenzene (TCAB)	LGC Standards, Teddington, England	DRE-C17340000
2,3,3,3-tetrafluoro-2-(heptafluoropropoxy)propanoate (GENX)	Manchester Organics, Cheshire, United Kingdom	N27218
Sodium arsenite	Thermo Fisher Scientific, Waltham, MA, USA	5/2330/48
Sodium oleate	Merck KGaA, Darmstadt, Germany	O3880
Sodium palmitate	Merck KGaA, Darmstadt, Germany	P9767
Thiabendazole	Santa Cruz Biotechnology, Inc., Dallas, Texas	SC-204913
Triclosan	Merck KGaA, Darmstadt, Germany	PHR1338
Triticonazole	Merck KGaA, Darmstadt, Germany	34172-100MG

2.1.4 Cell culture materials

Table 4 List of cell culture supplies

Supply	Company	Catalog number
Collagen lyophylized (rat tail), 10 mg	Roche Diagnostics GmbH, Mannheim, Germany	11171179001
CryoPure cryovials 1mL	Sarstedt, Numbrecht, Germany	72377992
Dexamethason	Merck KGaA, Darmstadt, Germany	D4902
Dulbecco's modified eagles medium (DMEM)	PAN Biotech GmbH, Aidenbach, Germany	P04-04500
Freezing container (Mr. Frosty)	Thermo Fisher Scientific, Waltham, MA, USA	5100-0001
Gentamicin	PAN Biotech GmbH, Aidenbach, Germany	P06-13001
Hemocytometer cover glasses	Marienfeld Superior, Germany	
Hemocytometer Neubauer improved	Marienfeld Superior, Germany	
Insulin transferrin selenite supplement (ITS)	Merck KGaA, Darmstadt, Germany	13146
Penicillin/Streptomycin	PAN Biotech GmbH, Aidenbach, Germany	P06-07100
Phosphate buffered saline (PBS) (-), (-) , 10x	Thermo Fisher Scientific, Waltham, MA, USA	70011-051
Sera Plus	PAN Biotech GmbH, Aidenbach, Germany	3702-P103009
FBS Good	PAN Biotech GmbH, Aidenbach, Germany	P40-37500
Stable – L Glutamine	PAN Biotech GmbH, Aidenbach, Germany	P04-82100
Trypan blue solution	Merck KGaA, Darmstadt, Germany	T8154
Trypsin/EDTA	Merck KGaA, Darmstadt, Germany	P10-023100
William's E medium	PAN Biotech GmbH, Aidenbach, Germany	P04-29510

2.1.5 Materials for rat liver perfusion

Table 5 List of materials for rat liver perfusion

Supply	Company	Catalog number
Albumin bovine fraction (BSA)	SERVA, Heidelberg, Germany	11926.02
Calcium chloride	Carl Roth, Karlsruhe, Germany	A119.1
Collagenase	Merck KGaA, Darmstadt, Germany	C2674
EGTA	Carl Roth, Karlsruhe, Germany	3054.2
Glutamine	Merck KGaA, Darmstadt, Germany	G3126
HEPES	Carl Roth, Karlsruhe, Germany	HN 77.5
Hydrochloric acid (HCl)	Carl Roth, Karlsruhe, Germany	X942.1
Magnesium sulfate (MgSO4)	Merck KGaA, Darmstadt, Germany	1.05886.0500
Potassium chloride	Carl Roth, Karlsruhe, Germany	6781.1
Potassium dihydrogen phosphate	Carl Roth, Karlsruhe, Germany	3904.1
Sodium chloride (NaCl)	Carl Roth, Karlsruhe, Germany	3957.2
Sodium hydroxide (NaOH)	Merck KGaA, Darmstadt, Germany	1.06482.5000

2.1.6 Cell systems

Three cell systems of hepatocytes were used for the *in vitro* work. Two cell lines (H4IIE and Zajdela) and freshly isolated hepatocytes from male Wistar rats.

2.1.6.1 H4IIE

The adherent H4IIE cell line was purchased from the American Type Culture Collection (ATCC) and is described as cells collected from liver tissue of a rat hepatoma (ATCC 2024).

2.1.6.2 Zajdela

The Zajdela rat cell line is derived from a hepatocellular carcinoma and was acquired from Cytion (formerly CLS, product number: 500306) (Cytion 2025). The adherent growing cells are described as an *in vitro* cell line established from the Zajdela ascites hepatoma (Van Renswoude et al. 1979).

2.1.6.3 Primary rat hepatocytes

Male Wistar rats (180 – 200 g) were ordered from Charles River Sulzfeld in Germany and housed for approximately one week before being used for experiments. The animals received normal feed ad libitum and were handled by trained staff (Elmar Kriek and Erik Willsch) in the animal facility. Hepatocytes were isolated as described in chapter 2.2.1.2.1 and cultured as described in chapter 2.2.1.2.2. The perfusion experiments were conducted as part of the approved animal study protocol "Liver Perfusion for the Isolation of Hepatocytes", reference number 81-02.04.2019.A399.

2.2 *In vitro* methods

2.2.1 Cell culture

Table 6 Cell culture media

Cell lines culture medium	
Component	**Volume [mL]**
DMEM (PAN Biotech)	500
Sera Plus/FBS Good	50
Penicillin/ Strepotomycin	5

Primary rat hepatocytes			
Plating medium		**Culture medium**	
Component	**Volume [mL]**	**Component**	**Volume [mL]**
William's E medium	500	William's E medium	500
Sera Plus / FBS Good	50		
Penicillin/ Strepotomycin	5	Penicillin/ Strepotomycin	5
Gentamicin	0.5	Gentamicin	0.5
Dexamethasone	0.02	Dexamethasone	0.02
ITS supplement	0.005	ITS supplement	0.005

Table 7 Cell line specifics

Specific	H4IIE	Zajdela
Centrifugation	5 min, 100 g	3 min, 300 g
Trypsinisation	5 min + bump	3 min
Passaging	once / week 0.3 x 10^6 cells / T75	twice / week 1.5 x 10^6 cells / T75
No. of passages after purchase	30	25
Volume of culture medium / T75	10 mL	25 mL
Medium change	3-4 days	2-3 days
Cultivation flask after thawing	T25	T75
Doubling time	~ 26 hours	~ 24 hours

2.2.1.1 Handling of cell lines

If not explicitly stated, the following descriptions apply to both cell lines. Cell line-specific instructions can be found in **Table 6** and **Table 7**.

2.2.1.1.1 Thawing and freezing cell lines

For the cell thawing process, a vial of cells was taken from the nitrogen storage tank and thawed in a 37 °C water bath for approximately one minute. The thawed cells were then transferred to 9 mL of cold medium (**Table 6**) and centrifuged at room temperature to remove residual DMSO from the freezing solution. The supernatant was carefully aspirated, and the cell pellet was resuspended in 10 mL of warm cell culture medium. Finally, the suspension was transferred to a culture flask and incubated at 37 °C with 5 % CO_2.

To freeze cells, an optimal cell density was required, ideally at 80-90 % confluence in a T75 flask. The medium was aspirated, and the cells were washed once with 10 mL PBS. Next, 2 mL of trypsin was added, and the flask was incubated as needed for each cell line. Under a brightfield microscope, it was confirmed that all cells had detached. Trypsinization was stopped by adding 8 mL of medium, and the cell suspension was centrifuged at 4° C. The supernatant was removed, and the cell pellet was resuspended in 3 mL of freezing solution (serum with 10 % DMSO). The suspension was aliquoted into three cryovials with 1 mL each. To cool the cells gradually, the cryovials were first placed on ice for 20 minutes and then moved to a freezing container at - 80°C. For long-term storage, the vials were transferred to liquid nitrogen tanks.

2.2.1.1.2 Subculturing cell lines

To maintain the cells in culture, they were kept in T75 flasks in culture medium at 37°C with 5 % CO_2 in the incubator. When the cells reached 70-90 % confluency, they were passaged. First, the confluent T75 flask was washed once with PBS, and then incubated with 2 mL of trypsin according to the conditions of the respective cell line to promote cell detachment (**Table 7**). The detached cells were then resuspended in 8 mL of culture medium and transferred to a 50 mL polystyrene tube, followed by centrifugation at room temperature. The supernatant was removed, and the resulting cell pellet was resuspended in 10 mL culture medium using a serological 10 mL pipette. After cell counting, the culture was maintained by routinely seeding a certain number of cells, tailored to the specific requirements of the cell type, into a T75 flask for further cultivation.

2.2.1.1.3 Counting cells

A 1:20 dilution in culture medium with Trypan Blue was optimal for counting cells from a confluent T75 flask (375 µL medium + 100 µL Trypan Blue + 25 µL cell suspension). Ten microliters of this dilution were placed in a Neubauer counting chamber to determine the cell number per milliliter (**Equation 1**) and the cell viability (**Equation 2**).

$$No.of\ cells\ per\ mL\ = \frac{counted\ viable\ cells}{no.\ of\ counted\ squares\ in\ Neubauer\ chamber}\ x\ dilution\ factor\ x\ 10^4 \qquad \textbf{Equation 1}$$

$$Viability\ [\%] = \frac{viable\ cells}{viable + dead\ cells} x\ 100 \qquad \textbf{Equation 2}$$

2.2.1.1.4 Plating of cell lines

Cells were plated one day prior to treatment (e.g., in 96-well plates). The procedure followed the steps outlined in the subculturing chapter 2.2.1.1.2. After counting the cells, a cell suspension was prepared with the desired number of cells per mL of culture medium. It was important to ensure that cell viability was not below 90 %: otherwise, the experiment would need to be reconsidered. For a 96-well plate, 200 µL of cell suspension per well were plated at room temperature. The plate was gently moved across the bench surface in a north-south and east-west direction (circular movements were avoided, as this may cause cells to accumulate primarily in the center of the wells). The plated cells were left standing at room temperature for 30 minutes and then transferred to the incubator at 37 °C with 5 % CO_2 until treatment.

2.2.1.2 Handling of primary rat hepatocytes

2.2.1.2.1 Isolating primary rat hepatocytes

The isolation of primary rat hepatocytes was conducted by trained personnel (Georgia Günther, Sara Bauer, Dr. Philip Gabrys and Katharina Grgas).

To initiate the isolation, the rat was anesthetized using a weight-appropriate dose of ketamine, xylazine and acepromazine (64 mg/kg bodyweight of ketamine and 7.2 mg/kg bodyweight xylazine, and 1.7 mg/kg bodyweight of acepromazine) which was given via intraperitoneal injection. The effectiveness of the anesthesia was confirmed through tests for pain sensitivity, mobility, and eyelid reflex.

After effective anesthesia, the rat was secured with tape on a grid, and the surgical area was moistened with ethanol. The abdomen was carefully opened starting with an incision in the suprapubic region, ensuring not to damage the peritoneum. A second incision was made from the middle of the first cut, running longitudinally cranial until the processus xiphoideus of the sternum was visible. From there, transversal incisions were made along the rib cage in the direction of the armpits. To fully expose the abdominal cavity, similar incisions were made in the peritoneum, taking care not to damage the liver or any other organs. The organs of the gastrointestinal tract were then set aside to access the inferior vena cava and the portal vein. A ligature was placed around the inferior vena cava but not yet tightened. The vena cava was then incised to insert the needle of the perfusion system, which was subsequently secured with the prepared ligature.

To flush the blood from the liver, the portal vein was cut, allowing the blood and the perfusion solutions to drain. Perfusion was initiated with EGTA perfusion buffer for approximately 10 minutes, leading to discoloration of the liver. In the next step, collagenase buffer was perfused to initiate liver digestion, which was stopped once the liver became soft and flaccid. The connections of the liver to other organs were then carefully removed by following the connective tissue and placed on a petri dish in suspension buffer.

Under a sterile hood, the connective tissue was carefully dissected away using forceps to release the cells. The resulting cell suspension was filtered through a sieve and centrifuged at 4 °C for 5 minutes at 50 g speed. The supernatant was discarded, and the cells were gently resuspended in suspension buffer in 50 mL polystyrene tubes by slowly inverting the tubes.

The cells were then counted and their viability assessed as described in paragraph 2.2.1.1.3.

2.2.1.2.2. Cultivation of primary rat hepatocytes

After isolating and counting the PRHs, and ensuring a viability above 60 %, a cell suspension of 500,000 cells per mL was prepared. For plating, 50,000 viable cells in 100 µL plating medium were seeded per well on pre-coated, PBS-washed (three times) 96-well plates. To avoid cell clumping and minimize potential cell damage, the suspension was gently and frequently resuspended and cut pipette tips were used to reduce shear stress during transfer.

The plates were then incubated for 3 to a maximum of 5 hours to allow the cells sufficient time to attach. Following the attachment, the cells were washed twice with warm serum-free culture medium to remove any non-attached dead cells. Finally, 200 µL of serum-free cultivation medium (or any other intended treatment) was added to each well for continued incubation at 37° C and 5 % CO_2.

2.2.2 Experiments

To maximize the use of each rat liver and use as many cells as possible, the experiments were performed with primary rat hepatocytes in high-throughput format and, where possible, simultaneously.

Collagen coating of 96-well plates

Note: For all experiments involving primary rat hepatocytes (PRHs), collagen coating was consistently applied. In contrast, for the cell lines, coating was performed only in the CTB assay, as we initially aimed to maintain comparability with the cytotoxicity tests in HepG2 cells conducted by Albrecht et al. (2019). All cell lines grew effectively without coating, so this step was omitted in the Nile Red and Hoechst assays.

To coat cell culture plates with collagen, a 0.25 mg/L rat tail collagen solution was prepared by dissolving the collagen in sterile 0.2 % acetic acid for a minimum of 4 hours at 4 °C. For coating a 96-well plate, 100 µL of the collagen solution was added to each well and left for 1-2 minutes before removal. The plates were then left to dry at room temperature for at least 3 hours. Before cell seeding, the collagen-coated plates were washed three times with 1 x PBS.

2.2.2.1 Cytotoxicity test

2.2.2.1.1 Background

The CellTiter-Blue® (CTB) Cell Viability Assay from Promega was used to assess cell viability. This assay utilizes a reagent that contains resazurin, a dark blue dye which is reduced to the fluorescent dye resorufin in metabolically active cells. As viable cells metabolize resazurin, the medium changes color from dark blue to pink, whereas dead cells do not induce any color change. The intensity of fluorescence is indicative of the cells' metabolic activity and overall viability.

2.2.2.1.2 Preparation and dilution of test substances for CTB assay

In the CTB assay, test substances were prepared in either five or nine concentrations, each tested in triplicate, along with a vehicle control for comparison. An example of the plate layout can be seen in **Figure 1**. For consistency across experiments, a serial dilution factor of 3.16 was used for concentration dilutions, a method validated in previous work (Albrecht et al. 2019). For water-soluble compounds, the dilution series was prepared directly in culture medium and sterile filtered prior to use. For compounds requiring solvents such as DMSO, ethanol, PBS, or methanol, the final solvent concentration was kept at 0.5 %, with a maximum permissible concentration of 1 % to maintain cell viability. Each well received 200 µL of the final diluted substance.

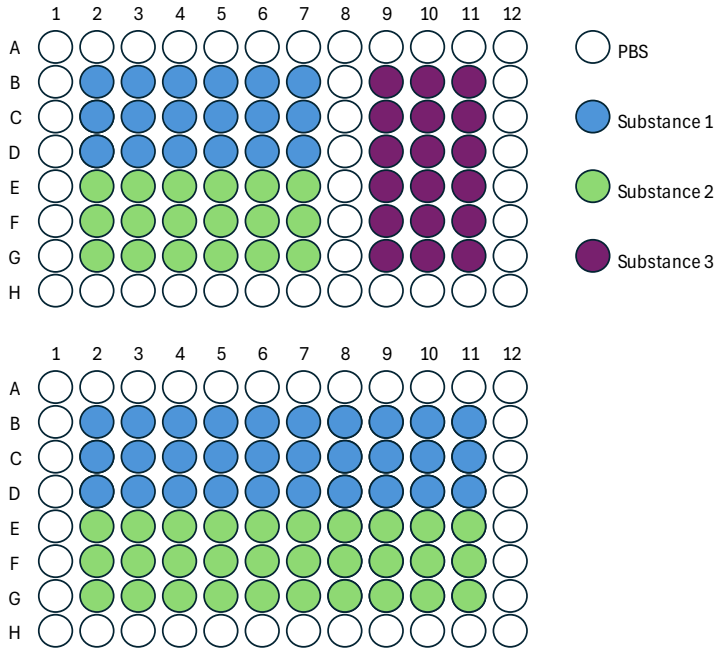

Figure 1 General plate design for cytotoxicity testing

2.2.2.1.3 CellTiter-Blue® cytotoxicity test in rat cell lines

The following experimental procedure is based on the CTB assay in HepG2 cells as described by Albrecht et al. (2019) and has been adapted for the Zajdela and H4IIE cell systems. Unless otherwise specified, the following instructions apply to both rat cell lines.

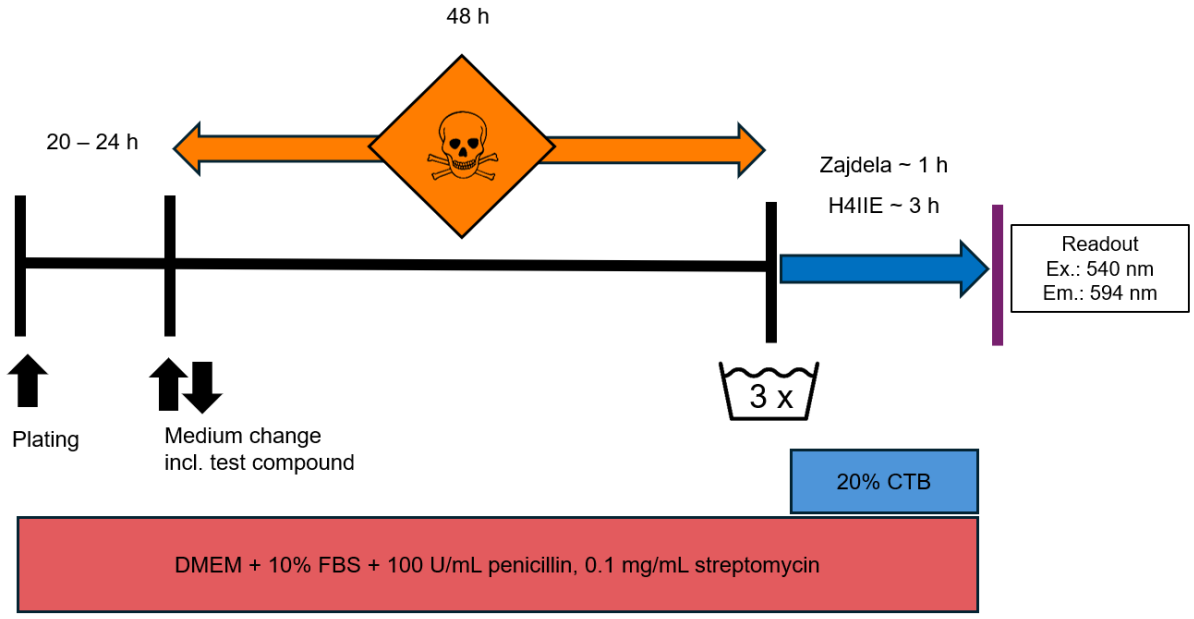

Figure 2 Time schedule and general overview of the CellTiterBlue® cytotoxicity test in Zajdela and H4IIE

Figure 2 provides a chronological sequence and general overview of the CTB assay. After washing the coated plates three times with 1 x PBS, 10,000 live cells were seeded per well. The cells were incubated for 20 to 24 hours at 37 °C with 5 % CO_2 and examined under a brightfield microscope to assess cell morphology prior to treatment. Each plate was treated with 2-3 substances according to the descriptions in paragraph 2.2.2.1.2.

The exposure period for the compounds was 48 hours. After this time, cells were re-examined under a brightfield microscope to assess their morphology. The assay was initiated by washing the plates three times with PBS and 100 µL of 20 % CTB reagent in medium were added to each well. Six wells without cells on each plate served as background controls. Cells were incubated until a color change was observed, which typically takes about one hour for Zajdela cells and approximately three hours for H4IIE cells. Fluorescence was measured using a plate reader with an excitation wavelength of 540 nm and an emission wavelength of 594 nm.

The average fluorescence of the CTB background control wells was subtracted from the fluorescence of the other wells. The viability of untreated cells was set to 100 %, since vehicle controls and compound-treated cells underwent the same procedure.

2.2.2.1.4 CellTiter-Blue® cytotoxicity test in primary rat hepatocytes (PRH)

The cytotoxicity test in primary rat hepatocytes is based on the CTB assay in primary human hepatocytes according to Albrecht et al. (2019).

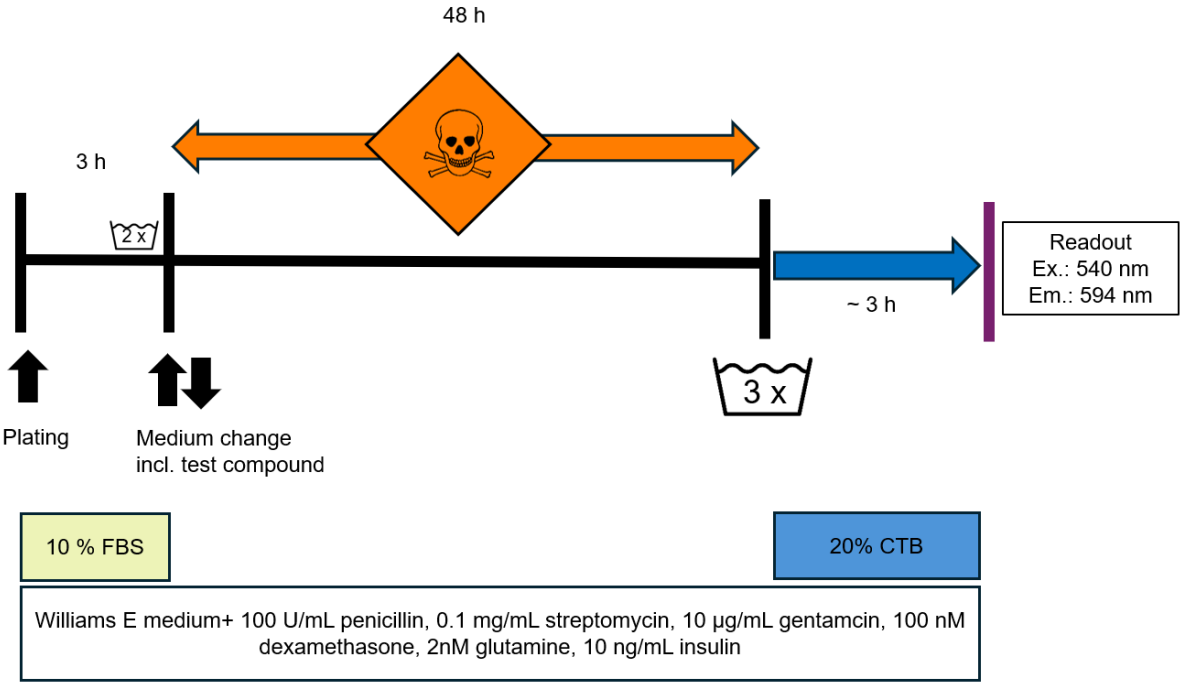

Figure 3 Time schedule and general overview of the CellTiterBlue® cytotoxicity test in primary rat hepatocytes

Where the physicochemical properties of a substance (e.g. volatility) allowed, the serial dilutions were prepared the day before perfusion. This pre-preparation ensured that all 40 substances could be tested in both assays during a single liver perfusion. Volatile substances and those soluble only in warm solvents were prepared on the day of treatment. The serial dilutions were placed in transparent 96-well plates and stored overnight at 4° C. On the day of treatment, these prepared dilution series were warmed in the incubator for three hours and then shaken on a shaker at 100 rpm for five minutes. After the freshly isolated rat hepatocytes had been attached for three hours, as described in section 2.2.1.2.2, 200 µL of the diluted compounds were applied to each well.

After a 48-hour incubation, the plates were first analyzed under a brightfield microscope and then washed three times with PBS. The CTB reagent was diluted to 20 % in serum-free culture medium specific to the primary rat hepatocytes, like the procedure used for cell lines. Following the washing with prewarmed 1 x PBS, 100 µL of the diluted CTB reagent was added to each well. The plates were then incubated for approximately 2 to 3 hours at 37 °C and 5 % CO_2, or until a color from blue to pink was observed. Finally, the fluorescence was measured using a plate reader (540 nm excitation, 594 nm emission).

2.2.2.2 Lipid droplet accumulation test

2.2.2.2.1 Background

The lipid droplet accumulation assay, also called Nile red assay, was performed according to Brecklinghaus et al. (2022a) and adapted to the rat cell lines and primary rat hepatocytes to measure lipid droplet formation at sub-cytotoxic concentrations (e.g. the EC_{50} of the cytotoxicity test). To quantify the intracellular lipids, a combination of the fluorescent Nile red with the DNA dye Hoechst was used and normalized to the Hoechst signal, by dividing Nile red fluorescence by Hoechst fluorescence.

2.2.2.2.2 Preparation and dilution of test substances for lipid droplet accumulation test

Test substance preparation was conducted with free fatty acids (FFA) supplementation. A 50 mM stock of palmitate was prepared in methanol and a 50 mM stock of oleate was prepared in DMEM or Williams E medium (plating medium). These stock solutions were used to set up a final medium containing a 62 µM FFA mixture in a 1:2 ratio of palmitate to oleate. To ensure proper dissolution of the free fatty acids, the FFA-containing medium was sonicated at 37 °C for 30 minutes.

The test substances were then dissolved in the 62 µM FFA mix medium at five concentrations, using DMSO, ethanol, methanol, PBS, or medium as solvents. Serial dilutions were performed with a factor of 3.16 as described in section 2.2.2.1.2.

Figure 4 illustrates the typical arrangement of substances in these experiments. In each experiment, two test substances per plate were analyzed in four technical replicates, with at least three independent replicates. Each 96-well plate also included a positive control (558 µM FFA mix) and a negative control (culture medium without FFA mix).

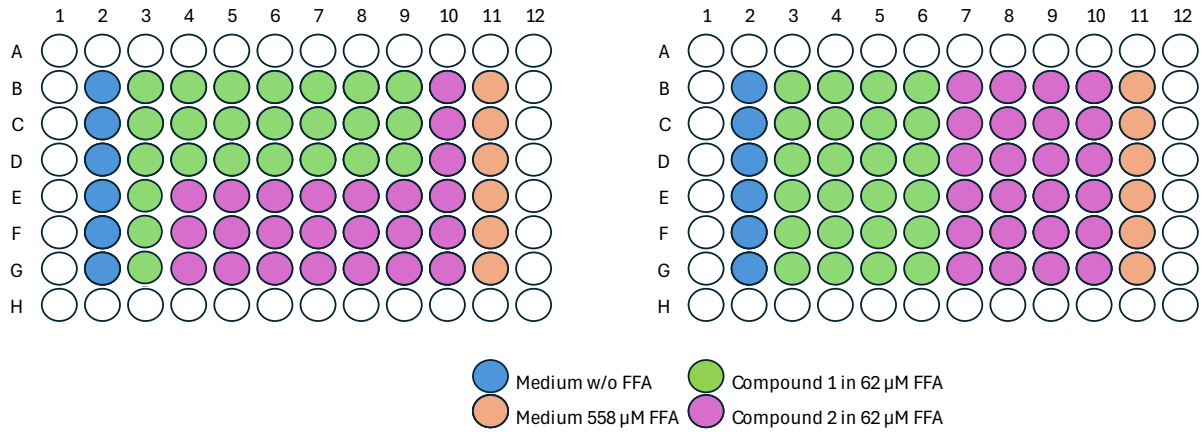

Figure 4 Plate layout for lipid droplet accumulation assay

2.2.2.2.3 Lipid droplet accumulation test in rat cell lines

The following experimental procedure is based on the Nile red assay in HepG2 cells as described by Brecklinghaus et al. (2022a) and has been adapted for the Zajdela and H4IIE cell systems. Unless otherwise specified, the following instructions apply to both rat cell lines.

Figure 5 provides a timeline and general overview of the lipid droplet accumulation assay. The experiment was initiated with the seeding of 15,000 live cells of H4IIE and 10,000 live cells of Zajdelas per well of a 96-well plate. The cells were then cultivated at 37 °C and 5 % CO_2 for a period of 20-24 hours. Subsequently, the cells' morphology was examined using a brightfield microscope, followed by treatment with the test substances, prepared as outlined in section 2.2.2.2.2, at a volume of 200 µL per well.

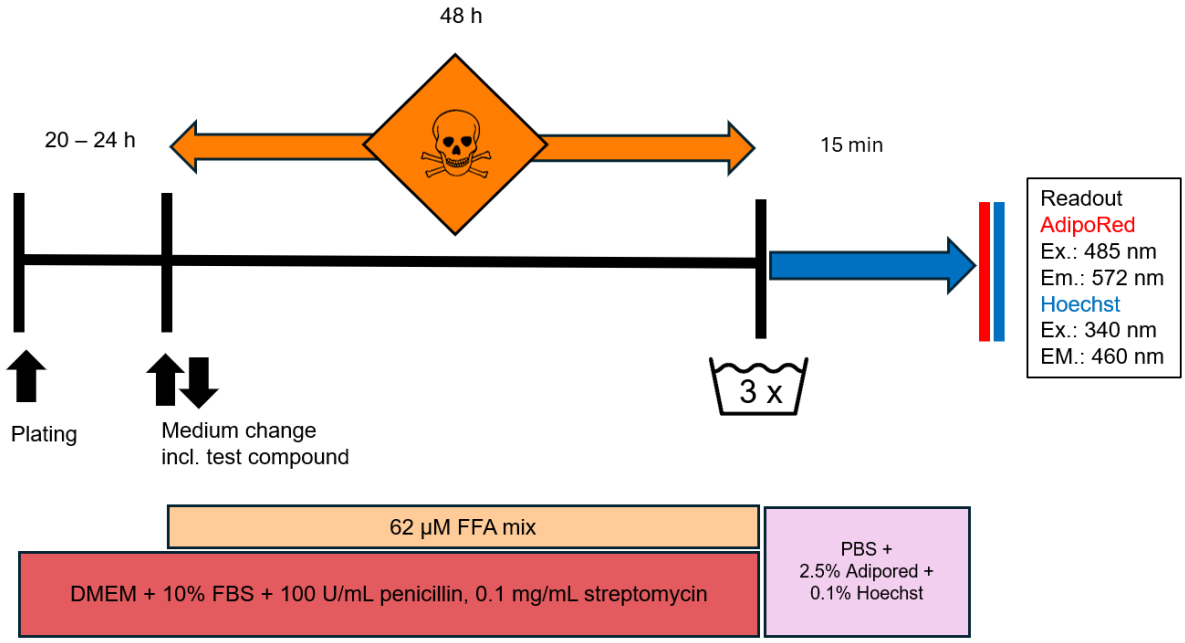

Figure 5 Time schedule & general overview of the lipid droplet accumulation test in rat cell lines

After 48 hours of exposure, cells were re-examined under a brightfield microscope to assess their morphology. The assay was initiated by washing the plates three times with PBS, followed by 200 µL of staining solution per well. The staining solution consisted of PBS with Nile red (1:40) and Hoechst (1:1000), specifically 194.8 µL PBS, 5 µL Nile red and 0.2 µL Hoechst per well. Six wells without cells on each plate served as background controls. The cells were incubated for 15 minutes at room temperature in the dark. After this, the fluorescence of Nile red (excitation: 485 nm, emission: 572 nm) and Hoechst (excitation: 340 nm, emission:460 nm) were measured using a plate reader.

For analysis, the background fluorescence, calculated as the mean signal from the six cell-free wells, was subtracted from all readings. After that the Nile red signal was normalized to the Hoechst signal by calculating their ratio.

2.2.2.2.4 Lipid droplet accumulation test in primary rat hepatocytes (PRH)

The procedure described here was optimized for primary rat hepatocytes based on the method by Brecklinghaus et al. 2022a. A chronological sequence and general overview of the assay can be seen in **Figure 6**.

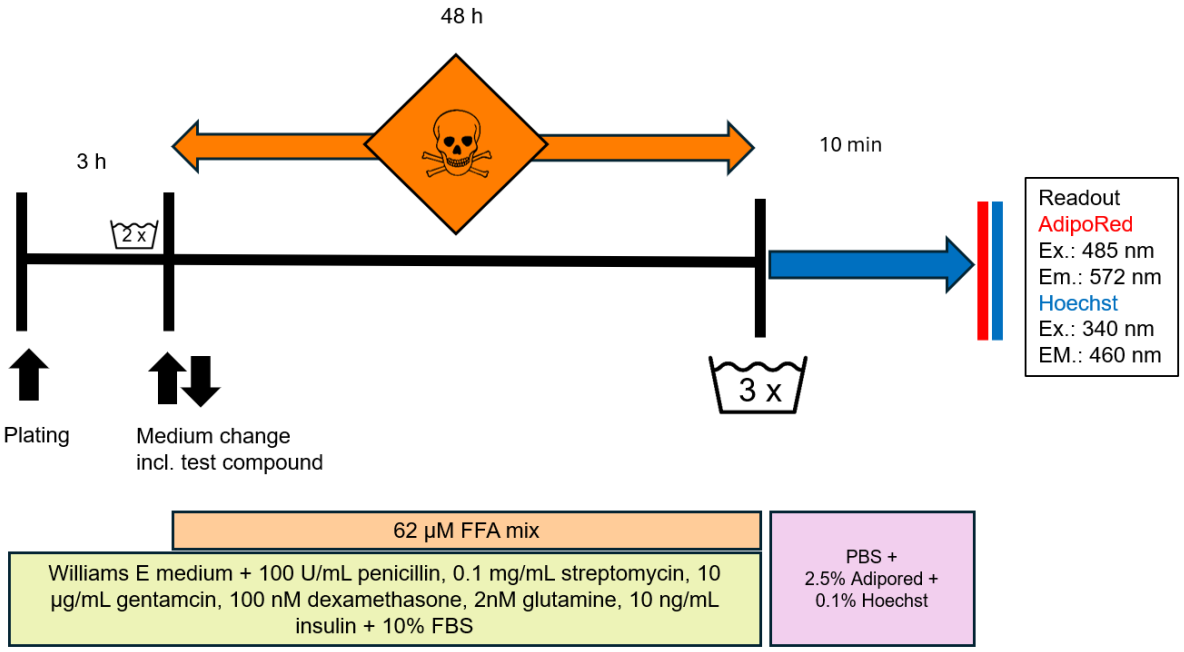

Figure 6 Time schedule & general overview of the lipid droplet accumulation test in primary rat hepatocytes

To improve the complexation of the free fatty acid mixture with albumin, the PRH were cultured in serum containing medium and the test substances were also prepared in this medium. The concentration series of test substances were prepared the day before rat liver perfusion to maximize the number of experiments. Volatile substances and those soluble only in warm solvents were prepared on the day of treatment. The serial dilutions were placed in transparent 96-well plates and stored overnight at 4 °C. On the day of treatment, these prepared dilution series were warmed in the incubator for three hours and then shaken on a shaker at 100 rpm for five minutes. After the freshly isolated rat hepatocytes had been attached for three hours, as described in section 2.2.1.2.1, 200 µL of the diluted compounds were applied to each well.

In comparison to the rat cell lines, a slightly shorter incubation time of 10 minutes was used for the AdipoRed-Hoechst staining solution. Aside from these adjustments, the procedure followed the same steps as described in 2.2.2.2.3 for the rat cell lines.

2.3 Methods for generating *in vivo* data

2.3.1 Physiologically based pharmacokinetic (PBPK) Modeling

Physiologically based pharmacokinetic modeling was performed by Dr. Wiebke Albrecht using the Simcyp Rat Simulator (Certera, Simcyp Versions 19 to 24). Certara UK Limited (Simcyp Division) granted access to the Simcyp Simulators through a sponsored academic license (subject to conditions).

A PBPK model was developed for each of the 40 test substances to simulate their pharmacokinetic behavior in rats at hepatotoxic LOAEL conditions.

The models incorporated a range of physicochemical properties, plasma protein binding parameters, and data on absorption, distribution, metabolism, and excretion. Those input parameters were derived from pharmacokinetic studies and various databases and, *in silico* prediction tools, including Pubchem (Kim et al. 2023), ChEMBL (Zdrazil et al. 2024), CompTox (Williams et al. 2017), ADMETlab 2.0 (Xiong et al. 2021), ADMETboost (Tian et al. 2022), pKCSM(Pires et al. 2015) and, PreADMET/Tox (Lee et al. 2002).

The simulations were conducted using a Sprague-Dawley rat model with a body weight of 0.25 kg. Each rat received a substance-specific hepatotoxic LOAEL orally every 24 hours for 30 consecutive days. The PBPK models were utilized to simulate peak concentrations (C_{max}) in the liver, portal vein and systemic circulation compartments. These compartments included plasma and whole blood, as well as the total and free composition and tissue concentrations for the liver. These C_{max} concentrations were used for the *in vitro – in vivo* comparison (extrapolation) to determine the similarity between the *in vivo* C_{max} and an effective concentration *in vitro*.

To ensure model reliability, all simulations were validated against available pharmacokinetic studies, focusing particularly on C_{max}, AUC and T_{max} values. Additionally, a second round of validation was performed by a pharmacokinetic expert Dr. Iain Gardner. A detailed overview of the input parameters, validation studies and model assumptions for each compound is provided in **Supplement 4**.

2.3.2 Validation data

To validate the *in vitro–in silico* approach of this study, robust experimental data from animal studies were required. These studies had to meet specific criteria to ensure their relevance and reliability for use in this analysis. The following sections will elucidate these criteria for pharmacokinetic studies and chronic toxicity studies to determine the LOAEL.

2.3.2.1 Pharmacokinetic studies

For pharmacokinetic validation, only studies meeting specific criteria were considered. The compound of interest had to be orally administered at a clearly defined dose. Both single and multiple dosing was permissible. If mixtures of substances were administered these studies were excluded.

The most reliable studies were those in which the test substance was directly measured in plasma, as opposed to indirect methods such as radiolabeled tracing, which were excluded. To guarantee a solid C_{max} determination, the studies must include sufficient sampling over time, since the C_{max} and T_{max} could not be reached at the first measurement after dosing.

2.3.2.2 Subchronic toxicity studies

A liver-specific LOAEL was defined by a significant hepatic adverse effect on a certain dose which is preceded by a NOAEL without an adverse liver effect. Standardized toxicity studies according to e.g. OECD 408 or 407 guidelines (OECD 1998) were the most suitable for determining adverse effects. The typical OECD 408 study was conducted for 90 days with enough animals (10/sex/group) and sufficient doses (at least three), serum analyses, especially clinical chemistry and, histopathological examinations. Studies that were not conducted according to validated standards but contained liver-specific LOAELs and NOAELs were also used.

2.3.2.2.1 LOAEL definition strategy

An overview of the decision-making process that led to the LOAEL definition can be seen in **Figure 7**. After clarification of the non-negotiable framework conditions (i.e. application form,

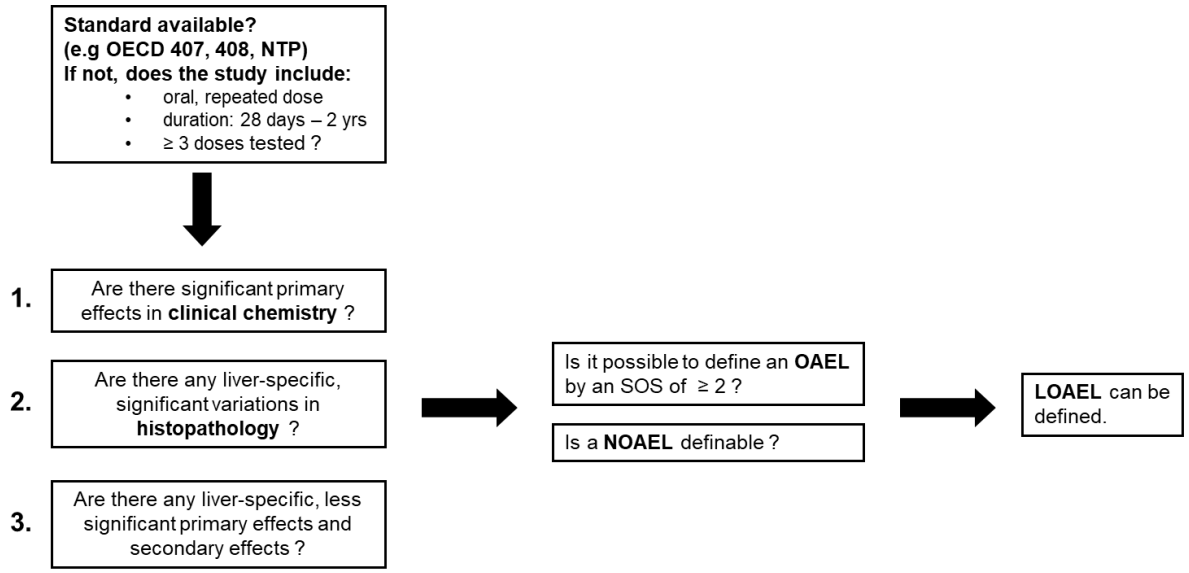

Figure 7 LOAEL definition strategy

LOAEL – Lowest Adverse Effect Level, NOAEL – No Observed Adverse Effect Level, NTP – National Toxicology Program, OAEL – Observed Adverse Effect Level, OECD – Organization for Economic Co-operation and Development, SOS – Score of significance

study duration and number of doses) the study could be used, and the available measurement data were examined for a dose-dependent effect and significance in comparison to the control measurement. The adverse effects were initially catalogued (OEAL: observed adverse effect level), and the lowest of these was designated as the LOAEL. A comprehensive list of all observed adverse effects can be found in **Supplement 3**. Since the measurable range of biochemical parameters varies greatly and depends on factors such as strain, sex and age (Giknis and Clifford 2006), pathological threshold values were not defined. The effects were classified as primary adverse effects, which alone can define a LOAEL (e.g. increased alanine aminotransferase (ALT), aspartate aminotransferase (AST) or direct bilirubin (Dbili)), or secondary effects (e.g. changes in liver weight), which cannot define a LOAEL (McInnes 2017) (**Table 8**).

Ultimately, this means that a liver LOAEL can only be established by a significant primary adverse effect or a less significant primary plus secondary effect. Sex-specific differences were recorded as accurately as possible if the data available allowed and sex-specific LOAELs were formulated accordingly. If no significant sex-specific differences were identifiable, the lowest observable adverse effect for both sexes were used.

To evaluate the quality level of the LOAELs, a scoring parameter was introduced: score of significance (SOS), which is described in more detail in chapter 3.1.1.1.

Table 8 Primary & secondary adverse effects

ALT – alanine aminotransferase, ALP – alkaline phosphatase, AST – aspartate aminotransferase, BUN – blood urea nitrogen, CHOL - cholesterol, CREA - creatinine, CYP – cytochrome P450, Dbili – direct bilirubin, GGT – gamma-glutamyltransferase, SBA – serum bile acids, TAG – triacylglyceride, TBili – total bilirubin, SOS – score of significance

	Primary adverse effects			**Secondary adverse effects**	
		SOS			**SOS**
		2	**1**		**1**
clinical chemistry	ALT	↑↑	↑	Albumin	↓
	AST	↑↑	↑	Protein	↓↑
	ALP	↑↑	↑	CHOL	↓↑
	GGT	↑↑	↑	TAG	↓↑
	Dbili	↑↑	↑	Tbili	↑
	SBA	↑↑	↑	Crea	↑
				BUN	↑
Histopathology	Hepatocyte Necrosis Fibrosis Hepatitis Steatosis Bile duct Hyperplasia	SOS = 2 if no. of affected animals ≥ ctrl + 30 %		Hepatocyte Vacuolization Hypertrophy	SOS = 1 if no. of affected animals ≥ ctrl + 30 %
Other effects	Glutathion	↓↓	↓	Changed liver weight	↓↑
	CYP activity	↓↓	↓	Liver coloration	

↑↑, ↓↓ ≥ 2 fold, ↑,↓ ≥ 1.3 - 2 fold, SOS = Score of Significance

2.4 Statistical analysis

The statistical analysis was done in close cooperation with Dr. Franziska Kappenberg and Dr. Julia Duda from the Department of Statistics at TU Dortmund University. For all statistical analysis the programming language R-version 3.6.0+ and the R-Studio version 2024.12.1+563 were utilized.

2.4.1 Curve fitting and determination of EC values

2.4.1.1 Cytotoxicity and Hoechst curve fitting

The concentration-response curves for the cytotoxicity and Hoechst readout were generated based on the model selection approach described in Albrecht et al. (2025), and Brecklinghaus et al. (2022b) using the R package drc (Ritz et al. 2015).

In summary, three different models (a four-parameter log-logistic model (4pLL), a Brain-Cousens model (Brain and Cousens 1989), and a flat profile) were fitted to the data. The Akaike Information Criterion (AIC) (Akaike 2011) was then calculated for each model, and the model with the lowest AIC was selected for normalization to obtain a response corresponding to 100 % viability at the control and for final curve fitting.

The effective concentration at which cell viability decreased to 90 %, 80 % and 50 % of the control (EC_{10}, EC_{20}, and EC_{50}, respectively) was determined for each compound and replicate. These values were defined as the concentration at which the fitted concentration–response curves intersected with an absolute viability value of 90 %, 80 % or 50 %.

For each fitted curve, a goodness-of-fit (GoF) value was calculated as described by Albrecht et al. (2019). The GoF was defined as 1 minus the ratio of the residual variation of the fitted model to the residual variation of the mean (**Equation 3**). A GoF value could not be determined for flat concentration profiles.

$$GOF = 1 - \frac{Sum\ of\ squared\ differences\ between\ the\ data\ points\ and\ fitted\ curve}{Sum\ of\ sqaured\ differences\ between\ the\ data\ points\ and\ the\ mean\ response}$$ **Equation 3**

If no EC_{10} value could be derived due to insufficient response (e.g., if the highest tested concentration yielded >90 % viability) or poor model fit (GoF < 0.55)), the EC_{10} was defined as “greater than the highest tested concentration”.

2.4.1.2 Nile red fit

The concentration–response modeling of the Nile red assay was performed according to the method described by Brecklinghaus et al. (2022a).

First, raw fluorescence data were normalized: for each independent experiment, the mean of the corresponding control values was calculated. All individual measurements were then divided by this mean and multiplied by 100 to obtain relative values expressed as percentages.

To analyze concentration–response relationships, the MCP-Mod method (Multiple Comparison Procedure and Modeling) was applied (Bretz et al. 2005). This two-step statistical approach accounts for model uncertainty by incorporating a range of plausible candidate models.

In the first step (MCP), the existence of a substance-related effect was assessed using two-sided contrast tests across the predefined candidate models. A family-wise error rate of $\alpha = 0.05$ is not exceeded to adjust for multiple testing.

In the second step (Mod), the best-fitting model was selected based on AIC, but only if the first step yielded a statistically significant result ($p < 0.05$). If no significance was observed, a flat concentration–response relationship was assumed. The selected model was then adjusted so that the response at concentration 0 equaled 100% (i.e., the baseline control level).

From the fitted model, EC_x values were derived, representing the concentration at which the response reaches (100 + x) % (e.g., EC_{10} corresponds to a 10% effect above control level).

For each compound, the median EC_x value from three independent experiments was reported as the representative value. Minimum and maximum EC_x values were also determined.

2.4.2 Calculation of the Toxicity Iso-concentration Index (TII)

A quantification parameter was introduced for systemic test system evaluation and optimization: Toxicity iso-concentration index (TII).

The TII measures how well hepatotoxic blood concentrations *in vivo* can be estimated for hepatotoxic compounds using the *in vitro* test system. A prerequisite for the use of the TII is a defined LOAEL and NOAEL. In cases where one is missing the Toxicity Estimation Index (TEI) described in Albrecht et al. (2019) should be used.

A TII of 1 represents an optimal match between an *in vitro–in vivo* concentration pair, a TII of 0.8 shows an average deviation from the iso-concentration line of 10.

The TII is calculated by the following formula:

$$\mathrm{TII} = 1 - \frac{1}{5}\,\frac{\sum_{i=1}^{n} \mid log10(\frac{x(i)}{y(i)}) \mid}{n} \qquad \textbf{Equation 4}$$

which represents a set of compounds with i ranging from 1 to n, and x(i) representing the effective concentration *in vitro* and y(i) denoting the *in vivo* concentration at the LOAEL.

The subsequent section will provide a concise overview of the algorithm. The sum of the absolute value of the concentration ratio in logarithm to base 10 was calculated from all hepatotoxic *in vitro–in vivo* pairs. The resultant value was then divided by the number of compounds, n, and subsequently scaled using a scaling factor of 5. The purpose of the scaling factor of 5 is as follows: when the distance increases by a factor of 10, TII decreases by 0.2. Consequently, TII decreases from 1.0 to 0.0 when the mean distance is 5 orders of magnitude or more. To obtain an index ranging from 0 to 1, with 1 representing the optimal value, the result of the summed and scaled ratios was subtracted from 1. The resulting measurement is the TII.

2.4.2.1 Penalty factors in case of missing positive effects.

For the TII based only on cytotoxicity data for the hepatocyte cell lines, no penalty factor was needed. However, for the indices based on lipid droplet accumulation or Hoechst alone a penalty factor was required. This aims to avoid overoptimistic calculations of the TII that would result from simply omitting compounds without a positive effect. For each compound with a missing positive effect, a replacement was calculated by multiplying the maximum tested concentration with a factor of 5. The result of this calculation was then used as the distance penalty for the calculation of TII.

2.4.2.2 Geometric mean fold error

The geometric mean fold error (GMFE), as defined in Equation 5 and described by (Y. Yang et al., 2024 was used to quantify the deviation between simulated *in vivo* concentrations at the LOAEL and *in vitro* concentrations for the best- performing cell system and assay, as it provides a robust metric for assessing average fold differences while minimizing the influence of outliers.

$$GMFE = 10^{\frac{1}{n}\sum_{i=1}^{n}|log_{10}(\frac{in\ vitro_i}{in\ vivo_i})|} \quad \textbf{Equation 5}$$

2.4.2.3 Geometric standard deviation

To describe the variability of the fold differences between *in vitro* and *in vivo* concentrations, the geometric standard deviation (GSD) was calculated according to the following equation:

$$GSD = 10^{STDEV.S(|log10(\frac{in\ vitro}{in\ vivo})|)} \quad \textbf{Equation 6}$$

Where STDEV.S denotes the sample standard deviation of the absolute base-10 logarithms of the concentration ratios. The GSD reflects the multiplicative spread of the fold differences and is expressed as a fold factor.

2.5 Use of artificial intelligence

In the course of this dissertation, artificial intelligence (AI) was used as a tool to assist in the formulation of the text and in the creation and optimization of R code. OpenAI was specifically employed for the composition and refinement of texts, DeepL was used for translations and linguistic fine-tuning, and the TU Dortmund Campus AI played a key role in the development and optimization of R code (DeepL GmbH 2025; OpenAI 2025; Technische Universität Dortmund 2025). No images were generated using AI, and no analyses based on raw data were conducted with AI. The AI-supported assistance was limited to improving the text and programming and did not influence the scientific analysis or results of this work.

3 Results

3.1 Test compounds and LOAEL definition

3.1.1 Hepatotoxicity of the selected test compounds

The first step of the present study was to identify the hepatotoxicity of the 40 test compounds using data from published rat toxicity studies. For this purpose, liver-specific lowest observed adverse effect levels (LOAELs) were systematically derived from the reported experimental measurements. These LOAELs were used to derive corresponding peak concentrations (C_{max}) in the portal vein plasma via pharmacokinetic modeling, allowing for a quantitative comparison with *in vitro* effective concentrations (e.g., $EC_{10}, EC_{20,} EC_{50}$). **Table 9** provides an overview of the animal toxicity studies used to define liver-specific LOAELs for the selected test compounds. Additional details on individual study characteristics can be found in **Supplement 3**.

Table 9 Overview of toxicity studies

Studies used for LOAEL definition, including characteristics, ATSDR – Agency for Toxic Substances and Disease Registry, F344 – Fischer 344 rats, N.A. – not available, NTP – National Toxicology Program, OECD – Organisation for Economic Co-operation and Development, SD – Sprague-Dawley rats, TRL – Toxicity Research Laboratories, US EPA – United States Environmental Protection Agency, W – Wistar rats

Compound	Abbreviation	Oral route	Study duration [weeks]	Rat strain	Tested doses [incl. control]	Sex	Animals/ sex/ dose	Reference
Aflatoxin B1	AFB1	gavage	5	F344	5	males	5	Qian et al. 2013
Acetaminophen	APAP	diet	13	F344	4	both	10	NTP 1993c
Arsenic	AS	drinking water	6	SD	4	males	18	ATSDR, Fowler et al. 1977
Butylated hydroxy toluene	BHT	gavage	4	W	4	males	10	Powell et al. 1986
Bisphenol - A	BPA	gavage	4	W	5	males	10	Hassan et al. 2012
Cannabidiol	CBD	gavage	13	SD	4	both	5	Henderson et al. 2023
Carbamazepine	CBZ	N.A.	3	N.A.	4	both	6	Akunne et al. 2017
Coumarin	COU	gavage	13	F344	6	both	10	NTP 1993b
Chrysin	CRY	gavage	13	SD	4	both	10	Yao et al. 2021
Copper	CU	drinking water	13	F344	6	both	10	NTP 1993a
Dibromoacetic acid	DBA	drinking water	13	F344	6	both	10	NTP 2007
Di(2-Ethylhexyl) Phthalate	DEHP	drinking water	4	SD	4	males	6	Wang et al. 2020
Di-isononylphthalate	DINP	diet	52	F344	4	both	10	Lington et al. 1997
1,4-dioxane	DIX	diet	13	F344	6	both	10	Kano et al. 2008
Emodin	EMO	diet	14	F344	6	both	10	NTP 2001

Table 9 (continued) Overview of toxicity studies

Studies used for LOAEL definition, including characteristics, ATSDR – Agency for Toxic Substances and Disease Registry, F344 – Fischer 344 rats, N.A. – not available, NTP – National Toxicology Program, OECD – Organisation for Economic Co-operation and Development, SD – Sprague-Dawley rats, TRL – Toxicity Research Laboratories, US EPA – United States Environmental Protection Agency, W – Wistar rats

Compound	Abbreviation	Oral route	Study duration [weeks]	Rat strain	Tested doses [incl. control]	Sex	Animals/ sex/ dose	Reference
Gallic acid	GA	diet	13	F344	5	both	10	Niho et al. 2001
2,3,3,3-tetrafluoro-2-(heptafluoropropoxy)propanoate	GENX	gavage	104	SD	4	both	80	Rae et al. 2015
Gemifloxacin mesylate	GFM	gavage	4	W	4	both	12	Roy et al. 2010
Genistein	GST	gavage	26	W	4	both	10	McClain et al. 2004
Imidacloprid	IMI	gavage	13	W	4	females	10	Bhardwaj et al. 2010
Isoeugenol	IEG	gavage	14	F344	6	both	10	NTP 2010a
Lindane	LIN	diet	104	W	5	both	15	Amyes 1990
Methyleugenol	MEG	gavage	14	F344	6	both	10	Abdo et al. 2002
Methanol	MET	gavage	13	SD	4	both	30	TRL 1986, US EPA 2013
Morin	MOR	diet	13	F344	5	both	10	Cho et al. 2005
Oxyresveratol	ORES	gavage	13	W	4	both	10	Alma et al. 2003
2,3',4,4',5-pentachlorobiphenyl	PCB118	gavage	14	SD	8	females	80	NTP, 2010c
3,3',4,4',5-pentachlorobiphenyl	PCB126	gavage	53	SD	8	females	80	NTP, 2006
Perfluorobutanoic acid	PFBA	gavage	13	SD	4	both	10	Butenhoff et al. 2012
Perfluorobutane sulfonic acid	PFBS	gavage	4	SD	6	both	10	NTP, 2019b
Perfluorohexanoic acid	PFHXA	gavage	4	SD	6	both	10	NTP, 2019a
Perfluorooctanoic acid	PFOA	gavage	4	SD	6	both	10	NTP, 2019b
Perfluorooctanesulfonate	PFOS	gavage	4	SD	6	both	10	NTP, 2019b
Pyridine	PYR	drinking water	13	F344	6	both	10	NTP, 2000
3,3',4,4'-tetrachloroazobenzene	TCAB	gavage	13	SD	8	both	10	NTP 2010b
Thiabendazole	THIA	diet	104	F344	5	both	30	Fujii et al. 1991
Triticonazole	TRI	diet	13	SD	5	both	10	US EPA 2000
Triclosan	TSN	gavage	9	SD	5	males	6	Ena et al. 2018

The available studies vary in terms of experimental design, which poses challenges for comparability. For instance, different oral administration routes were used, 60 % of the compounds were administered via gavage, 25 % via diet, and 12.5 % via drinking water. Study durations ranged from 3 weeks to 104 weeks, but the majority (55 %) lasted between 13 and 14 weeks. Various rat strains were employed: 45 % of the studies used Sprague-Dawley rats,

35 % used Fischer 344 rats and 17.5% Wistar rats. Furthermore, most studies included both sexes (75 %), while only a few were limited to females (7.5 %) or males (15 %).

3.1.1.1 Systematic derivation of hepatotoxic LOAELs with a novel scoring system (SOS)

To account for the variability in study design and adherence to standardized protocols a scoring system was introduced to assess the reliability of the liver-specific derived LOAELs. The score of significance (SOS) standardizes the LOAEL definition by quantitatively assessing the severity and reliability of observed adverse effects. Adverse effects were categorized into primary and secondary effects (see chapter 2.3.2.2.1), with primary effects being more directly indicative of significant toxicological outcomes. For primary adverse effects, an SOS of 2 points was assigned for significant effects and 1 point for less significant effects. Secondary adverse effects, which were less directly linked to hepatotoxicity, were uniformly assigned an SOS of 1 point. Each observed effect was evaluated and assigned to a corresponding SOS.

To establish a LOAEL, the cumulative SOS of adverse effects must reach at least 2 points, of which at least 1 point must originate from the primary effects category. Additional scoring adjustments ensure a more nuanced evaluation:

1. Dose-dependency: If the incidence or severity of the adverse effects was clearly dose-dependent, or if additional adverse effects were observed at doses exceeding the LOAEL, this was interpreted as further evidence of frank, relevant hepatotoxicity. To account for the increased reliability of the study, an additional point was awarded per effect displaying dose-dependency.

2. Study quality: An additional 2 points were assigned if the study was conducted following established and validated standards, enhancing the reliability of the LOAEL determination.

3. Limited data availability: Adverse effects described as 'severe', 'significant', or estimated (e.g., '30 % higher compared to control') without specific numerical information (e.g., number of affected animals, measured values) were scored with only 1 point.

An illustration of the rationale and use of the score of significance is provided in **Table 10**, which shows five representative case examples with varying degrees of study details. The studies differ in type and amount of available data used for LOAEL determination, including clinical chemistry, histopathology of the liver, and other endpoints.

Table 10 Application of the Score of Significance (SOS)

The application of the SOS is demonstrated using four example substances.
Significant effects (2 points): ↑↑, ↓↓ ≥ 2 fold, ++
Less significant effects (1 point): ↑, ↓ ≥ 1.1 - 2 fold, +
ALP – alkaline phosphatase, AST – aspartate aminotransferase, ALT – alanine aminotransferase, f – female, GSH – Glutathione, LOAEL – Lowest Observed Adverse Effect Level, m – male, N.A. – not available, NTP – National Toxicology Program, SBA – Serum bile acids, TBili – Total bilirubin
histopathology with number of affected individuals/ total number of individuals

Compound	LOAEL [mg/kg/bw day]	Clinical chemistry		Histopathology		Additional categories				Total points = SOS
		Adverse effect	Points	Adverse effect	Points	Other effects	Dose dependency	Study quality	Points	
Acetaminophen	1000 (f)	N.A.	0	Necrosis (5/10) ++, Postnecrotic cirrhosis (10/10) ++, Hepatocytomegaly (10/10) ++	6	N.A.	N.A.	NTP 13 weeks	2	8
Bisphenol A	10 (m)	↑ALT, ↑ALP, ↑↑Tbili	4	N.A.	0	↓GSH	3 effects	N.A	4	8
Copper	68.09 (f)	↑ALT, ↑SBA, ↓Albumin	3	Chronic active inflammation (6/10) ++	2	Liver weight +	1 effect	NTP 13 weeks	4	9
Copper	68.09 (m)	↑↑ALT, ↑SBA	3	Chronic active inflammation (10/10) ++	2	Liver weight +	1 effect	NTP 13 weeks	4	9
Ethanol	3600	N.A.	0	Centrilobular steatosis +, Mallory bodies +, Necrosis +	3	Liver discoloratation +	N.A.	N.A.	1	4
Methanol	2500	↑ALP, ↑ALT	2	N.A.	0	N.A.	N.A.	N.A.	0	2

3.1.1.2 Defined hepatotoxic LOAELs

Finally, the systematically derived LOAELs and the corresponding scores of significance (SOS), are summarized in **Table 11**. These doses serve as hepatotoxic input parameters for the pharmacokinetic modeling, which translates them into corresponding portal vein plasma concentrations. In cases where possible, sex-specific LOAELs were determined to account for potential sex differences in hepatotoxicity. While some compounds, such as CRY, GST, or PFHXA, exhibited identical LOAELs across sexes, notable variation in the corresponding SOS was observed. The LOAELs span a wide range, from just a few nanograms (e.g., PCB126) to several grams (e.g., ethanol). This variability reflects the broad spectrum of compound types included in the test set, such as plant constituents, pharmaceuticals, environmental contaminants, industrial chemicals and pesticides.

Table 11 Overview of hepatotoxicity

Unless stated otherwise, data refer to both male and female animals.
ATSDR – Agency for Toxic Substances and Disease Registry, f – females, m – males, NTP – National Toxicology Program, OECD – Organisation for Economic Co-operation and Development, PCB - Polychlorinated biphenyl, PFAS - Per- and polyfluoroalkyl substances, SOS – Score of significance, TRL – Toxicity Research Laboratories, US EPA – United States Environmental Protection Agency

Compound	Abbreviation	Compound type	LOAEL [mg/kg/bw]	SOS	Reference
Aflatoxin B1	AFB1	Mycotoxin	0.01	5	Qian et al. 2013
Acetaminophen	APAP	Drug (analgesic, antipyretic)	1000 (f)	8 (f)	NTP 1993a
Arsenic	AS	Element	6 (m)	3 (m)	ATSDR 2007, Fowler et al. 1977
Butylated hydroxy toluene	BHT	Preservative	250 (m)	5 (m)	Powell et al. 1986
Bisphenol - A	BPA	Plasticizer	10 (m)	8 (m)	Hassan et al. 2012
Cannabidiol	CBD	Component of cannabis (cannabinoid)	140 (f)	7 (f)	Henderson et al. 2023
Carbamazepine	CBZ	Drug (anticonvulsant)	400	4	Okafor et al. 2017
Coumarin	COU	Component of cinnamon	150	11 (f), 12 (m)	NTP 1993b
Chrysin	CRY	Component of e.g., honey, passion flowers (flavone)	1000	4 (f), 9 (m)	Yao et al. 2021
Copper	CU	Element	68.09	9	NTP 1993c
Dibromoacetic acid	DBA	Water disinfection related contaminant	20 (m)	6 (m)	NTP 2007
Di(2-Ethylhexyl) Phthalate	DEHP	Plasticizer	3000 (m)	4 (m)	Wang et al. 2020
Di-isononylphthalate	DINP	Plasticizer	184 (f), 152 (m)	7 (f), 8 (m)	Lington et al. 1997
1,4-dioxane	DIX	Solvent	1614 (f), 657 (m)	8	Kano et al. 2008
Emodin	EMO	Component of e.g., rhubarb, buckthorn	340 (f), 170 (m)	6 (f), 5 (m)	NTP 2001
Ethanol	ETOH	Solvent	3600	4	OECD 2004
8-2 fluorotelomer alcohol	FTOH	PFAS precursor	25 (m)	7 (m)	Ladics et al. 2008

Table 11 (continued) Overview of hepatotoxicity

Unless stated otherwise, data refer to both male and female animals.
ATSDR – Agency for Toxic Substances and Disease Registry, f – females, m – males, NTP – National Toxicology Program, OECD – Organisation for Economic Co-operation and Development, PCB - Polychlorinated biphenyl, PFAS - Per- and polyfluoroalkyl substances, SOS – Score of significance, TRL – Toxicity Research Laboratories, US EPA – United States Environmental Protection Agency

Compound	Abbreviation	Compound type	LOAEL [mg/kg/bw]	SOS	Reference
Gallic acid	GA	Component of e.g., gallnuts, sumac, tea, grapes and lemon	70.5 (f), 64.9 (m)	7 (f), 5 (m)	Niho et al. 2001
2,3,3,3-tetrafluoro-2-(heptafluoropropoxy)propanoate	GENX	Environmental contaminant (PFAS)	50 (m)	8 (m)	Rae et al. 2015
Gemifloxacin mesylate	GFM	Drug (broad-spectrum quinolone antibacterial agent)	200 (f), 100 (m)	7 (f), 8 (m)	Roy et al. 2010
Genistein	GST	Component of e.g., soybeans and soy products	500	7 (f), 2 (m)	McClain et al. 2006
Imidacloprid	IMI	Insecticide	20 (f)	3 (f)	Bhardwaj et al. 2010
Isoeugenol	IEG	Component of e.g., ylang-ylang (essential oil)	300	4	NTP 2010a
Lindane	LIN	Insecticide	24 (f)	4 (f)	Amyes 1990
Methyleugenol	MEG	Component of e.g., fennel, roses, basil (essential oil)	100	9	Abdo et al. 2001
Methanol	MET	Solvent	2500	2	TRL 1986, US EPA 2013
Morin	MOR	Component of e.g., Maclura tinctoria (flavonol)	1701 (f), 613 (m)	6 (f), 7 (m)	Cho et al. 2006
Oxyresveratol	ORES	Component of e.g., white mulberry (stilbenoid)	150	8	Alam et al. 2023
2,3',4,4',5-pentachlorobiphenyl	PCB118	Environmental contaminant (PCB)	4.6 (f)	9 (f)	NTP, 2010b
3,3',4,4',5-pentachlorobiphenyl	PCB126	Environmental contaminant (PCB)	0.00055 (f)	7 (f)	NTP, 2006
Perfluorobutanoic acid	PFBA	Environmental contaminant (PFAS)	32 (m)	4 (m)	Butenhoff et al. 2012
Perfluorobutane sulfonic acid	PFBS	Environmental contaminant (PFAS)	250 (f), 500 (m)	10 (f), 10 (m)	NTP, 2019b
Perfluorohexanoic acid	PFHXA	Environmental contaminant (PFAS)	500	10 (f), 12 (m)	NTP, 2019a
Perfluorooctanoic acid	PFOA	Environmental contaminant (PFAS)	100 (f), 1.25 (m)	9 (f), 12 (m)	NTP, 2019b
Perfluorooctanesulfonate	PFOS	Environmental contaminant (PFAS)	1.25 (f), 0.625 (m)	10 (f), 9 (m)	NTP, 2019b
Pyridine	PYR	Solvent	90 (f), 25 (m)	9 (f), 8 (m)	NTP, 2000
3,3',4,4'-tetrachloroazobenzene	TCAB	Contaminant of herbicide synthesis	3	8 (f), 11 (m)	NTP 2010c
Thiabendazole	THIA	Fungicide	112 (f), 90 (m)	3 (f), 2 (m)	Fujii et al. 1991
Triticonazole	TRI	Fungicide	22.3 (f), 1117 (m)	7 (f), 7 (m)	US EPA 2000
Triclosan	TSN	Disinfectant, preservative, and deodorant agent	750 (m)	2 (m)	Ena et al. 2018

3.2 *In vitro*

3.2.1 *In vitro* hepatotoxicity screening

Once the hepatotoxicity of the compounds was established from literature, cytotoxicity was assessed *in vitro*. The effective concentrations (EC) obtained through experimentation were then compared with the modeled *in vivo* peak concentration (C_{max}) at the hepatotoxic LOAEL in the portal vein plasma. For this purpose, three hepatocyte cell systems and three readouts were used to obtain effective concentrations at 10, 20 and 50 % change relative to the control measurement. Primary rat hepatocytes and the liver carcinoma cell lines H4IIE and Zajdela were tested for cytotoxicity using resazurin, lipid droplet accumulation through Nile red dye and nuclear enumeration via Hoechst staining. For all assays, the cell systems were exposed to six different concentrations (including control) of the test compounds for 48 hours.

As illustrated in **Figure 8**, three distinct examples are presented, demonstrating the determination of effective concentrations from experimental data for three compounds. The cytotoxicity and Hoechst measurements demonstrate how cell viability changes with varying concentrations (Figure 8 A and C), while the lipid droplet measurments shows the concentration-dependent increase in lipid droplets (Figure 8 B). The concentration-response curves for all experiments can be found in **Supplement 5**.

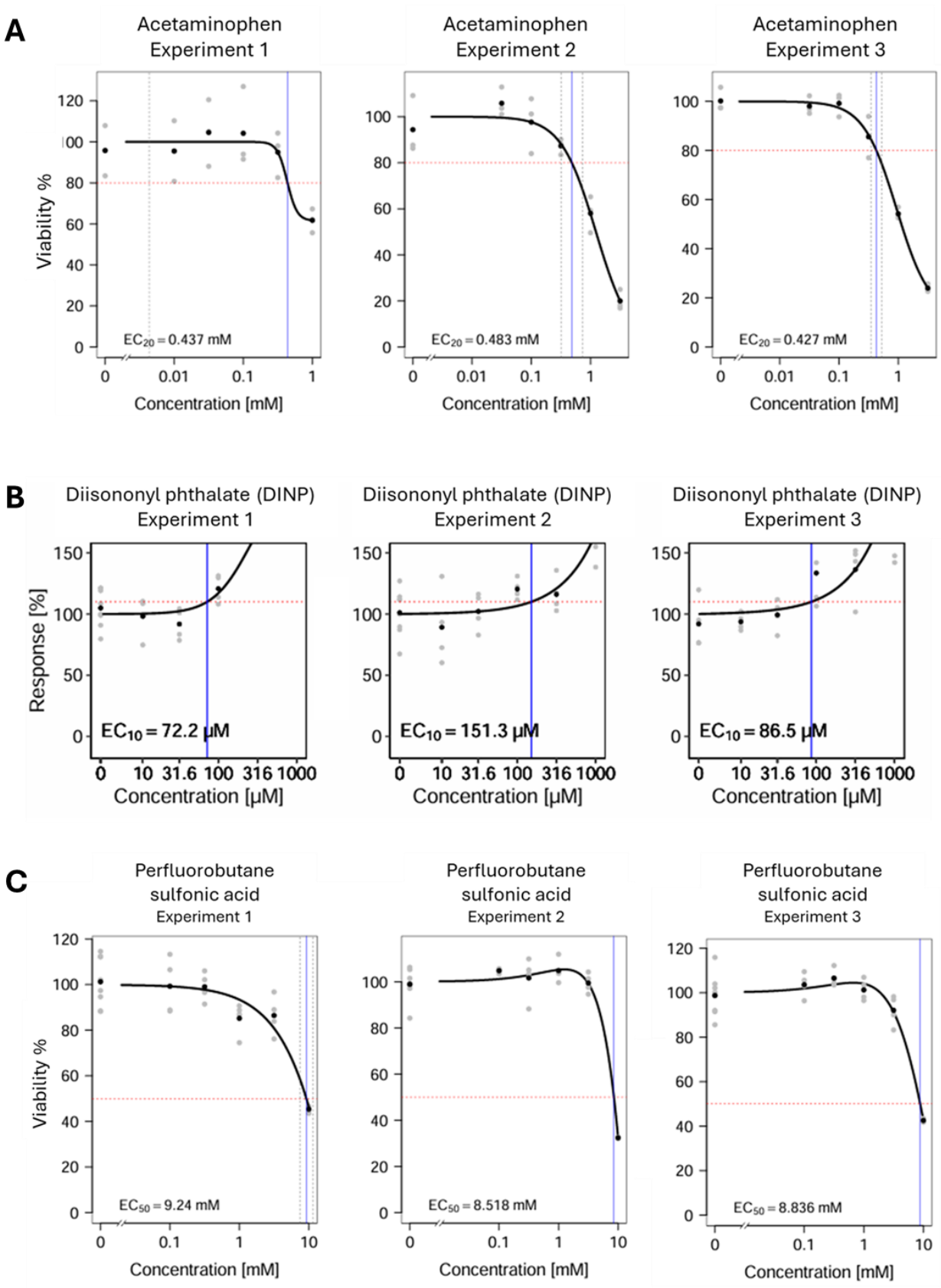

Figure 8 Concentration-response curve for APAP, DINP, and PFBS

Representative measurements after 48 hours of compound exposure (n = at least 3 independent experiments). **A**: EC_{20} cytotoxicity in H4IIE cells, **B**: EC_{10} lipid droplet accumulation in Zajdela cells, **C**: EC_{50} Hoechst in primary rat hepatocytes. Red and blue lines indicate the respective effective concentrations (EC_{10}, EC_{20}, EC_{50}). Blue and grey lines represent the confidence intervals of the effective concentrations.

3.2.1.1 Overview of assay perfomance based on positive test results across cell systems

In order to determine which cell system and assay delivers the most suitable *in vitro* effective concentration for the later *in vitro—in vivo* extrapolation, the number of positive test results from the cell systems and readouts is first recorded below. For this purpose, the median values of all effective concentrations are presented in tabular form (**Table 12** - **Table 20**). The median values were determined from at least three independent replicates and are presented along with the lowest (EC min) and highest (EC max) effective concentrations measured in each test series.

In the H4IIE cells, a positive test result for EC_{10} and EC_{20} was observed for all substances using the cytotoxicity assay (**Table 12**). An EC_{50} was determined for 32 substances. The Nile red assay (**Table 13**) yielded a total of 16 compounds with positive test results for EC_{10}, 14 for EC_{20}, and 6 for EC_{50}. In the Hoechst readout (**Table 14**), 35 positive test results were recorded for EC_{10} in the H4IIE cells, with 25 for EC_{20} and 21 for EC_{50}. For the second liver cancer cell line, the Zajdela cells, the cytotoxicity assay (**Table 15**) also showed positive test results for all tested compounds at an effective concentration at 90 % viability, with 39 positive test results for EC_{20} and 31 for EC_{50}. For the lipid droplet assay (**Table 16**), a total of 17 positive test results were recorded for EC_{10}, with 14 compounds showing EC_{20}, and 7 of these also showing EC_{50}. In the Hoechst assay (**Table 17**), EC_{10} and EC_{20} were initially determined for 28 compounds, and 16 of these still showed EC_{50}. The distribution of positive test results for the primary rat hepatocytes demonstrated a total of 29 positive test results for EC_{10} in the cytotoxicity assay (**Table 18**), 27 for EC_{20} and 22 for EC_{50}. The evaluation of lipid droplet accumulation (**Table 19**) yielded 14 positive test results for EC_{10}, 10 for EC_{20} and 3 for EC_{50}. In the Hoechst assay (**Table 20**) 20 compounds were identified as positive for a EC_{10} and 17 for EC_{20}, while 7 were identified as positive for EC_{50}.

The cytotoxicity assay yielded the most positive test results across all cell systems for effective concentrations, although the primary rat hepatocytes produced no positive test result for 11 compounds (BHT, CBZ, DEHP, DINP, IMI, LIN, MEG, PCB126, TCAB, THIA, TRI). The lipid droplet accumulation test showed the fewest positive test results, with the Zajdela cells exhibiting the highest number of positive outcomes and primary rat hepatocytes showing the least. It was also observed, that the Zajdela cells displayed the highest number of EC_{50} values in both cytotxicity and Nile red assays. The H4IIE cells showed the highest number of EC_{50} values in the Hoechst readout. Primary rat hepatocytes demonstrated the lowest number of EC_{50} values across all three assays. That indicates, that the cell lines (H4IIE and Zajdela) are more sensitive at detecting a broader spectrum of the toxicity than the primary rat hepatocytes.

Table 12 Effective concentrations (EC) of cytotoxicity testing in H4IIE cells
The median was calculated from at least three independent replicates. EC min and EC max show the lowest and highest measurements respectively.

Compound	Abbreviation	EC_{10} median [M]	EC_{10} min [M]	EC_{10} max [M]	EC_{20} median [M]	EC_{20} min [M]	EC_{20} max [M]	EC_{50} median [M]	EC_{50} min [M]	EC_{50} max [M]
Aflatoxin B1	AFB1	2.30E-08	1.20E-08	2.70E-08	6.20E-08	3.90E-08	6.80E-08	3.56E-07	2.96E-07	4.49E-07
Acetaminophen	APAP	2.64E-04	1.46E-04	4.89E-04	4.32E-04	3.00E-04	7.09E-04	1.23E-03	1.13E-03	2.45E-03
Arsenic	AS	1.94E-05	1.24E-05	3.28E-05	2.54E-05	2.18E-05	3.38E-05			
Butylated hydroxy toluene	BHT	3.19E-04	2.93E-04	5.78E-04	3.68E-04	3.58E-04	6.42E-04	6.03E-04	4.37E-04	7.63E-04
Bisphenol - A	BPA	1.78E-05	1.40E-05	4.87E-05	2.91E-05	2.60E-05	4.93E-05	6.67E-05	5.12E-05	7.25E-05
Cannabidiol	CBD	2.36E-05	1.07E-05	2.75E-05	2.49E-05	1.19E-05	2.79E-05	2.91E-05	1.61E-05	2.93E-05
Carbamazepine	CBZ	1.15E-04	7.14E-05	1.34E-04	1.70E-04	1.25E-04	1.72E-04	3.09E-04	3.03E-04	3.41E-04
Coumarin	COU	2.94E-04	2.76E-04	3.54E-04	4.59E-04	4.23E-04	4.60E-04			
Chrysin	CRY	2.60E-05	2.26E-05	3.14E-05	2.88E-05	2.65E-05	4.01E-05	4.20E-05	3.82E-05	6.08E-05
Copper	CU	2.44E-05	1.61E-05	2.55E-05	2.44E-05	1.45E-04	6.71E-04	6.89E-04	2.10E-04	7.09E-04
Dibromoacetic acid	DBA	9.33E-04	8.69E-04	1.36E-03	1.04E-03	9.35E-04	1.54E-03	1.24E-03	1.16E-03	2.02E-03
Di(2-Ethylhexyl) Phthalate	DEHP	1.51E-05	3.76E-06	1.90E-05	2.14E-05	5.88E-06	2.24E-05	3.29E-05	1.26E-05	3.88E-05
Di-isononylphthalate	DINP	9.11E-05	7.18E-05	1.15E-04	1.51E-04	1.47E-04	1.70E-04			
1,4-dioxane	DIX	6.36E-02	4.10E-02	7.02E-02	7.64E-02	6.83E-02	9.12E-02			
Emodin	EMO	9.34E-06	8.42E-06	2.27E-05	1.57E-05	1.30E-05	2.52E-05	3.31E-05	2.67E-05	3.46E-05
Ethanol	ETOH	6.80E-02	5.83E-02	1.13E-01	9.53E-02	7.04E-02	1.60E-01	1.69E-01	1.23E-01	2.88E-01
8-2 fluorotelomer alcohol	FTOH	1.02E-04	9.41E-05	1.15E-04	1.02E-04	1.01E-04	1.25E-04	1.23E-04	1.04E-04	1.54E-04
Gallic acid	GA	2.95E-05	1.57E-05	3.08E-05	3.11E-05	1.92E-05	3.40E-05	3.20E-05	2.71E-05	4.31E-05
2,3,3,3-tetrafluoro-2-(heptafluoropropoxy)propanoate	GENX	4.07E-04	3.32E-04	5.89E-04	6.33E-04	4.98E-04	9.22E-04	1.80E-03	9.86E-04	2.00E-03

Table 12 (continued) Effective concentrations (EC) of cytotoxicity testing in H4IIE cells

The median was calculated from at least three independent replicates. EC min and EC max show the lowest and highest measurements respectively.

Compound	Abbreviation	EC_{10} median [M]	EC_{10} min [M]	EC_{10} max [M]	EC_{20} median [M]	EC_{20} min [M]	EC_{20} max [M]	EC_{50} median [M]	EC_{50} min [M]	EC_{50} max [M]
Gemifloxacin mesylate	GFM	6.78E-05	4.40E-05	7.36E-05	9.26E-05	7.05E-05	9.97E-05	2.01E-04	1.87E-04	2.10E-04
Genistein	GST	2.12E-05	2.04E-05	7.45E-05	3.40E-05	3.05E-05	8.16E-05	7.74E-05	6.11E-05	9.58E-05
Imidacloprid	IMI	1.77E-04	1.44E-04	1.95E-04	2.77E-04	2.39E-04	2.81E-04	5.56E-04	5.24E-04	5.96E-04
Isoeugenol	IEG	6.37E-05	1.86E-05	7.54E-05	8.42E-05	4.14E-05	1.08E-04	1.76E-04	1.49E-04	2.36E-04
Lindane	LIN	2.03E-05	1.45E-05	3.33E-05	3.41E-05	3.07E-05	4.96E-05	1.01E-04	8.36E-05	1.09E-04
Methyleugenol	MEG	2.16E-04	1.26E-04	3.04E-04	2.80E-04	2.63E-04	3.51E-04			
Methanol	MET	4.18E-01	3.29E-01	5.94E-01	6.45E-01	4.51E-01	7.51E-01	1.23E+00	8.85E-01	1.24E+00
Morin	MOR	1.14E-04	1.05E-04	1.80E-04	1.40E-04	1.30E-04	2.06E-04	1.98E-04	1.86E-04	2.58E-04
Oxyresveratol	ORES	8.02E-05	3.90E-05	8.63E-05	8.24E-05	4.30E-05	8.76E-05	8.95E-05	5.67E-05	9.13E-05
2,3',4,4',5-pentachlorobiphenyl	PCB118	9.13E-05	7.82E-05	1.45E-04	1.06E-04	9.07E-05	1.48E-04			
3,3',4,4',5-pentachlorobiphenyl	PCB126	3.59E-05	3.44E-05	4.45E-05	4.45E-05	9.48E-06	5.00E-05			
Perfluorobutanoic acid	PFBA	2.12E-04	1.42E-04	4.19E-04	5.19E-04	2.61E-04	7.18E-04			
Perfluorobutane sulfonic acid	PFBS	4.89E-04	1.48E-04	7.40E-04	6.48E-04	2.89E-04	9.52E-04	1.44E-03	8.88E-04	2.03E-03
Perfluorohexanoic acid	PFHXA	2.94E-04	2.51E-04	5.32E-04	4.41E-04	4.21E-04	8.24E-04			
Perfluorooctanoic acid	PFOA	1.70E-04	1.59E-04	1.99E-04	2.03E-04	1.64E-04	2.37E-04	2.75E-04	1.73E-04	3.17E-04
Perfluorooctanesulfonate	PFOS	2.31E-04	1.61E-04	3.79E-04	2.82E-04	1.85E-04	4.44E-04			
Pyridine	PYR	5.22E-03	2.35E-03	6.11E-03	1.24E-02	5.86E-03	1.34E-02	3.54E-02	2.37E-02	8.41E-02
3,3',4,4'-tetrachloroazobenzene	TCAB	1.43E-05	1.40E-05	1.69E-05	1.46E-05	1.46E-05	2.04E-05			
Thiabendazole	THIA	1.87E-04	1.17E-04	2.07E-04	2.03E-04	1.40E-04	2.17E-04	2.43E-04	2.33E-04	2.47E-04
Triticonazole	TRI	3.12E-05	2.76E-05	4.40E-05	4.43E-05	4.23E-05	7.11E-05	9.96E-05	9.15E-05	1.56E-04
Triclosan	TSN	2.19E-05	1.31E-05	2.70E-05	2.38E-05	1.68E-05	2.77E-05	2.75E-05	2.57E-05	2.98E-05

Table 13 Effective concentrations (EC) of lipid droplet accumulation testing in H4IIE cells

The median was calculated from at least three independent replicates. EC min and EC max show the lowest and highest measurements respectively

Compound	Abbreviation	EC_{10} median [M]	EC_{10} min [M]	EC_{10} max [M]	EC_{20} median [M]	EC_{20} min [M]	EC_{20} max [M]	EC_{50} median [M]	EC_{50} min [M]	EC_{50} max [M]
Aflatoxin B1	AFB1									
Acetaminophen	APAP									
Arsenic	AS	2.91E-07	4.33E-08	3.17E-07						
Butylated hydroxy toluene	BHT	3.69E-06	2.11E-06	1.44E-05	8.61E-06	5.19E-06	2.25E-05	4.16E-05	3.01E-05	4.33E-05
Bisphenol - A	BPA									
Cannabidiol	CBD									
Carbamazepine	CBZ									
Coumarin	COU									
Chrysin	CRY									
Copper	CU	6.47E-05	9.66E-06	7.41E-05	1.29E-04	1.05E-05	1.48E-04			
Dibromoacetic acid	DBA	2.69E-05	6.21E-06	1.76E-05	2.69E-05	1.24E-05	3.54E-05	6.82E-05	3.13E-05	9.01E-05
Di(2-Ethylhexyl) Phthalate	DEHP									
Di-isononylphthalate	DINP	5.85E-05	2.38E-05	8.65E-05	1.08E-04	2.64E-05	1.73E-04	3.30E-04	3.66E-05	5.74E-04
1,4-dioxane	DIX									
Emodin	EMO									
Ethanol	ETOH	2.84E-02	1.73E-02	7.19E-02						
8-2 fluorotelomer alcohol	FTOH	3.43E-05	2.08E-05	4.30E-05	8.32E-05	4.17E-05	1.27E-04			
Gallic acid	GA									
2,3,3,3-tetrafluoro-2-(heptafluoropropoxy)propanoate	GENX									

Table 13 (continued) Effective concentrations (EC) of lipid droplet accumulation testing in H4IIE cells

The median was calculated from at least three independent replicates. EC min and EC max show the lowest and highest measurements respectively

Compound	Abbreviation	EC_{10} median [M]	EC_{10} min [M]	EC_{10} max [M]	EC_{20} median [M]	EC_{20} min [M]	EC_{20} max [M]	EC_{50} median [M]	EC_{50} min [M]	EC_{50} max [M]
Gemifloxacin mesylate	GFM									
Genistein	GST									
Imidacloprid	IMI									
Isoeugenol	IEG									
Lindane	LIN									
Methyleugenol	MEG									
Methanol	MET									
Morin	MOR	3.48E-06	7.71E-07	6.49E-06	4.61E-06	4.31E-06	6.98E-06			
Oxyresveratol	ORES	1.01E-06	1.93E-07	1.27E-06	2.40E-06	4.45E-07	2.74E-06			
2,3',4,4',5-pentachlorobiphenyl	PCB118	3.80E-05	3.40E-05	5.69E-05	7.17E-05	6.38E-05	7.65E-05	1.88E-04	1.70E-04	1.91E-04
3,3',4,4',5-pentachlorobiphenyl	PCB126									
Perfluorobutanoic acid	PFBA	2.86E-04	1.01E-04	7.18E-04	5.72E-04	2.09E-04	1.44E-03			
Perfluorobutane sulfonic acid	PFBS	1.69E-04	1.16E-04	5.78E-04	3.59E-04	2.39E-04	1.16E-03			
Perfluorohexanoic acid	PFHXA	2.00E-04	1.32E-04	2.17E-04	4.00E-04	2.65E-04	4.34E-04			
Perfluorooctanoic acid	PFOA	2.81E-05	2.40E-05	3.06E-05	5.63E-05	4.80E-05	6.11E-05	1.41E-04	1.20E-04	1.53E-04
Perfluorooctanesulfonate	PFOS									
Pyridine	PYR									
3,3',4,4'-tetrachloroazobenzene	TCAB	3.38E-07	1.37E-07	5.66E-07	8.60E-07	3.12E-07	1.15E-06			
Thiabendazole	THIA									
Triticonazole	TRI	6.32E-06	1.35E-06	1.25E-05	6.24E-06	3.06E-06	2.60E-05	1.79E-05	1.00E-05	7.43E-05
Triclosan	TSN									

Table 14 Effective concentrations (EC) of nuclear enumeration by Hoechst staining in H4IIE cells

The median was calculated from at least three independent replicates. EC min and EC max show the lowest and highest measurements respectively

Compound	Abbreviation	EC_{10} median [M]	EC_{10} min [M]	EC_{10} max [M]	EC_{20} median [M]	EC_{20} min [M]	EC_{20} max [M]	EC_{50} median [M]	EC_{50} min [M]	EC_{50} max [M]
Aflatoxin B1	AFB1	2.90E-08	1.20E-08	5.10E-08	7.00E-08	4.30E-08	1.14E-07			
Acetaminophen	APAP	1.90E-04	1.21E-04	4.31E-04	2.84E-04	1.99E-04	6.61E-04	9.63E-04	3.72E-04	1.78E-03
Arsenic	AS	1.94E-06	7.39E-07	3.42E-06	3.96E-06	1.07E-06	4.86E-06	5.31E-06	2.63E-06	1.29E-05
Butylated hydroxy toluene	BHT	2.09E-04	9.68E-05	3.41E-04	3.42E-04	1.97E-04	4.09E-04	6.03E-04	5.08E-04	7.45E-04
Bisphenol - A	BPA	3.30E-05	2.07E-05	3.76E-05	4.14E-05	4.13E-05	5.03E-05	1.04E-04	4.93E-05	1.24E-04
Cannabidiol	CBD	3.10E-06	2.87E-06	8.79E-06	6.10E-06	3.53E-06	1.15E-05	1.98E-05	4.41E-06	2.61E-05
Carbamazepine	CBZ	2.63E-04	1.67E-04	4.20E-04	3.58E-04	2.65E-04	4.63E-04			
Coumarin	COU									
Chrysin	CRY	1.46E-05	5.90E-06	2.71E-05	1.98E-05	1.10E-05	3.60E-05	3.35E-05	3.22E-05	6.04E-05
Copper	CU	1.27E-05	8.35E-06	3.11E-05	1.57E-05	1.08E-05	3.14E-05			
Dibromoacetic acid	DBA	1.92E-05	8.78E-06	2.73E-05	2.81E-05	2.66E-05	3.55E-05	9.90E-05	5.47E-05	1.67E-04
Di(2-Ethylhexyl) Phthalate	DEHP									
Di-isononylphthalate	DINP									
1,4-dioxane	DIX	6.85E-02	4.96E-02	1.28E-01	8.58E-02	8.24E-02	1.76E-01			
Emodin	EMO	1.97E-05	1.26E-05	2.60E-05	2.64E-05	2.05E-05	2.80E-05	4.07E-05	3.18E-05	5.19E-05
Ethanol	ETOH	7.40E-02	3.47E-02	1.62E-01	1.10E-01	6.88E-02	1.88E-01	2.27E-01	1.99E-01	2.92E-01
8-2 fluorotelomer alcohol	FTOH	1.33E-04	1.04E-04	1.72E-04	1.64E-04	1.14E-04	2.11E-04	2.27E-04	1.35E-04	3.46E-04
Gallic acid	GA	1.84E-05	1.02E-05	2.63E-05	1.98E-05	1.03E-05	2.83E-05	2.29E-05	1.07E-05	3.22E-05
2,3,3,3-tetrafluoro-2-(heptafluoropropoxy)propanoate	GENX	4.48E-04	2.02E-04	9.03E-04	6.46E-04	2.57E-04	1.03E-03	1.22E-03	6.10E-04	1.42E-03

Table 14 (continued) Effective concentrations (EC) of nuclear enumeration by Hoechst staining in H4IIE cells

The median was calculated from at least three independent replicates. EC min and EC max show the lowest and highest measurements respectively

Compound	Abbreviation	EC_{10} median [M]	EC_{10} min [M]	EC_{10} max [M]	EC_{20} median [M]	EC_{20} min [M]	EC_{20} max [M]	EC_{50} median [M]	EC_{50} min [M]	EC_{50} max [M]
Gemifloxacin mesylate	GFM	1.41E-05	1.18E-05	3.13E-05	3.59E-05	1.90E-05	5.05E-05			
Genistein	GST	2.06E-05	1.79E-05	3.03E-05	4.27E-05	2.84E-05	4.38E-05	9.04E-05	6.41E-05	1.41E-04
Imidacloprid	IMI	3.73E-05	2.76E-05	1.30E-04	7.38E-05	5.92E-05	2.09E-04	2.98E-04	2.12E-04	4.86E-04
Isoeugenol	IEG	1.55E-04	1.13E-04	2.50E-04						
Lindane	LIN	3.51E-05	2.40E-05	6.28E-05	4.93E-05	3.58E-05	9.36E-05	9.15E-05	6.95E-05	2.49E-04
Methyleugenol	MEG	1.07E-04	4.61E-05	1.87E-04	1.92E-04	1.02E-04	4.11E-04			
Methanol	MET	2.00E-01	4.88E-02	2.53E-01	3.32E-01	1.07E-01	3.66E-01			
Morin	MOR									
Oxyresveratol	ORES	9.83E-06	9.29E-06	3.64E-05	2.13E-05	9.43E-06	4.57E-05	6.80E-05	1.01E-05	7.23E-05
2,3',4,4',5-pentachlorobiphenyl	PCB118	7.61E-05	2.41E-05	1.40E-04	7.73E-05	5.11E-05	1.55E-04			
3,3',4,4',5-pentachlorobiphenyl	PCB126									
Perfluorobutanoic acid	PFBA	9.49E-04	5.29E-04	2.56E-03	1.16E-03	5.62E-04	2.90E-03			
Perfluorobutane sulfonic acid	PFBS	4.49E-04	4.49E-04	1.02E-03	9.19E-04	5.69E-04	1.43E-03	2.46E-03	8.67E-04	2.74E-03
Perfluorohexanoic acid	PFHXA	6.44E-04	1.58E-04	7.58E-04	8.36E-04	3.61E-04	8.53E-04			
Perfluorooctanoic acid	PFOA	9.29E-05	7.83E-05	1.91E-04	1.40E-04	1.14E-04	2.14E-04	2.58E-04	1.51E-04	3.04E-04
Perfluorooctanesulfonate	PFOS	2.27E-04	2.04E-04	3.17E-04	2.65E-04	2.37E-04	3.47E-04	3.86E-04	3.04E-04	4.04E-04
Pyridine	PYR	2.10E-02	7.12E-03	2.68E-02	2.58E-02	1.17E-02	4.48E-02			
3,3',4,4'-tetrachloroazobenzene	TCAB	9.99E-07	7.68E-07	1.24E-06						
Thiabendazole	THIA	9.99E-05	6.91E-05	2.33E-04	1.23E-04	7.94E-05	2.55E-04			
Triticonazole	TRI	1.66E-05	8.37E-06	2.06E-05	2.86E-05	2.03E-05	3.78E-05	8.21E-05	5.15E-05	1.35E-04
Triclosan	TSN	2.74E-05	1.15E-05	4.38E-05	3.29E-05	1.32E-05	5.33E-05	4.54E-05	1.68E-05	7.24E-05

Table 15 Effective concentrations (EC) of cytotoxicity test in Zajdela cells

The median was calculated from at least three independent replicates. EC min and EC max show the lowest and highest measurements respectively

Compound	Abbreviation	EC_{10} median [M]	EC_{10} min [M]	EC_{10} max [M]	EC_{20} median [M]	EC_{20} min [M]	EC_{20} max [M]	EC_{50} median [M]	EC_{50} min [M]	EC_{50} max [M]
Aflatoxin B1	AFB1	5.00E-09	3.00E-09	1.60E-08	4.40E-08	2.40E-08	1.48E-07			
Acetaminophen	APAP	1.08E-04	3.77E-05	1.39E-04	2.05E-04	9.54E-05	2.61E-04	5.97E-04	4.15E-04	8.52E-04
Arsenic	AS	7.51E-06	7.16E-06	8.17E-06	1.10E-05	8.87E-06	1.16E-05	2.12E-05	1.28E-05	2.12E-05
Butylated hydroxy toluene	BHT	3.96E-04	1.55E-04	4.49E-04	4.89E-04	2.47E-04	5.16E-04			
Bisphenol - A	BPA	7.22E-05	6.25E-05	1.17E-04	8.96E-05	7.84E-05	1.29E-04	1.29E-04	1.15E-04	1.53E-04
Cannabidiol	CBD	8.56E-06	6.81E-06	1.02E-05	1.02E-05	9.60E-06	1.28E-05	1.91E-05	1.17E-05	2.01E-05
Carbamazepine	CBZ	1.91E-04	1.48E-04	2.75E-04	2.31E-04	1.66E-04	3.82E-04	3.57E-04	2.12E-04	6.25E-04
Coumarin	COU	8.68E-04	6.83E-04	1.16E-03	1.23E-03	1.06E-03	1.47E-03	2.39E-03	1.66E-03	2.84E-03
Chrysin	CRY	4.13E-05	3.16E-05	8.58E-05	5.03E-05	4.66E-05	8.92E-05	9.94E-05	9.23E-05	1.00E-04
Copper	CU	1.99E-04	1.26E-04	2.06E-04	2.52E-04	2.35E-04	3.11E-04	3.54E-04	3.48E-04	1.10E-03
Dibromoacetic acid	DBA	4.55E-04	3.08E-04	7.07E-04	5.87E-04	3.85E-04	8.66E-04	9.06E-04	6.54E-04	1.23E-03
Di(2-Ethylhexyl) Phthalate	DEHP	1.98E-04	5.88E-05	2.18E-04	2.81E-04	2.54E-04	3.13E-04			
Di-isononylphthalate	DINP	4.61E-05	3.29E-05	6.21E-05						
1,4-dioxane	DIX	1.49E-02	6.05E-03	3.24E-02	2.87E-02	1.86E-02	3.74E-02	7.18E-02	5.72E-02	8.36E-02
Emodin	EMO	2.59E-05	1.47E-05	2.95E-05	3.07E-05	2.90E-05	4.49E-05			
Ethanol	ETOH	9.11E-02	6.70E-02	9.61E-02	1.29E-01	1.02E-01	1.35E-01	2.34E-01	2.06E-01	2.40E-01
8-2 fluorotelomer alcohol	FTOH	2.83E-04	9.74E-05	3.04E-04	3.15E-04	1.11E-04	3.48E-04	3.81E-04	1.38E-04	4.40E-04
Gallic acid	GA	2.66E-05	1.00E-05	3.46E-05	3.28E-05	1.89E-05	3.90E-05	5.32E-05	4.70E-05	5.50E-05
2,3,3,3-tetrafluoro-2-(heptafluoropropoxy)propanoate	GENX	2.40E-03	6.01E-04	2.43E-03	2.76E-03	1.01E-03	3.04E-03	3.44E-03	2.37E-03	5.09E-03

Table 15 (continued) Effective concentrations (EC) of cytotoxicity test in Zajdela cells

The median was calculated from at least three independent replicates. EC min and EC max show the lowest and highest measurements respectively

Compound	Abbreviation	EC_{10} median [M]	EC_{10} min [M]	EC_{10} max [M]	EC_{20} median [M]	EC_{20} min [M]	EC_{20} max [M]	EC_{50} median [M]	EC_{50} min [M]	EC_{50} max [M]
Gemifloxacin mesylate	GFM	6.92E-05	4.64E-05	9.29E-05	9.14E-05	5.55E-05	9.41E-05	9.80E-05	9.40E-05	1.53E-04
Genistein	GST	7.65E-05	7.31E-05	1.14E-04	1.47E-05	1.33E-05	1.50E-05	3.07E-05	2.82E-05	5.66E-05
Imidacloprid	IMI	8.51E-06	6.37E-06	1.20E-05	1.87E-03	1.40E-03	3.14E-03			
Isoeugenol	IEG	1.02E-03	5.79E-04	2.54E-03	9.82E-05	9.20E-05	1.45E-04	1.82E-04	1.71E-04	2.68E-04
Lindane	LIN	9.08E-05	2.24E-05	1.08E-04	1.46E-04	3.43E-05	1.85E-04	2.84E-04	7.39E-05	4.78E-04
Methyleugenol	MEG	8.97E-04	4.42E-04	1.40E-03	1.00E-03	8.42E-04	1.70E-03	2.01E-03	1.21E-03	2.34E-03
Methanol	MET	1.62E-01	9.07E-02	2.23E-01	2.60E-01	1.84E-01	4.06E-01	5.86E-01	5.79E-01	9.97E-01
Morin	MOR	6.69E-05	3.28E-05	1.64E-04	1.02E-04	7.47E-05	1.97E-04	2.71E-04	2.08E-04	3.52E-04
Oxyresveratol	ORES	1.40E-04	1.17E-04	2.18E-04	1.55E-04	1.37E-04	2.41E-04	1.98E-04	1.83E-04	2.78E-04
2,3',4,4',5-pentachlorobiphenyl	PCB118	1.30E-04	8.00E-05	1.43E-04	1.36E-04	8.20E-05	1.52E-04			
3,3',4,4',5-pentachlorobiphenyl	PCB126	1.26E-05	1.23E-05	1.73E-05	2.03E-05	1.52E-05	2.47E-05	3.90E-05	3.19E-05	3.98E-05
Perfluorobutanoic acid	PFBA	1.09E-04	1.04E-04	4.04E-04	4.32E-04	2.23E-04	1.93E-03			
Perfluorobutane sulfonic acid	PFBS	2.16E-03	1.02E-03	2.17E-03	2.46E-03	1.29E-03	2.87E-03	3.31E-03	2.43E-03	4.57E-03
Perfluorohexanoic acid	PFHXA	4.05E-04	1.15E-04	4.10E-04	7.95E-04	3.81E-04	8.02E-04	2.14E-03	1.87E-03	2.15E-03
Perfluorooctanoic acid	PFOA	1.12E-04	6.06E-05	2.81E-04	2.14E-04	1.23E-04	3.30E-04	4.60E-04	3.51E-04	5.35E-04
Perfluorooctanesulfonate	PFOS	2.25E-04	1.60E-04	6.79E-04	2.76E-04	2.02E-04	7.36E-04	4.16E-04	3.59E-04	8.58E-04
Pyridine	PYR	6.33E-03	5.76E-03	1.15E-02	1.60E-02	1.25E-02	2.14E-02	5.14E-02	4.19E-02	7.10E-02
3,3',4,4'-tetrachloroazobenzene	TCAB	1.22E-05	9.11E-06	1.44E-05	1.64E-05	1.52E-05	2.28E-05			
Thiabendazole	THIA	1.32E-04	8.83E-05	2.23E-04	1.82E-04	1.72E-04	3.28E-04	4.81E-04	2.74E-04	5.53E-04
Triticonazole	TRI	5.90E-05	4.21E-05	9.19E-05	1.21E-04	1.07E-04	1.56E-04	3.17E-04	3.14E-04	4.01E-04
Triclosan	TSN	3.82E-05	3.05E-05	6.54E-05	4.23E-05	3.14E-05	6.90E-05	5.57E-05	3.37E-05	7.56E-05

Table 16 Effective concentrations (EC) of lipid droplet accumulation test in Zajdela cells

The median was calculated from at least three independent replicates. EC min and EC max show the lowest and highest measurements respectively

Compound	Abbreviation	EC_{10} median [M]	EC_{10} min [M]	EC_{10} max [M]	EC_{20} median [M]	EC_{20} min [M]	EC_{20} max [M]	EC_{50} median [M]	EC_{50} min [M]	EC_{50} max [M]
Aflatoxin B1	AFB1									
Acetaminophen	APAP									
Arsenic	AS									
Butylated hydroxy toluene	BHT	1.69E-05	9.93E-06	5.91E-05						
Bisphenol - A	BPA	1.73E-05	1.04E-05	4.55E-05						
Cannabidiol	CBD									
Carbamazepine	CBZ	4.35E-05	2.02E-05	1.01E-04	9.43E-05	4.32E-05	2.02E-04			
Coumarin	COU	6.26E-05	4.20E-05	3.92E-04	8.41E-05	7.52E-05	7.83E-04			
Chrysin	CRY	2.09E-05	9.42E-06	4.45E-05	4.47E-05	1.94E-05	8.90E-05			
Copper	CU									
Dibromoacetic acid	DBA									
Di(2-Ethylhexyl) Phthalate	DEHP									
Di-isononylphthalate	DINP									
1,4-dioxane	DIX									
Emodin	EMO									
Ethanol	ETOH	1.01E-02	8.66E-03	1.06E-02						
8-2 fluorotelomer alcohol	FTOH									
Gallic acid	GA									
2,3,3,3-tetrafluoro-2-(heptafluoropropoxy)propanoate	GENX	7.23E-04	5.81E-04	2.68E-03	9.28E-04	8.57E-04	5.36E-03			

Table 16 (continued) Effective concentrations (EC) of lipid droplet accumulation test in Zajdela cells

The median was calculated from at least three independent replicates. EC min and EC max show the lowest and highest measurements respectively

Compound	Abbreviation	EC_{10} median [M]	EC_{10} min [M]	EC_{10} max [M]	EC_{20} median [M]	EC_{20} min [M]	EC_{20} max [M]	EC_{50} median [M]	EC_{50} min [M]	EC_{50} max [M]
Gemifloxacin mesylate	GFM									
Genistein	GST									
Imidacloprid	IMI	2.24E-04	1.31E-04	3.65E-04	4.49E-04	2.63E-04	7.29E-04	1.12E-03	6.56E-04	1.82E-03
Isoeugenol	IEG									
Lindane	LIN									
Methyleugenol	MEG	6.68E-06	6.43E-06	6.76E-06	1.56E-05	1.45E-05	1.73E-05	1.09E-04	4.61E-05	3.48E-04
Methanol	MET									
Morin	MOR									
Oxyresveratol	ORES									
2,3',4,4',5-pentachlorobiphenyl	PCB118									
3,3',4,4',5-pentachlorobiphenyl	PCB126									
Perfluorobutanoic acid	PFBA	3.64E-04	2.55E-04	8.61E-04	7.28E-04	5.11E-04	1.72E-03	1.46E-03	1.28E-03	2.17E-03
Perfluorobutane sulfonic acid	PFBS	1.36E-04	1.02E-04	1.82E-04	2.73E-04	2.03E-04	3.63E-04	6.82E-04	5.08E-04	9.08E-04
Perfluorohexanoic acid	PFHXA	9.73E-05	9.17E-05	2.37E-04	1.95E-04	1.83E-04	4.75E-04			
Perfluorooctanoic acid	PFOA	4.63E-05	3.43E-05	5.15E-05	8.19E-05	6.54E-05	8.94E-05	1.61E-04	1.45E-04	2.29E-04
Perfluorooctanesulfonate	PFOS	1.08E-04	4.14E-05	1.80E-04	1.69E-04	1.09E-04	2.17E-04	2.72E-04	7.46E-05	3.82E-04
Pyridine	PYR									
3,3',4,4'-tetrachloroazobenzene	TCAB									
Thiabendazole	THIA	1.31E-05	1.02E-05	7.69E-05	2.73E-05	2.10E-05	1.54E-04			
Triticonazole	TRI	3.52E-06	2.94E-06	4.78E-06	7.78E-06	7.38E-06	8.98E-06	2.82E-05	1.68E-05	3.25E-05
Triclosan	TSN	6.22E-06	5.57E-06	7.23E-06	1.41E-05	1.24E-05	1.93E-05			

Table 17 Effective concentrations (EC) of nuclear enumeration by Hoechst staining in Zajdela cells

The median was calculated from at least three independent replicates. EC min and EC max show the lowest and highest measurements respectively

Compound	Abbreviation	EC_{10} median [M]	EC_{10} min [M]	EC_{10} max [M]	EC_{20} median [M]	EC_{20} min [M]	EC_{20} max [M]	EC_{50} median [M]	EC_{50} min [M]	EC_{50} max [M]
Aflatoxin B1	AFB1	6.31E-07	3.48E-07	7.40E-07	1.32E-06	1.28E-06	1.70E-06			
Acetaminophen	APAP	7.16E-05	5.14E-05	7.57E-05	1.12E-04	9.36E-05	1.52E-04	5.56E-04	1.40E-04	5.77E-04
Arsenic	AS	2.43E-06	7.33E-07	2.82E-06	3.33E-06	1.06E-06	4.04E-06	3.97E-06	2.23E-06	8.31E-06
Butylated hydroxy toluene	BHT	3.00E-04	1.76E-04	3.53E-04	4.25E-04	3.09E-04	7.27E-04			
Bisphenol - A	BPA	8.90E-05	5.16E-05	1.26E-04	1.03E-04	7.28E-05	1.53E-04	1.33E-04	1.09E-04	2.49E-04
Cannabidiol	CBD									
Carbamazepine	CBZ	1.52E-04	1.36E-04	3.08E-04	1.98E-04	1.76E-04	3.51E-04	3.77E-04	2.69E-04	4.79E-04
Coumarin	COU									
Chrysin	CRY	1.45E-05	1.02E-05	3.55E-05	2.77E-05	2.30E-05	5.82E-05	9.96E-05	5.52E-05	1.39E-04
Copper	CU	2.19E-05	8.52E-06	3.86E-05	5.18E-05	9.39E-06	9.57E-05			
Dibromoacetic acid	DBA									
Di(2-Ethylhexyl) Phthalate	DEHP									
Di-isononylphthalate	DINP									
1,4-dioxane	DIX	3.11E-03	2.51E-03	8.04E-03	1.12E-02	6.36E-03	2.35E-02	8.28E-02	4.63E-02	1.19E-01
Emodin	EMO	4.00E-05	1.18E-05	7.01E-05	5.37E-05	2.10E-05	7.86E-05			
Ethanol	ETOH	1.01E-01	7.45E-02	1.75E-01	2.11E-01	1.15E-01	2.39E-01			
8-2 fluorotelomer alcohol	FTOH	3.72E-05	3.36E-05	9.67E-05	7.63E-05	4.61E-05	1.57E-04	2.28E-04	6.69E-05	3.01E-04
Gallic acid	GA	3.25E-05	1.88E-05	5.73E-05	3.34E-05	2.69E-05	6.13E-05	4.89E-05	3.64E-05	6.90E-05
2,3,3,3-tetrafluoro-2-(heptafluoropropoxy)propanoate	GENX	9.22E-04	3.94E-04	1.33E-03	1.50E-03	5.16E-04	1.71E-03	2.37E-03	1.21E-03	4.33E-03

Table 17 (continued) Effective concentrations (EC) of nuclear enumeration by Hoechst staining in Zajdela cells

The median was calculated from at least three independent replicates. EC min and EC max show the lowest and highest measurements respectively

Compound	Abbreviation	EC_{10} median [M]	EC_{10} min [M]	EC_{10} max [M]	EC_{20} median [M]	EC_{20} min [M]	EC_{20} max [M]	EC_{50} median [M]	EC_{50} min [M]	EC_{50} max [M]
Gemifloxacin mesylate	GFM									
Genistein	GST	6.60E-06	6.11E-06	9.72E-06	8.87E-06	8.43E-06	1.39E-05	1.91E-05	1.78E-05	2.77E-05
Imidacloprid	IMI									
Isoeugenol	IEG	3.45E-05	1.91E-05	4.68E-05	6.99E-05	2.97E-05	8.67E-05			
Lindane	LIN	6.33E-05	2.12E-05	1.04E-04	7.53E-05	2.85E-05	1.33E-04	1.31E-04	5.24E-05	2.78E-04
Methyleugenol	MEG	3.01E-04	1.58E-04	4.22E-04	4.56E-04	3.93E-04	5.59E-04			
Methanol	MET									
Morin	MOR									
Oxyresveratol	ORES	1.04E-04	7.31E-05	1.31E-04	1.20E-04	1.11E-04	1.57E-04	1.98E-04	1.53E-04	2.12E-04
2,3',4,4',5-pentachlorobiphenyl	PCB118	6.04E-06	3.82E-06	9.64E-06	1.46E-05	9.25E-06	2.72E-05			
3,3',4,4',5-pentachlorobiphenyl	PCB126	3.69E-05	1.15E-05	4.75E-05	4.05E-05	2.10E-05	4.78E-05	4.77E-05	4.64E-05	4.87E-05
Perfluorobutanoic acid	PFBA									
Perfluorobutane sulfonic acid	PFBS	2.82E-04	8.35E-05	3.61E-04	3.89E-04	9.20E-05	8.38E-04			
Perfluorohexanoic acid	PFHXA	1.35E-05	1.16E-05	3.17E-05	2.60E-05	1.59E-05	4.80E-05			
Perfluorooctanoic acid	PFOA									
Perfluorooctanesulfonate	PFOS	3.18E-04	3.12E-04	3.26E-04	3.64E-04	3.57E-04	3.76E-04	4.37E-04	4.34E-04	4.53E-04
Pyridine	PYR	2.80E-02	2.09E-02	8.42E-02	3.13E-02	2.95E-02	9.46E-02			
3,3',4,4'-tetrachloroazobenzene	TCAB	1.25E-05	2.25E-06	1.38E-05	1.63E-05	6.56E-06	1.98E-05			
Thiabendazole	THIA									
Triticonazole	TRI	1.35E-04	5.32E-05	2.21E-04	1.82E-04	1.03E-04	2.75E-04	3.62E-04	2.54E-04	3.93E-04
Triclosan	TSN	5.29E-05	2.01E-05	6.26E-05	6.12E-05	2.46E-05	6.62E-05	7.30E-05	3.50E-05	7.68E-05

Table 18 Effective concentrations (EC) of cytotoxicity of primary rat hepatocytes

The median was calculated from at least three independent replicates. EC min and EC max show the lowest and highest measurements respectively

Compound	Abbreviation	EC_{10} median [M]	EC_{10} min [M]	EC_{10} max [M]	EC_{20} median [M]	EC_{20} min [M]	EC_{20} max [M]	EC_{50} median [M]	EC_{50} min [M]	EC_{50} max [M]
Aflatoxin B1	AFB1	2.11E-07	6.00E-08	2.90E-07	3.63E-07	7.60E-08	4.43E-07	8.00E-07	1.18E-07	9.01E-07
Acetaminophen	APAP	9.95E-04	3.83E-04	2.75E-03	1.47E-03	9.84E-04	2.90E-03			
Arsenic	AS	9.51E-06	6.91E-06	3.20E-05	9.62E-06	7.37E-06	3.25E-05	9.90E-06	8.20E-06	3.42E-05
Butylated hydroxy toluene	BHT									
Bisphenol - A	BPA	5.24E-05	1.70E-05	8.64E-05	5.57E-05	2.18E-05	8.73E-05	6.28E-05	3.33E-05	9.00E-05
Cannabidiol	CBD	7.85E-05	3.44E-05	9.21E-05	8.55E-05	4.21E-05	9.29E-05	9.56E-05	5.95E-05	9.90E-05
Carbamazepine	CBZ									
Coumarin	COU	2.38E-04	9.02E-05	3.99E-04	2.89E-04	1.93E-04	4.50E-04	6.38E-04	3.99E-04	8.74E-04
Chrysin	CRY	1.07E-04	1.04E-04	1.82E-04	1.14E-04	1.05E-04	2.04E-04	1.43E-04	1.12E-04	2.72E-04
Copper	CU	1.21E-05	9.19E-06	1.79E-05	1.37E-05	9.40E-06	2.35E-05	1.90E-05	1.00E-05	3.70E-05
Dibromoacetic acid	DBA	8.24E-04	5.30E-04	9.40E-04	1.09E-03	6.30E-04	1.62E-03	1.74E-03	9.79E-04	3.75E-03
Di(2-Ethylhexyl) Phthalate	DEHP									
Di-isononylphthalate	DINP									
1,4-dioxane	DIX	4.92E-02	2.36E-02	1.25E-01	6.94E-02	2.80E-02	8.22E-02			
Emodin	EMO	1.62E-05	8.65E-06	2.76E-05	2.14E-05	1.02E-05	3.41E-05	3.60E-05	1.35E-05	5.45E-05
Ethanol	ETOH	2.09E-01	1.15E-01	2.49E-01	2.40E-01	1.38E-01	2.70E-01	3.37E-01	2.23E-01	4.29E-01
8-2 fluorotelomer alcohol	FTOH	3.71E-04	2.20E-04	6.05E-04	5.24E-04	2.53E-04	6.74E-04	8.35E-04	3.21E-04	8.46E-04
Gallic acid	GA	2.29E-04	1.51E-04	2.39E-04	2.85E-04	1.82E-04	3.62E-04			
2,3,3,3-tetrafluoro-2-(heptafluoropropoxy)propanoate	GENX	3.81E-04	3.39E-04	5.17E-04	5.73E-04	5.12E-04	7.36E-04	1.14E-03	1.03E-03	1.33E-03

Table 18 (continued) Effective concentrations (EC) of cytotoxicity of primary rat hepatocytes

The median was calculated from at least three independent replicates. EC min and EC max show the lowest and highest measurements respectively

Compound	Abbreviation	EC_{10} median [M]	EC_{10} min [M]	EC_{10} max [M]	EC_{20} median [M]	EC_{20} min [M]	EC_{20} max [M]	EC_{50} median [M]	EC_{50} min [M]	EC_{50} max [M]
Gemifloxacin mesylate	GFM	1.06E-04	6.49E-05	2.92E-04						
Genistein	GST	6.00E-05	1.62E-05	6.84E-05	7.53E-05	3.85E-05	7.93E-05	1.25E-04	8.88E-05	1.27E-04
Imidacloprid	IMI							1.18E-04	8.94E-05	1.73E-04
Isoeugenol	IEG	8.39E-05	6.67E-05	8.97E-05	9.51E-05	7.43E-05	1.09E-04			
Lindane	LIN									
Methyleugenol	MEG									
Methanol	MET	8.13E-02	2.75E-02	1.06E-01	2.10E-01	5.67E-02	2.46E-01	8.03E-01	1.96E-01	8.27E-01
Morin	MOR	7.85E-05	2.57E-05	9.33E-05	9.05E-05	3.45E-05	9.47E-05			
Oxyresveratol	ORES	2.72E-05	2.63E-05	3.41E-05	2.77E-05	2.69E-05	3.62E-05	2.95E-05	2.89E-05	4.44E-05
2,3',4,4',5-pentachlorobiphenyl	PCB118	3.89E-05	7.15E-06	7.41E-05	5.10E-05	1.37E-05	7.59E-05	8.10E-05	4.07E-05	1.03E-04
3,3',4,4',5-pentachlorobiphenyl	PCB126									
Perfluorobutanoic acid	PFBA	2.41E-03	1.02E-03	3.09E-03	2.83E-03	1.44E-03	4.32E-03			
Perfluorobutane sulfonic acid	PFBS	1.93E-03	8.17E-04	3.68E-03	2.66E-03	1.23E-03	4.02E-03	4.54E-03	2.43E-03	4.92E-03
Perfluorohexanoic acid	PFHXA	3.46E-04	1.54E-04	4.93E-04						
Perfluorooctanoic acid	PFOA	6.74E-05	5.93E-05	9.46E-05	1.12E-04	9.22E-05	1.37E-04	1.85E-04	1.57E-04	4.24E-04
Perfluorooctanesulfonate	PFOS	5.44E-05	4.26E-05	6.20E-05	5.99E-05	4.88E-05	7.52E-05	8.02E-05	6.98E-05	1.37E-04
Pyridine	PYR	1.27E-02	9.86E-03	2.10E-02	2.12E-02	2.01E-02	3.05E-02	5.65E-02	5.08E-02	5.98E-02
3,3',4,4'-tetrachloroazobenzene	TCAB									
Thiabendazole	THIA									
Triticonazole	TRI									
Triclosan	TSN	8.11E-05	3.32E-05	1.58E-04	9.65E-05	3.41E-05	1.77E-04	1.40E-04	3.68E-05	2.29E-04

Table 19 Effective concentrations (EC) of lipid droplet accumulation of primary rat hepatocytes

The median was calculated from at least three independent replicates. EC min and EC max show the lowest and highest measurements respectively

Compound	Abbreviation	EC_{10} median [M]	EC_{10} min [M]	EC_{10} max [M]	EC_{20} median [M]	EC_{20} min [M]	EC_{20} max [M]	EC_{50} median [M]	EC_{50} min [M]	EC_{50} max [M]
Aflatoxin B1	AFB1									
Acetaminophen	APAP									
Arsenic	AS									
Butylated hydroxy toluene	BHT									
Bisphenol - A	BPA									
Cannabidiol	CBD									
Carbamazepine	CBZ									
Coumarin	COU									
Chrysin	CRY									
Copper	CU									
Dibromoacetic acid	DBA	5.42E-05	7.40E-06	7.23E-05	7.66E-05	1.70E-05	1.53E-04			
Di(2-Ethylhexyl) Phthalate	DEHP	2.76E-04	7.49E-05	3.01E-04						
Di-isononylphthalate	DINP									
1,4-dioxane	DIX									
Emodin	EMO									
Ethanol	ETOH	4.85E-02	3.93E-02	2.16E-01						
8-2 fluorotelomer alcohol	FTOH									
Gallic acid	GA									
2,3,3,3-tetrafluoro-2-(heptafluoropropoxy)propanoate	GENX	2.13E-04	1.70E-04	4.84E-04	4.28E-04	4.01E-04	9.68E-04			

Table 19 (continued) Effective concentrations (EC) of lipid droplet accumulation of primary rat hepatocytes

The median was calculated from at least three independent replicates. EC min and EC max show the lowest and highest measurements respectively

Compound	Abbreviation	EC_{10} median [M]	EC_{10} min [M]	EC_{10} max [M]	EC_{20} median [M]	EC_{20} min [M]	EC_{20} max [M]	EC_{50} median [M]	EC_{50} min [M]	EC_{50} max [M]
Gemifloxacin mesylate	GFM									
Genistein	GST									
Imidacloprid	IMI									
Isoeugenol	IEG									
Lindane	LIN	2.55E-05	1.07E-05	2.88E-05	5.67E-05	2.56E-05	6.58E-05			
Methyleugenol	MEG									
Methanol	MET									
Morin	MOR									
Oxyresveratol	ORES									
2,3',4,4',5-pentachlorobiphenyl	PCB118	2.16E-05	1.81E-05	7.71E-05						
3,3',4,4',5-pentachlorobiphenyl	PCB126									
Perfluorobutanoic acid	PFBA	2.19E-03	8.87E-04	2.31E-03	2.56E-03	7.82E-04	4.38E-03			
Perfluorobutane sulfonic acid	PFBS	3.39E-04	2.27E-04	3.92E-04	6.79E-04	4.67E-04	7.84E-04	1.70E-03	1.31E-03	1.96E-03
Perfluorohexanoic acid	PFHXA	2.69E-04	1.81E-04	4.93E-04	4.95E-04	3.63E-04	6.56E-04			
Perfluorooctanoic acid	PFOA	2.34E-05	1.95E-05	4.49E-05	4.80E-05	3.99E-05	3.63E-04	1.23E-04	1.08E-04	1.42E-04
Perfluorooctanesulfonate	PFOS	1.27E-04	9.00E-05	1.66E-04	1.65E-04	1.40E-04	2.11E-04	2.58E-04	2.08E-04	3.29E-04
Pyridine	PYR									
3,3',4,4'-tetrachloroazobenzene	TCAB	1.14E-05	2.86E-06	1.17E-05	1.25E-05	5.93E-06	1.31E-05			
Thiabendazole	THIA	1.68E-04	5.81E-05	2.39E-04	4.78E-04	2.83E-04	5.02E-04			
Triticonazole	TRI	2.16E-04	1.75E-04	4.17E-04						
Triclosan	TSN									

Table 20 Effective concentrations (EC) of nuclear enumeration by Hoechst staining of primary rat hepatocytes

The median was calculated from at least three independent replicates. EC min and EC max show the lowest and highest measurements respectively

Compound	Abbreviation	EC_{10} median [M]	EC_{10} min [M]	EC_{10} max [M]	EC_{20} median [M]	EC_{20} min [M]	EC_{20} max [M]	EC_{50} median [M]	EC_{50} min [M]	EC_{50} max [M]
Aflatoxin B1	AFB1	3.16E-07	3.00E-07	4.22E-07	4.98E-07	4.66E-07	5.53E-07			
Acetaminophen	APAP									
Arsenic	AS	4.08E-06	1.29E-06	4.70E-06	5.32E-06	3.00E-06	6.38E-06	9.35E-06	9.30E-06	9.68E-06
Butylated hydroxy toluene	BHT	3.29E-04	3.14E-04	6.31E-04	4.26E-04	3.79E-04	7.19E-04			
Bisphenol - A	BPA	1.65E-04	8.28E-05	3.09E-04	1.76E-04	9.20E-05	3.60E-04			
Cannabidiol	CBD	1.61E-04	9.33E-05	2.75E-04	1.94E-04	9.77E-05	2.83E-04			
Carbamazepine	CBZ									
Coumarin	COU	3.06E-04	8.77E-05	3.86E-04	3.81E-04	1.44E-04	9.47E-04			
Chrysin	CRY	7.79E-05	1.77E-05	8.24E-05						
Copper	CU									
Dibromoacetic acid	DBA									
Di(2-Ethylhexyl) Phthalate	DEHP									
Di-isononylphthalate	DINP									
1,4-dioxane	DIX									
Emodin	EMO	5.22E-05	3.42E-05	6.88E-05	6.43E-05	3.64E-05	7.60E-05	8.95E-05	4.62E-05	9.23E-05
Ethanol	ETOH	6.45E-01	3.56E-01	7.93E-01	7.55E-01	3.91E-01	9.03E-01			
8-2 fluorotelomer alcohol	FTOH	6.81E-05	2.70E-05	8.90E-05	1.02E-04	8.99E-05	1.50E-04	2.98E-04	1.92E-04	8.04E-04
Gallic acid	GA									
2,3,3,3-tetrafluoro-2-(heptafluoropropoxy)propanoate	GENX	1.47E-03	1.07E-03	1.86E-03	1.72E-03	1.11E-03	2.00E-03	2.06E-03	1.35E-03	3.53E-03

Table 20 (continued) Effective concentrations (EC) of nuclear enumeration by Hoechst staining of primary rat hepatocytes

The median was calculated from at least three independent replicates. EC min and EC max show the lowest and highest measurements respectively

Compound	Abbreviation	EC_{10} median [M]	EC_{10} min [M]	EC_{10} max [M]	EC_{20} median [M]	EC_{20} min [M]	EC_{20} max [M]	EC_{50} median [M]	EC_{50} min [M]	EC_{50} max [M]
Gemifloxacin mesylate	GFM	2.36E-04	7.45E-05	2.75E-04						
Genistein	GST	1.04E-04	8.48E-05	2.21E-04						
Imidacloprid	IMI	8.83E-05	3.38E-05	1.20E-04	9.69E-05	4.55E-05	1.32E-04	1.49E-04	9.67E-05	1.93E-04
Isoeugenol	IEG									
Lindane	LIN									
Methyleugenol	MEG									
Methanol	MET	1.05E+00	6.03E-01	1.96E+00	1.33E+00	7.89E-01	2.18E+00			
Morin	MOR									
Oxyresveratol	ORES	1.13E-04	9.65E-05	2.00E-04	1.27E-04	9.94E-05	2.24E-04			
2,3',4,4',5-pentachlorobiphenyl	PCB118									
3,3',4,4',5-pentachlorobiphenyl	PCB126									
Perfluorobutanoic acid	PFBA									
Perfluorobutane sulfonic acid	PFBS	3.93E-03	1.56E-03	7.03E-03	5.16E-03	3.31E-03	7.64E-03	8.89E-03	8.52E-03	9.24E-03
Perfluorohexanoic acid	PFHXA									
Perfluorooctanoic acid	PFOA	4.70E-04	4.52E-04	8.99E-04	5.64E-04	5.53E-04	9.18E-04	9.16E-04	8.63E-04	9.67E-04
Perfluorooctanesulfonate	PFOS									
Pyridine	PYR	3.01E-02	1.37E-02	8.27E-02	3.60E-02	2.43E-02	8.63E-02			
3,3',4,4'-tetrachloroazobenzene	TCAB									
Thiabendazole	THIA									
Triticonazole	TRI									
Triclosan	TSN	5.28E-05	3.33E-05	5.53E-05	5.48E-05	3.39E-05	5.65E-05			

3.2.1.2 Systematic comparison of effective concentrations and assay variability across cell systems

In the previous section, all effective concentrations (EC_{10}, EC_{20}, EC_{50}) of the tested compounds were summarized for each assay and cell system. To further explore the sensitivity and reliability of the *in vitro* models, the following section is structured in two parts: First, assay-specific trends within each individual cell system are analyzed to identify which assays yield the lowest concentrations and thus the highest sensitivity (see Section 3.2.1.2.1). Second, the performance of the three cell systems is compared for each assay, to assess which cell model is most sensitive towards individual substances (see Section 3.2.1.2.2).

Since EC_{10} values were most frequently available and provide a more sensitive estimate of the cellular response than EC_{50} values, all comparisons are based on EC_{10} data. Scatter plots and ratio plots (**Figure 18** - **Figure 26**) were used to visualize differences in sensitivity across a wide concentration range, using decadic logarithms to improve comparability and clarity. All compounds are shown in the scatterplots. Compounds without a measurable effect are indicated by triangles and assigned a penalty value corresponding to 5 times the highest concentration tested. Compounds with a measurable effect are represented as circles. In the ratio plots, the $\log_{10}(x/y)$ is displayed only for compounds that showed a positive test result in both systems. For example, if a data point is located below the iso-concentration line in the scatterplot ($x > y$), it will appear in the ratio plot with a positive $\log_{10}$ value (> 0), and vice versa.

Color scheme of visualizations

To ensure clarity and consistency, the plots follow a defined color scheme. In chapter 3.2 *In vitro*, red indicates substances with confirmed hepatotoxicity. In chapter 3.4 *In vitro–in vivo* analysis, colors represent the respective assay types (e.g., CTB, NR, Hoechst), allowing for a differentiated comparison of the test systems.

3.2.1.2.1 Intra-system comparison: Sensitivity of assays within each cell system

To evaluate assay-specific performance within each individual cell system, EC_{10} values of the three assays—cytotoxicity (CTB), lipid droplet accumulation (Nile red) and nuclear enumeration (Hoechst)—were compared across all tested compounds. This intra-system analysis aims to identify which assay yields the lowest effective concentrations, thereby indicating the highest sensitivity. The comparison helps determine the most suitable assay for each cell model in terms of sensitivity to specific tested compounds.

H4IIE

Intra-system comparison of CTB and Nile red assay in H4IIE

The ratio plot (**Figure 9**) reveals a clear trend toward higher sensitivity of the Nile Red assay compared to the cytotoxicity assay in the H4IIE cell line. Although the overall number of positive test results is lower in the Nile Red assay, several compounds show markedly lower EC_{10} values in this assay. Notably, six substances—BHT, ORES, AS, TCAB, DBA, and MOR—exhibit EC_{10} values in the Nile red assay that are over 30-fold lower than in the CTB assay.

Intra-system comparison of CTB and Hoechst assay in H4IIE

When comparing the cytotoxicity and Hoechst assays in the H4IIE cell line (**Figure 10**), the Hoechst assay consistently demonstrates higher sensitivity across several test compounds. While the number of positive test results is comparable (CTB: 40; Hoechst: 35), the effective concentrations tend to be lower in the Hoechst assay. This is particularly evident for DBA, which shows a more than 30-fold lower EC_{10} in the Hoechst assay. Additionally, TCAB and AS also exhibit EC_{10} values that are more than 10-fold lower in the Hoechst assay compared to CTB. However, for most compounds, the differences in EC_{10} values between the two assays remain within a 3-fold range, indicating a generally good agreement between the two readouts. Notably, some substances—including the plasticizers DEHP and DINP, as well as morin, coumarin, and PCB126—could not be evaluated in the Hoechst assay.

Intra-system comparison of Nile red and Hoechst assay in H4IIE

Comparing the readouts in H4IIE cells—Nile red and Hoechst (**Figure 11**)—reveals that Nile red is again the more sensitive assay. Two compounds stand out in particular: BHT, which shows more than a 30-fold lower EC_{10} value in the Nile red assay, and ORES, with a roughly 10-fold lower effective concentration.

In contrast, the Hoechst assay yielded lower EC_{10} values for some individual compounds, most notably PFOS, which exhibited a more than 10-fold lower EC_{10} value compared to Nile Red.

In summary, among the three assays evaluated in H4IIE cells, the Nile red assay demonstrated the highest sensitivity, yielding the lowest EC_{10} values for selected compounds, albeit with the fewest overall positive results. The Hoechst assay ranked second in sensitivity, while the CTB assay was the least sensitive but provided the most comprehensive coverage, detecting a response for all tested compounds. Notably, DEHP and PCB126 elicited effects exclusively in the CTB assay.

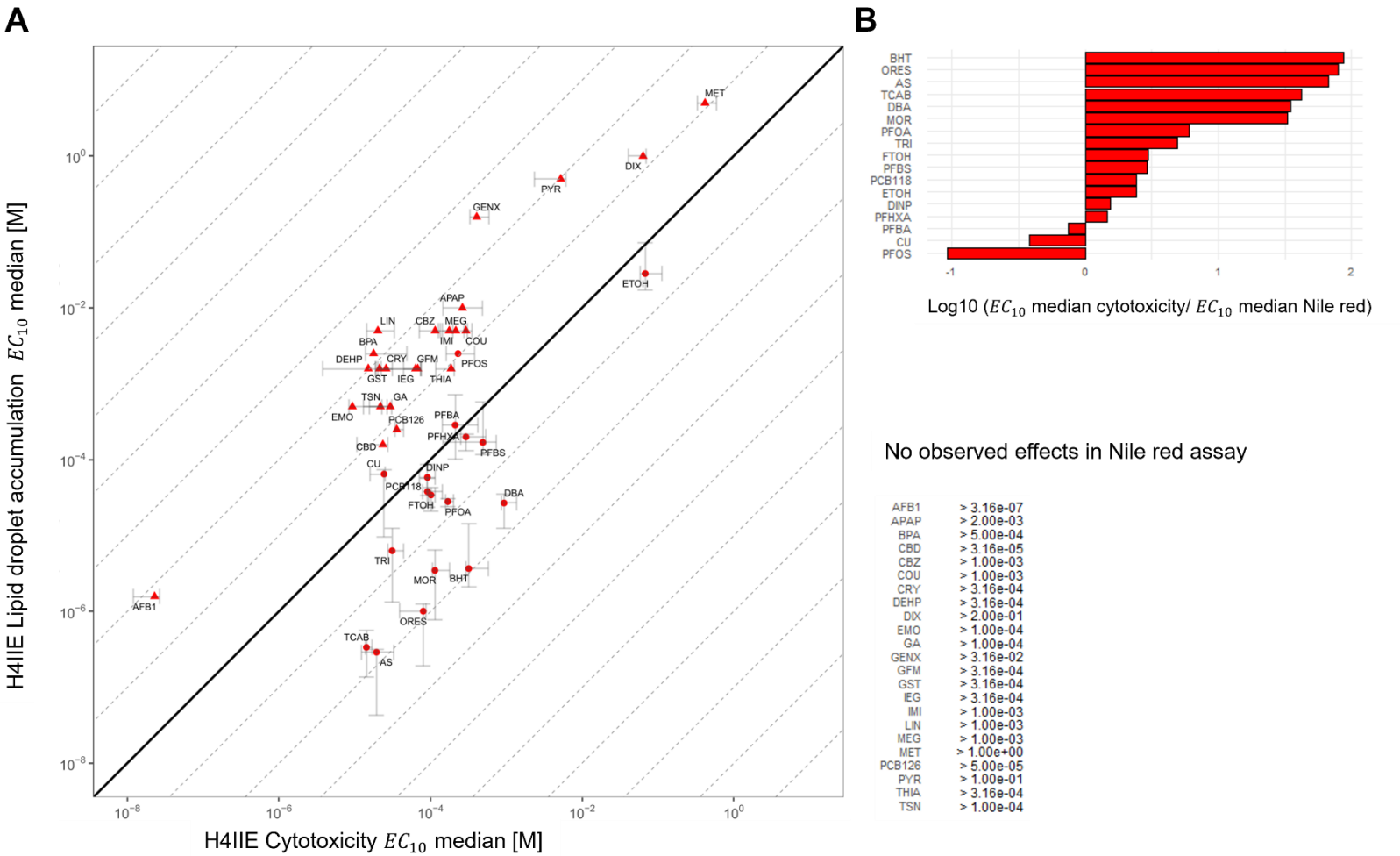

Figure 9 Comparison of the performance of cytotoxicity test and lipid droplet accumulation in H4IIE cells

A Scatterplot of the median EC_{10} values (n = at least 3 independent experiments) for two assays with logarithmic scales on both axes. Error bars represent the minimum and maximum EC_{10} values. The black solid line represents the line of identity. Gray dashed lines mark constant factor differences (in decadic log scale) of the EC_{10} values between the assays. Each line corresponds to a 10^n-fold deviation from the line of identity (n = ±1, ±2, etc.). Compounds with no observed effect in one or both systems were assigned a penalty (5× highest tested concentration) and shown as triangles; those with effects in both systems appear as circles. Unilateral detection is indicated by directional error bars. **B** Ratio plot displaying the ratio of effective concentrations of two assays on a decadic logarithmic scale. Only positive test results without penalties were compared. For substance with no observed effects, the highest tested concentration in M is listed below the ratio plot for each assay. All data points and bars are colored in red, denoting hepatotoxicity.

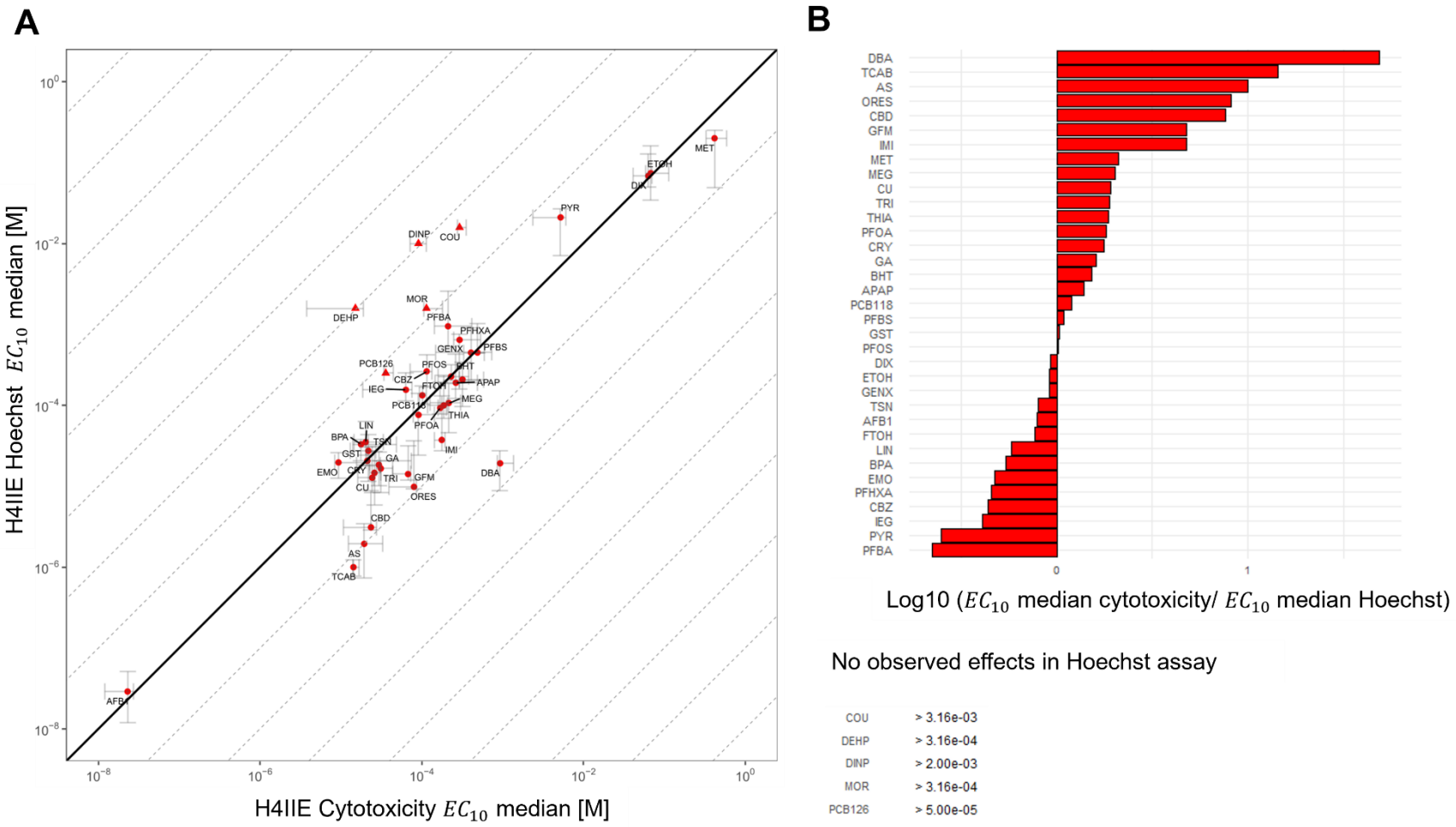

Figure 10 Comparison of the performance of cytotoxicity test and nuclear enumeration via Hoechst staining in H4IIE cells

A Scatterplot of the median EC_{10} values (n = at least 3 independent experiments) for two assays with logarithmic scales on both axes. Error bars represent the minimum and maximum EC_{10} values. The black solid line represents the line of identity. Gray dashed lines mark constant factor differences (in decadic log scale) of the EC_{10} values between the assays. Each line corresponds to a 10^n-fold deviation from the line of identity (n = ±1, ±2, etc.). Compounds with no observed effect in one or both systems were assigned a penalty (5× highest tested concentration) and shown as triangles; those with effects in both systems appear as circles. Unilateral detection is indicated by directional error bars. **B** Ratio plot displaying the ratio of effective concentrations of two assays on a decadic logarithmic scale. Only positive test results without penalties were compared. For substance with no observed effects, the highest tested concentration in M is listed below the ratio plot for each assay. All data points and bars are colored in red, denoting hepatotoxicity.

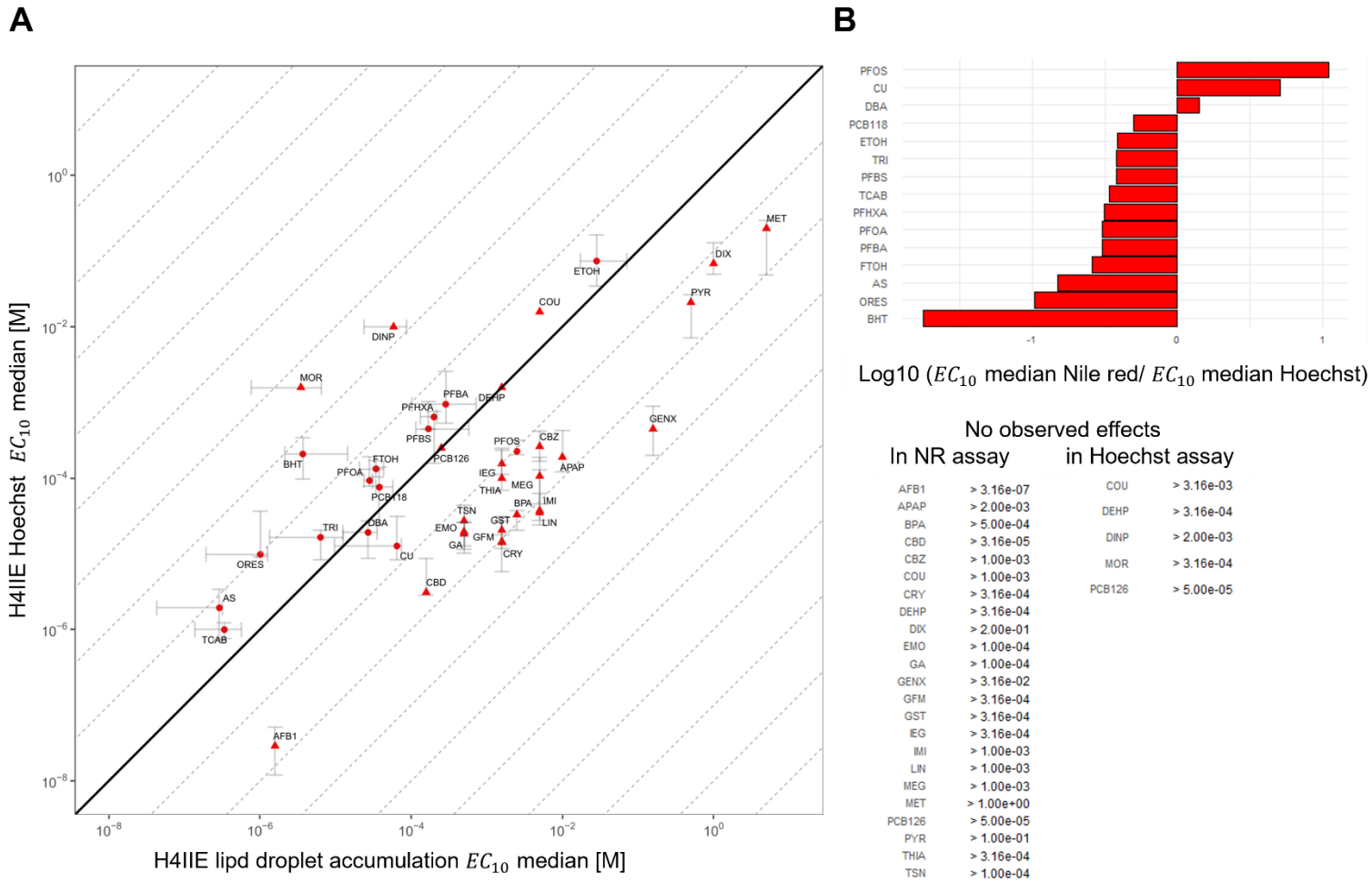

Figure 11 Comparison of the performance of lipid droplet accumulation and nuclear enumeration via Hoechst staining in H4IIE cells

A Scatterplot of the median EC_{10} values (n = at least 3 independent experiments) for two assays with logarithmic scales on both axes. Error bars represent the minimum and maximum EC_{10} values. The black solid line represents the line of identity. Gray dashed lines mark constant factor differences (in decadic log scale) of the EC_{10} values between the assays. Each line corresponds to a 10^n-fold deviation from the line of identity (n = ±1, ±2, etc.). Compounds with no observed effect in one or both systems were assigned a penalty (5× highest tested concentration) and shown as triangles; those with effects in both systems appear as circles. Unilateral detection is indicated by directional error bars**. B** Ratio plot displaying the ratio of effective concentrations of two assays on a decadic logarithmic scale. Only positive test results without penalties were compared. For substance with no observed effects, the highest tested concentration in M is listed below the ratio plot for each assay. All data points and bars are colored in red, denoting hepatotoxicity.

Zajdela

Intra-system comparison of CTB and Nile red assays in Zajdela cells

In the Zajdela hepatoma cell line, comparison of the cytotoxicity and Nile Red assays (**Figure 12**) demonstrates a pronounced shift in assay sensitivity. Among the 17 compounds tested, 16 displayed substantially lower EC_{10} values in the Nile Red assay. Only PFBA showed greater sensitivity in the CTB assay. Notably, several compounds—such as MEG, BHT, TRI, PFBS, COU, and THIA—exhibited EC_{10} values more than tenfold lower in the Nile Red assay.

Intra-system comparison of CTB and Hoechst assays in Zajdela cells

In Zajdela cells, the comparison between the cytotoxicity and Hoechst assays (**Figure 13**) shows that, the Hoechst assay is generally more sensitive. Most compounds differ by less than a factor of 3 between the two assays. However, notable exceptions include PFHxA and PCB118, which show more than tenfold lower EC_{10} values in the Hoechst assay. In contrast, AFB1 is detected with markedly higher sensitivity—over a hundredfold—in the cytotoxicity assay.

Intra-system comparison of Nile red and Hoechst assays in Zajdela cells

A comparison between Nile red and Hoechst assay in Zajdela cells in **Figure 14** shows a clear trend toward higher sensitivity in the Nile red readout. Among the twelve compounds assessed, BHT, TRI, ETOH and MEG show more than tenfold lower EC_{10} values in the Nile red assay. In contrast, PFHxA is notably more sensitively detected in the Hoechst assay—approximately fivefold lower. The remaining substances differ by less than a factor of ten between assays.

Across the evaluated assays in Zajdela cells, a consistent sensitivity ranking can be observed, closely mirroring the pattern seen in H4IIE cells. The Nile Red assay is the most sensitive, though it yields the fewest positive readouts. It is followed by the Hoechst assay, while the cytotoxicity assay is the least sensitive but detects the largest number of positive results. Notably, several compounds are exclusively detected by the cytotoxicity assay, including CBD, DBA, DEHP, DINP, GFM, MET, and MOR.

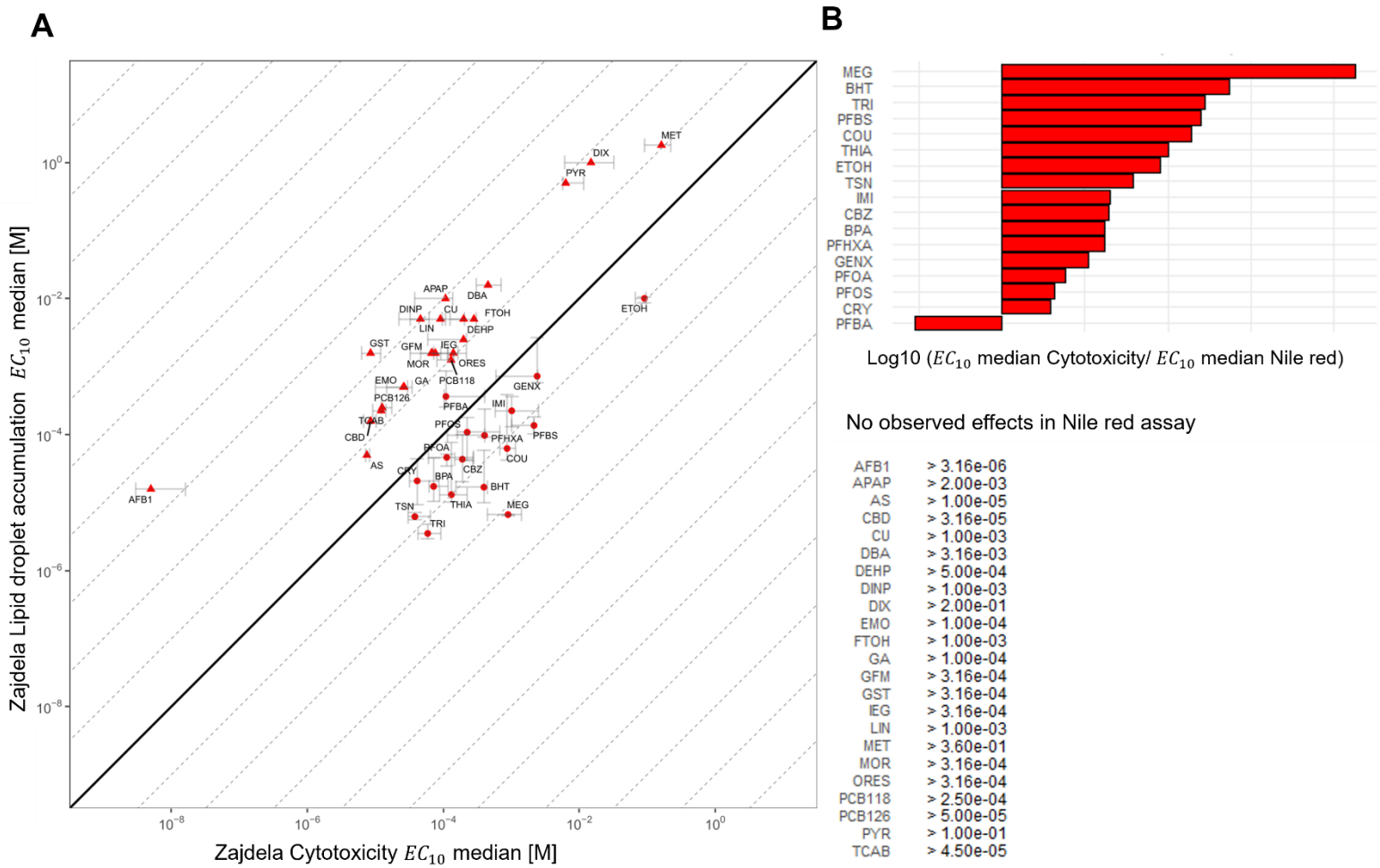

Figure 12 Comparison of the performance of cytotoxicity and lipid droplet accumulation in Zajdela cells

A Scatterplot of the median EC_{10} values (n = at least 3 independent experiments) for two assays with logarithmic scales on both axes. Error bars represent the minimum and maximum EC_{10} values. The black solid line represents the line of identity. Gray dashed lines mark constant factor differences (in decadic log scale) of the EC_{10} values between the assays. Each line corresponds to a 10^n-fold deviation from the line of identity (n = ±1, ±2, etc.). Compounds with no observed effect in one or both systems were assigned a penalty (5× highest tested concentration) and shown as triangles; those with effects in both systems appear as circles. Unilateral detection is indicated by directional error bars**. B** Ratio plot displaying the ratio of effective concentrations of two assays on a decadic logarithmic scale. Only positive test results without penalties were compared. For substance with no observed effects, the highest tested concentration in M is listed below the ratio plot for each assay. All data points and bars are colored in red, denoting hepatotoxicity.

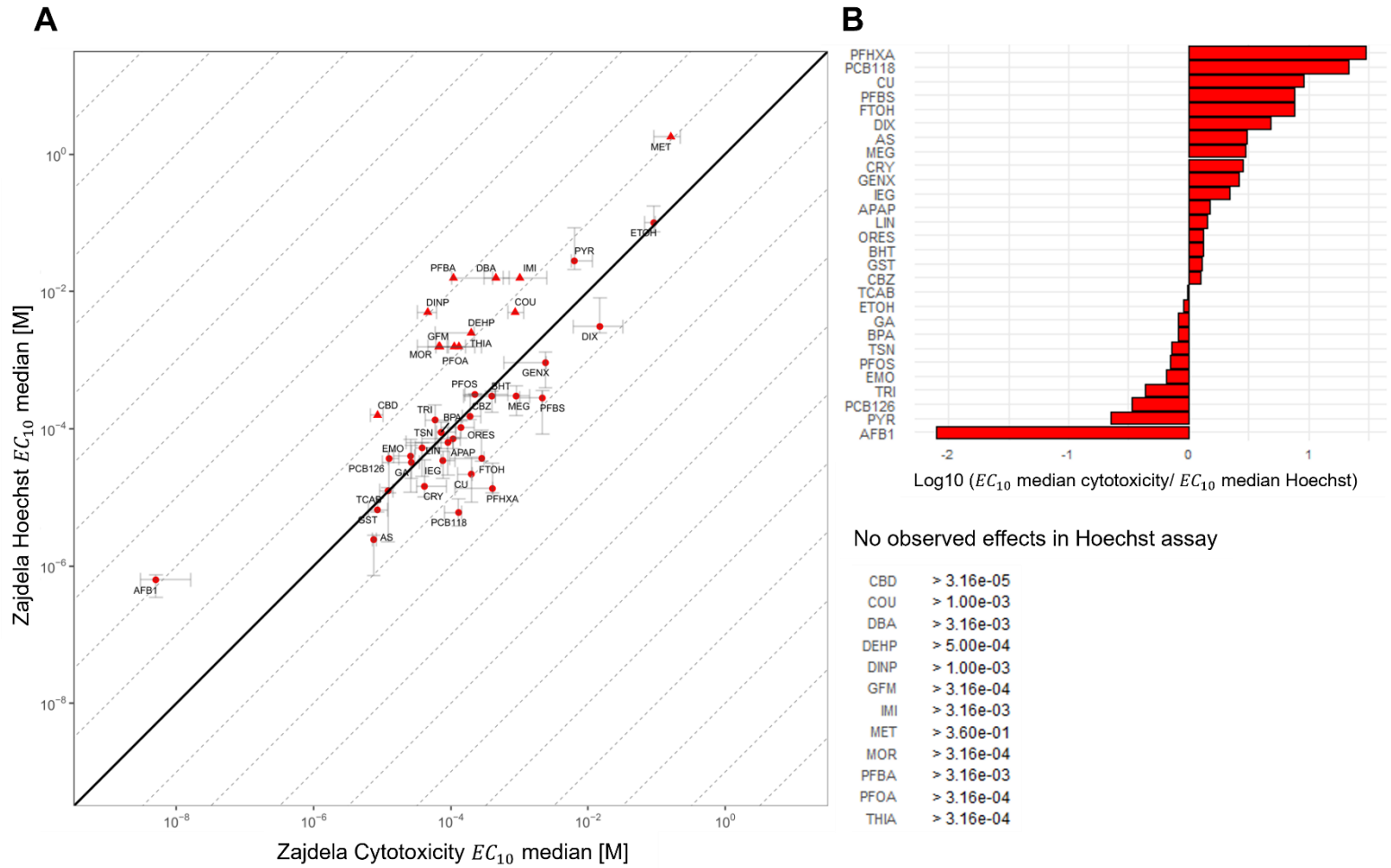

Figure 13 Comparison of the performance of cytotoxicity and nuclear enumeration via Hoechst staining in Zajdela cells

A Scatterplot of the median EC_{10} values (n = at least 3 independent experiments) for two assays with logarithmic scales on both axes. Error bars represent the minimum and maximum EC_{10} values. The black solid line represents the line of identity. Gray dashed lines mark constant factor differences (in decadic log scale) of the EC_{10} values between the assays. Each line corresponds to a 10^n-fold deviation from the line of identity (n = ±1, ±2, etc.). Compounds with no observed effect in one or both systems were assigned a penalty (5× highest tested concentration) and shown as triangles; those with effects in both systems appear as circles. Unilateral detection is indicated by directional error bars**. B** Ratio plot displaying the ratio of effective concentrations of two assays on a decadic logarithmic scale. Only positive test results without penalties were compared. For substance with no observed effects, the highest tested concentration in M is listed below the ratio plot for each assay. All data points and bars are colored in red, denoting hepatotoxicity.

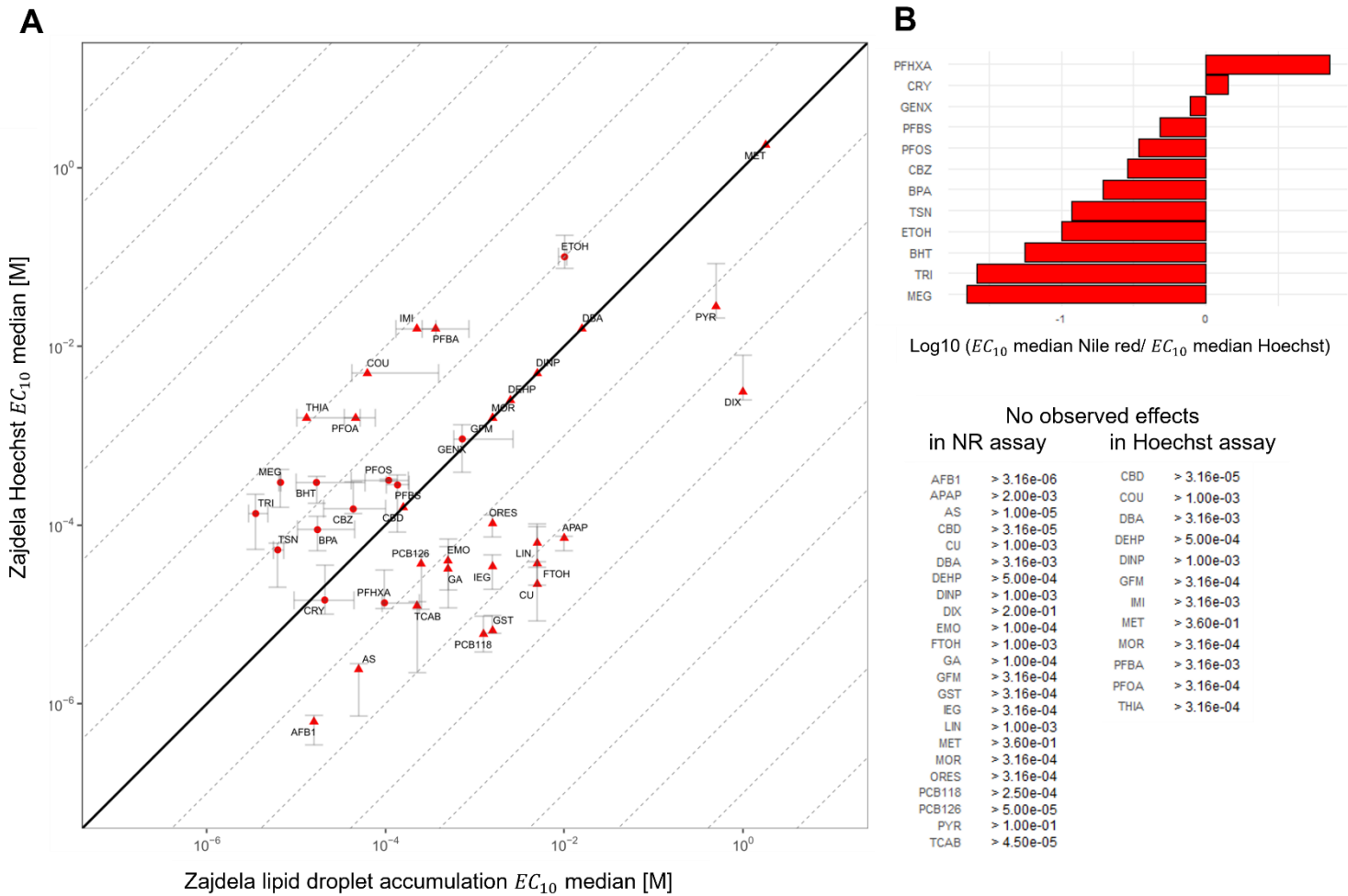

Figure 14 Comparison of the performance of lipid droplet accumulation and nuclear enumeration via Hoechst staining in Zajdela cells

A Scatterplot of the median EC_{10} values (n = at least 3 independent experiments) for two assays with logarithmic scales on both axes. Error bars represent the minimum and maximum EC_{10} values. The black solid line represents the line of identity. Gray dashed lines mark constant factor differences (in decadic log scale) of the EC_{10} values between the assays. Each line corresponds to a 10^n-fold deviation from the line of identity (n = ±1, ±2, etc.). Compounds with no observed effect in one or both systems were assigned a penalty (5× highest tested concentration) and shown as triangles; those with effects in both systems appear as circles. Unilateral detection is indicated by directional error bars**. B** Ratio plot displaying the ratio of effective concentrations of two assays on a decadic logarithmic scale. Only positive test results without penalties were compared. For substance with no observed effects, the highest tested concentration in M is listed below the ratio plot for each assay. All data points and bars are colored in red, denoting hepatotoxicity.

Primary rat hepatocytes

Intra-system comparison of cytotoxicity and Nile red assays in primary red hepatocytes

In **Figure 15** the comparison of the cytotoxicity and Nile red assay in primary red hepatocytes shows a greater sensitivity for Nile red measurements. Of the nine compounds that could be measured in both assays, eight showed lower effective concentrations in the Nile red assay. Only PFOS was detected at a slightly lower concentration in the cytotoxicity assay (less than a 3-fold difference). Most differences between the assays were within a 5-fold range. One notable exception is DBA, which exhibited a 10-fold higher sensitivity in the Nile red assay.

Intra-system comparison of cytotoxicity and Hoechst assays in primary red hepatocytes

When comparing the cytotoxicity assay to nuclear enumeration via Hoechst staining in primary rat hepatocytes (**Figure 16**), most compounds appear to be more sensitively detected in the cytotoxicity assay. Only four compounds showed lower concentrations in the Hoechst assay: AS, TSN, CRY, and notably FTOH, which stood out with significantly higher sensitivity. In contrast, methanol displayed a more than 10-fold lower detection level in the cytotoxicity assay, and PFOA was detected over 5 times lower. The remaining compounds showed differences below a 5-fold range.

Intra-system comparison of Nile red and Hoechst assays in primary red hepatocytes

The Nile red and Hoechst assay comparison in **Figure 17** displays, that only four compounds could be compared at all: GENX, PFBS, ethanol and PFOA. All of them showed lower effective concentrations in the Nile red assay. PFBS, ethanol and PFOA were detected at concentrations more than tenfold lower by the Nile red readout.

In primary hepatocyte system, a slightly different pattern emerges compared to heptamona cell lines. While the Nile red assay remains the most sensitive in terms of detecting lower concentrations, the Hoechst assay now appears to be the least sensitive, with cytotoxicity occupying an intermediate position. Several compounds could only be assessed via the cytotoxicity assay, these include APAP, CU, DIX, GA, and MOR. Conversely, four compounds—DINP, IMI, MEG, and PCB126—could not be detected in any of the three assays tested.

Conclusion of intra-system comparison

The intra-system comparison across the three cell systems revealed consistent patterns regarding both the number of detectable compounds and assay sensitivity. In terms of the number of positive test results (**Table 21**), the CTB assay consistently produced the most results in all three systems, with H4IIE cells yielding the highest number overall. Zajdela cells demonstrated intermediate coverage, while primary hepatocytes had the lowest number of compounds detected across all assays. Notably, the CTB assay was the only readout to detect all tested compounds in the cell lines (H4IIE and Zajdela).

Table 21 Overview of positive test results across cell systems

+++ all compounds, ++ 30-40 compounds, + < 30 compounds

Number of positive tested results	CTB	Nile red	Hoechst
H4IIE	+++	+	++
Zajdela	+++	+	+
Primary rat hepatocytes	+	+	+

Regarding sensitivity (**Table 22**), the Nile red assay emerged as the most sensitive across all three systems, particularly in H4IIE and Zajdela cells. In contrast, the CTB assay—while providing the most hits—was generally the least sensitive. Interestingly, the Hoechst assay ranked in the middle for H4IIE and Zajdela but showed the lowest sensitivity in the primary rat hepatocytes.

Table 22 Overview of cells system specific assay sensitivity

+++ most sensitive, ++ intermediate sensitivity, + lowest sensitivity

Readout sensitivity	CTB	Nile red	Hoechst
H4IIE	+	+++	++
Zajdela	+	+++	++
Primary rat hepatocytes	++	+++	+

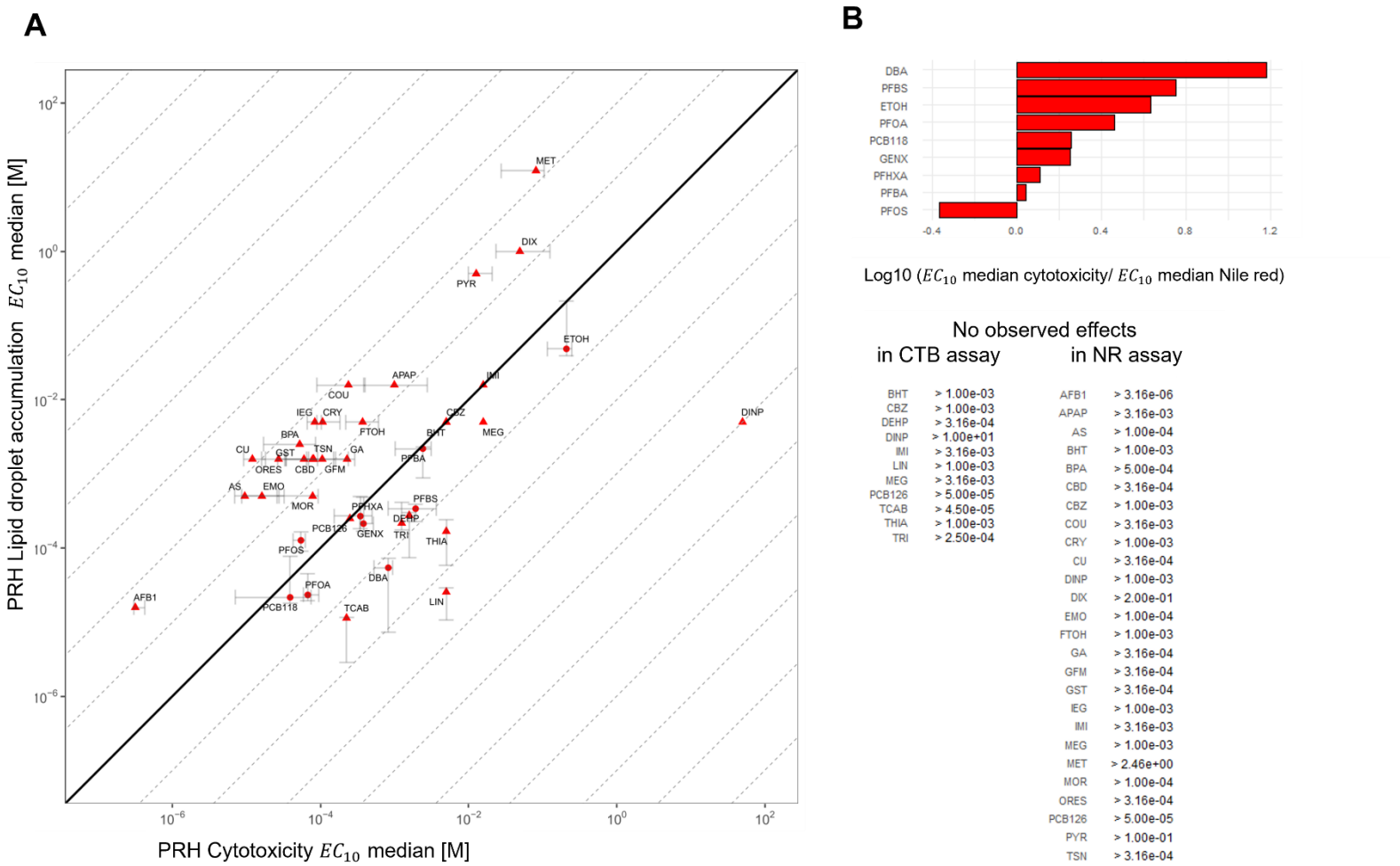

Figure 15 Comparison of the performance of cytotoxicity and lipid droplet accumulation in primary rat hepatocytes

A Scatterplot of the median EC_{10} values (n = at least 3 independent experiments) for two assays with logarithmic scales on both axes. Error bars represent the minimum and maximum EC_{10} values. The black solid line represents the line of identity. Gray dashed lines mark constant factor differences (in decadic log scale) of the EC_{10} values between the assays. Each line corresponds to a 10^n-fold deviation from the line of identity (n = ±1, ±2, etc.). Compounds with no observed effect in one or both systems were assigned a penalty (5× highest tested concentration) and shown as triangles; those with effects in both systems appear as circles. Unilateral detection is indicated by directional error bars. **B** Ratio plot displaying the ratio of effective concentrations of two assays on a decadic logarithmic scale. Only positive test results without penalties were compared. For substance with no observed effects, the highest tested concentration in M is listed below the ratio plot for each assay. All data points and bars are colored in red, denoting hepatotoxicity.

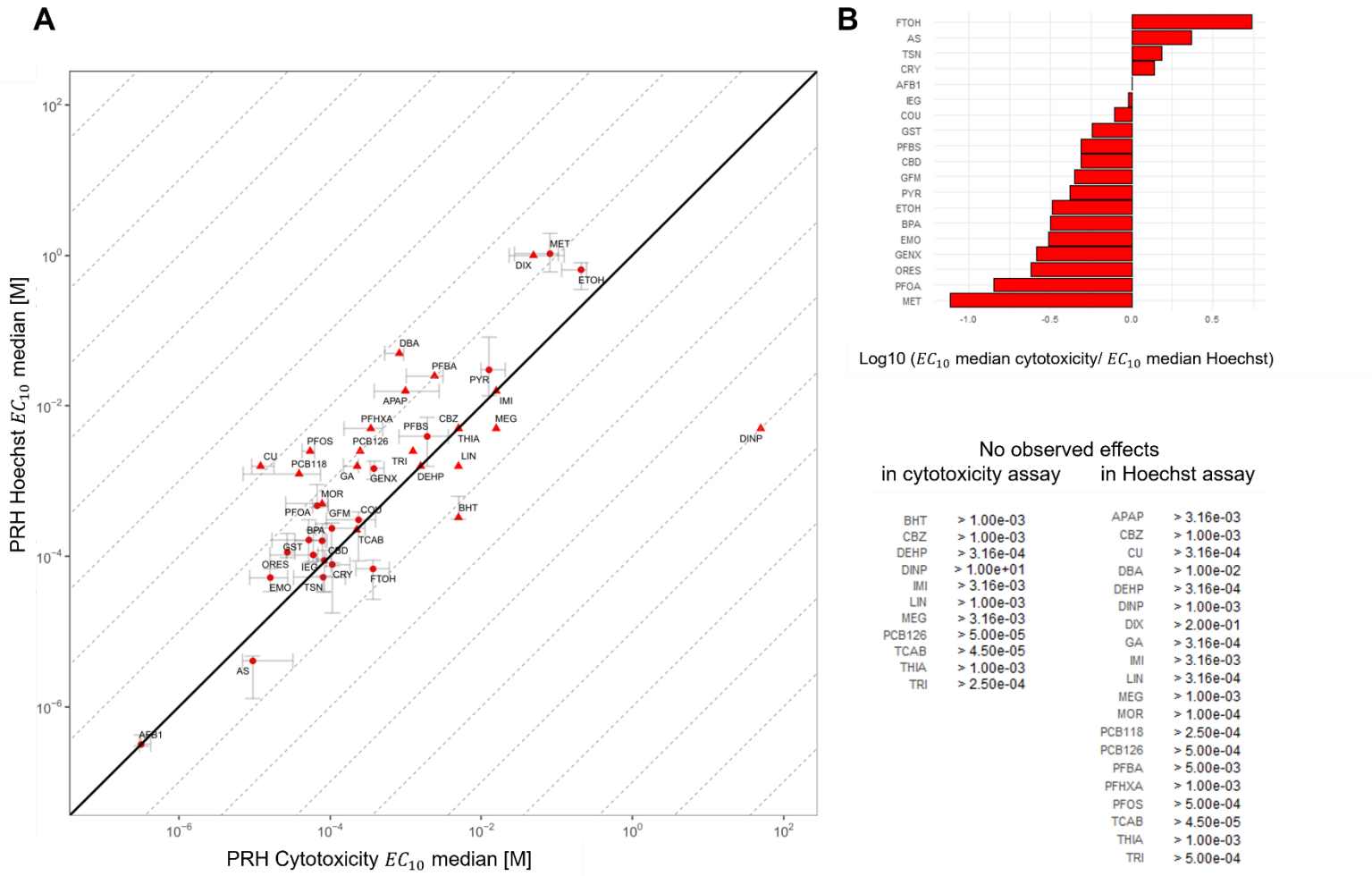

Figure 16 Comparison of the performance of cytotoxicity and nuclear enumeration via Hoechst staining in primary rat hepatocytes

A Scatterplot of the median EC_{10} values (n = at least 3 independent experiments) for two assays with logarithmic scales on both axes. Error bars represent the minimum and maximum EC_{10} values. The black solid line represents the line of identity. Gray dashed lines mark constant factor differences (in decadic log scale) of the EC_{10} values between the assays. Each line corresponds to a 10^n-fold deviation from the line of identity (n = ±1, ±2, etc.). Compounds with no observed effect in one or both systems were assigned a penalty (5× highest tested concentration) and shown as triangles; those with effects in both systems appear as circles. Unilateral detection is indicated by directional error bars. **B** Ratio plot displaying the ratio of effective concentrations of two assays on a decadic logarithmic scale. Only positive test results without penalties were compared. For substance with no observed effects, the highest tested concentration in M is listed below the ratio plot for each assay. All data points and bars are colored in red, denoting hepatotoxicity.

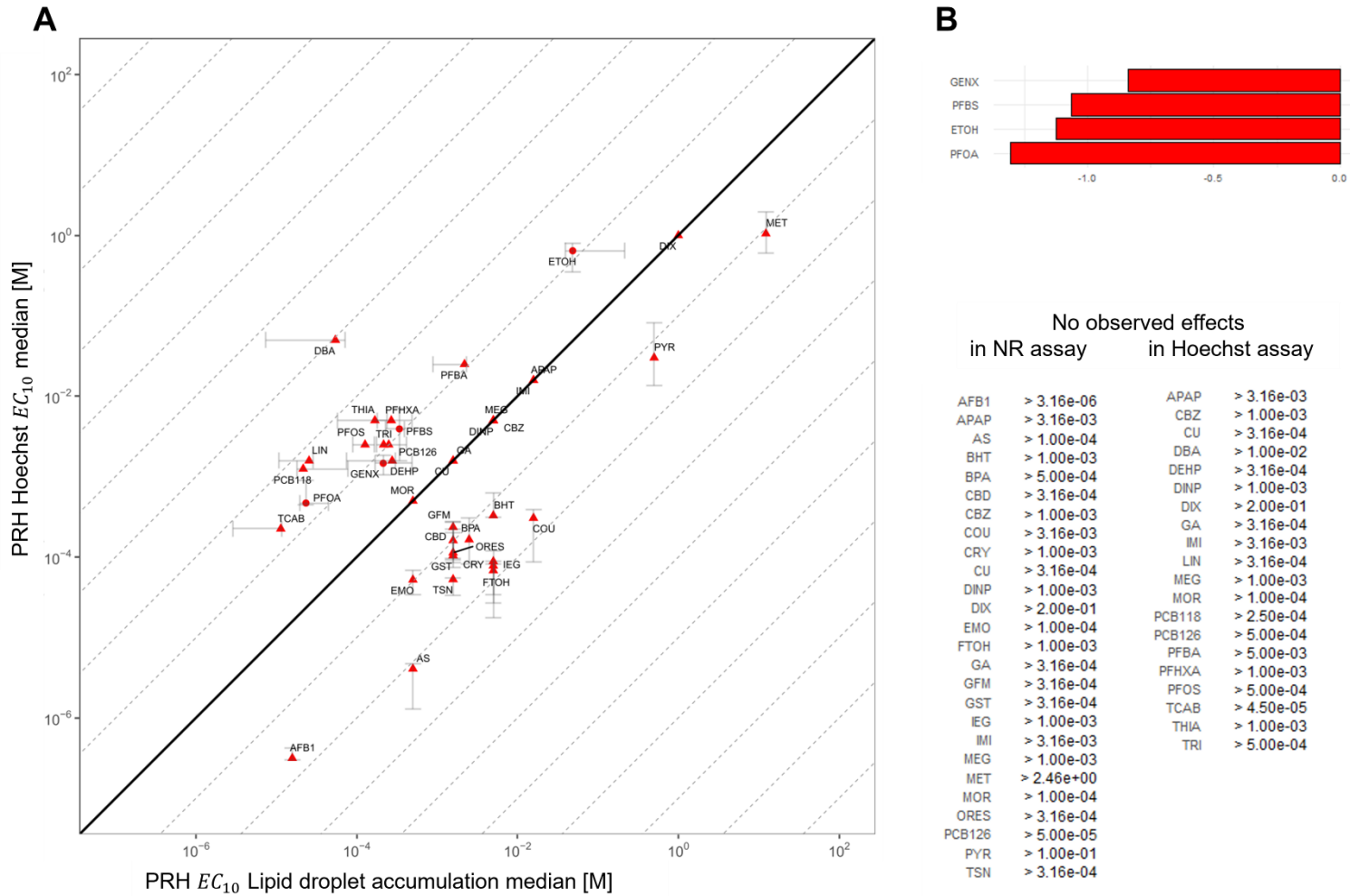

No observed effects

	in NR assay		in Hoechst assay
AFB1	> 3.16e-06	APAP	> 3.16e-03
APAP	> 3.16e-03	CBZ	> 1.00e-03
AS	> 1.00e-04	CU	> 3.16e-04
BHT	> 1.00e-03	DBA	> 1.00e-02
BPA	> 5.00e-04	DEHP	> 3.16e-04
CBD	> 3.16e-04	DINP	> 1.00e-03
CBZ	> 1.00e-03	DIX	> 2.00e-01
COU	> 3.16e-03	GA	> 3.16e-04
CRY	> 1.00e-03	IMI	> 3.16e-03
CU	> 3.16e-04	LIN	> 3.16e-04
DINP	> 1.00e-03	MEG	> 1.00e-03
DIX	> 2.00e-01	MOR	> 1.00e-04
EMO	> 1.00e-04	PCB118	> 2.50e-04
FTOH	> 1.00e-03	PCB126	> 5.00e-04
GA	> 3.16e-04	PFBA	> 5.00e-03
GFM	> 3.16e-04	PFHXA	> 1.00e-03
GST	> 3.16e-04	PFOS	> 5.00e-04
IEG	> 1.00e-03	TCAB	> 4.50e-05
IMI	> 3.16e-03	THIA	> 1.00e-03
MEG	> 1.00e-03	TRI	> 5.00e-04
MET	> 2.46e+00		
MOR	> 1.00e-04		
ORES	> 3.16e-04		
PCB126	> 5.00e-05		
PYR	> 1.00e-01		
TSN	> 3.16e-04		

Figure 17 Comparison of the performance of lipid droplet accumulation and nuclear enumeration via Hoechst staining in primary rat hepatocytes

A Scatterplot of the median EC_{10} values (n = at least 3 independent experiments) for two assays with logarithmic scales on both axes. Error bars represent the minimum and maximum EC_{10} values. The black solid line represents the line of identity. Gray dashed lines mark constant factor differences (in decadic log scale) of the EC_{10} values between the assays. Each line corresponds to a 10^{n}-fold deviation from the line of identity (n = ±1, ±2, etc.). Compounds with no observed effect in one or both systems were assigned a penalty (5× highest tested concentration) and shown as triangles; those with effects in both systems appear as circles. Unilateral detection is indicated by directional error bars**. B** Ratio plot displaying the ratio of effective concentrations of two assays on a decadic logarithmic scale. Only positive test results without penalties were compared. For substance with no observed effects, the highest tested concentration in M is listed below the ratio plot for each assay. All data points and bars are colored in red, denoting hepatotoxicity.

3.2.1.2.2 Inter-system comparison: Sensitivity of cell systems within each assay

Cytotoxicity test

Inter-system comparison of the cytotoxicity readout in H4IIE and Zajdela cells

The comparison of the cytotoxicity readouts of the cell lines H4IIE and Zajdela cells (**Figure 18**) demonstrates a high degree of similarity. For 30 compounds, the EC_{10} values differ by no more than a factor of 3.16, while 9 substances fall within a 3.16- to 10-fold range. Only one compound, DEHP, shows a deviation greater than tenfold, with H4IIE cells being markedly more sensitive. Overall, H4IIE cells tend to exhibit slightly lower EC_{10} values more frequently.

Inter-system comparison of the cytotoxicity readout in H4IIE and primary rat hepatocytes

As illustrated in **Figure 19**, the cytotoxic responses of H4IIE cells and primary rat hepatocytes are compared. H4IIE cells exhibited lower EC_{10} values in 17 out of 29 tested substances. Although no effect was observed in primary hepatocytes for 11 compounds, the remaining data show a high degree of agreement: 18 substances fall within a deviation of less than 3.16-fold, 10 substances within a 3.16–10-fold range, and only one compound (PFBA) exceeds a tenfold difference, with H4IIE being more sensitive. Additionally, H4IIE detected GA and AFB1 at lower concentrations, whereas primary hepatocytes showed increased sensitivity—by more than a factor of 3.16—to MET and PFOS.

Inter-system comparison of the cytotoxicity readout in Zajdela and primary rat hepatocytes

In the cytotoxicity comparison between Zajdela cells and primary rat hepatocytes (**Figure 20**), the Zajdela cells show lower EC_{10} values for 17 out of 29 comparable substances. Notable outliers include AFB1 and PFBA, where the Zajdela cells are more than tenfold more sensitive. In contrast, primary rat hepatocytes show particularly low EC_{10} values for CU, which is detected at more than tenfold lower concentrations in these cells.

Overall, the cell lines show the highest level of similarity in terms of both the number of positive test results and the number of compounds with deviations below a factor of 3.16. When compared with primary rat hepatocytes, the H4IIE cells display slightly more comparable sensitivity, with 28 compounds falling below the factor 10 threshold, compared to 26 for the Zajdela cells. This indicates that, among the substances with a positive test result from the cytotoxicity test (n = 29), H4IIE cells behave slightly more "primary-like" than Zajdela cells.

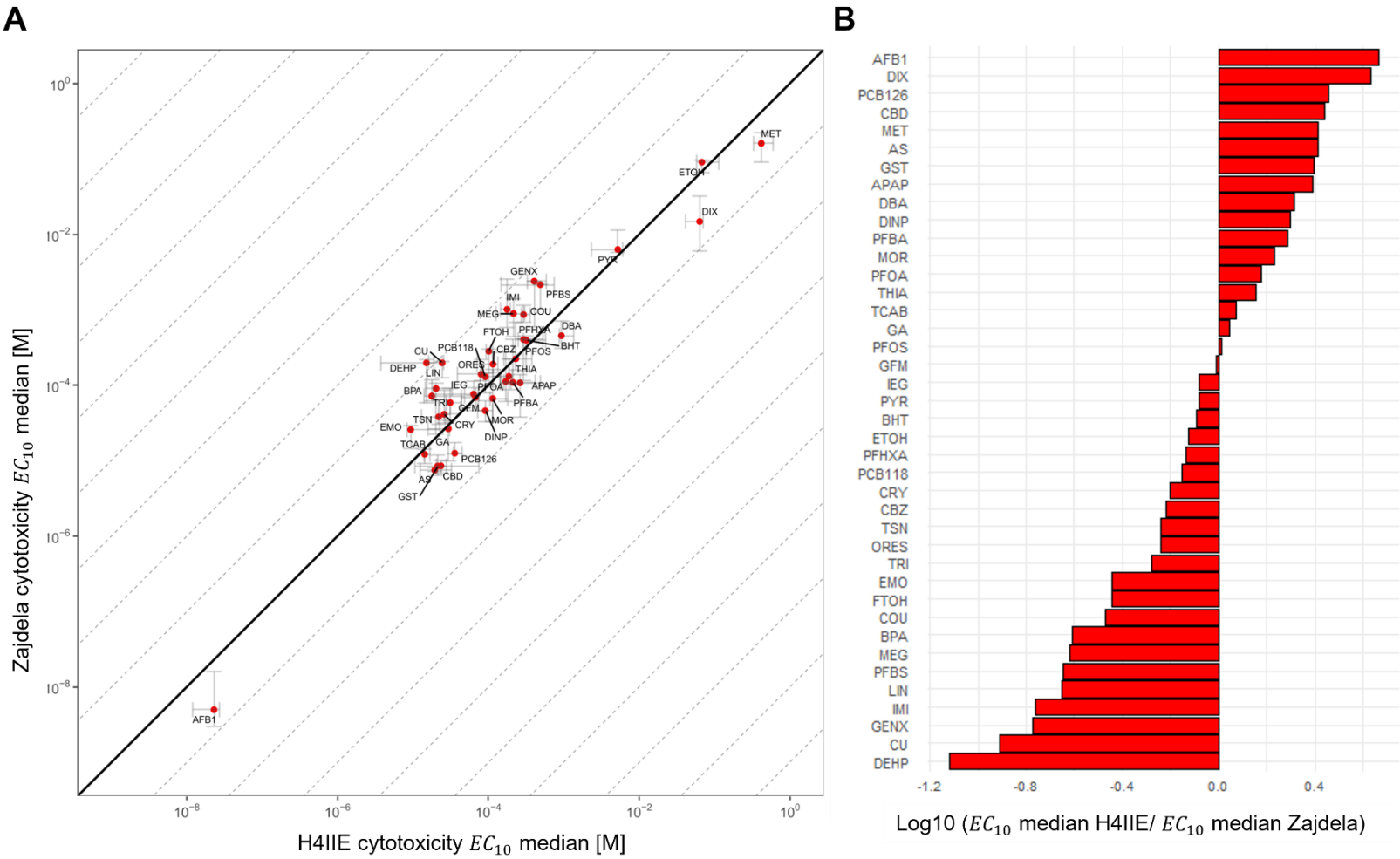

Figure 18 Comparison of the performance of H4IIE and Zajdela hepatocytes in the cytotoxicity test

A Scatterplot of the median EC_{10} values (n = at least 3 independent experiments) for two cell systems with logarithmic scales on both axes. Error bars represent the minimum and maximum EC_{10} values. The black solid line represents the line of identity. Gray dashed lines mark constant factor differences (in decadic log scale) of the EC_{10} values between the assays. Each line corresponds to a 10^n-fold deviation from the line of identity (n = ±1, ±2, etc.). Compounds with no observed effect in one or both systems were assigned a penalty (5× highest tested concentration) and shown as triangles; those with effects in both systems appear as circles. Unilateral detection is indicated by directional error bars**. B** Ratio plot displaying the ratio of effective concentrations of two cell systems on a decadic logarithmic scale. Only positive test results without penalties were compared. For substance with no observed effects, the highest tested concentration in M is listed below the ratio plot for each cell system. All data points and bars are colored in red, denoting hepatotoxicity.

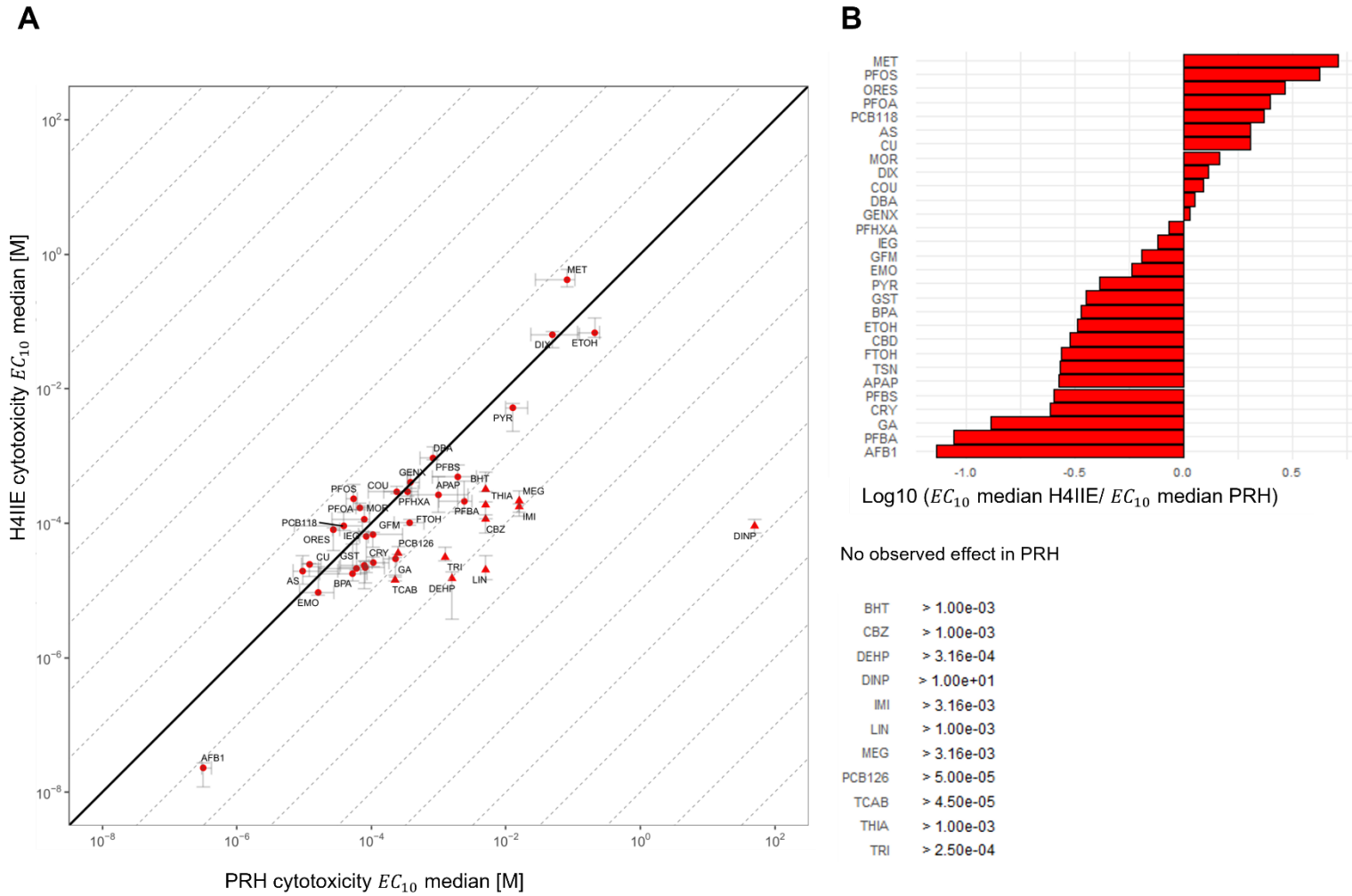

Figure 19 Comparison of the performance of H4IIE and primary rat hepatocytes in the cytotoxicity test

A Scatterplot of the median EC_{10} values (n = at least 3 independent experiments) for two cell systems with logarithmic scales on both axes. Error bars represent the minimum and maximum EC_{10} values. The black solid line represents the line of identity. Gray dashed lines mark constant factor differences (in decadic log scale) of the EC_{10} values between the assays. Each line corresponds to a 10^n-fold deviation from the line of identity (n = ±1, ±2, etc.). Compounds with no observed effect in one or both systems were assigned a penalty (5× highest tested concentration) and shown as triangles; those with effects in both systems appear as circles. Unilateral detection is indicated by directional error bars**. B** Ratio plot displaying the ratio of effective concentrations of two cell systems on a decadic logarithmic scale. Only positive test results without penalties were compared. For substance with no observed effects, the highest tested concentration in M is listed below the ratio plot for each cell system. All data points and bars are colored in red, denoting hepatotoxicity.

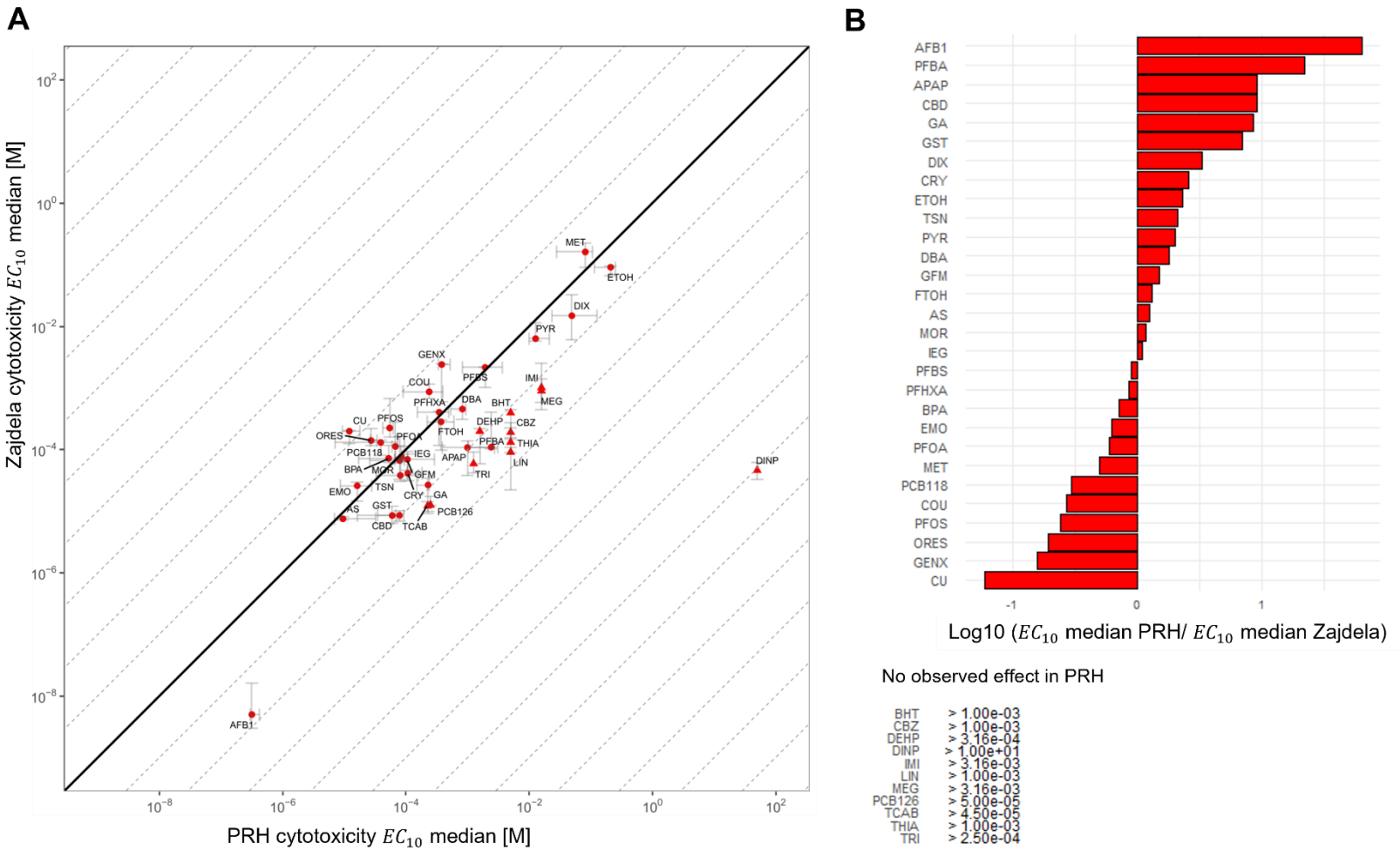

Figure 20 Comparison of the performance of Zajdela and primary rat hepatocytes in the cytotoxicity test

A Scatterplot of the median EC_{10} values (n = at least 3 independent experiments) for two cell systems with logarithmic scales on both axes. Error bars represent the minimum and maximum EC_{10} values. The black solid line represents the line of identity. Gray dashed lines mark constant factor differences (in decadic log scale) of the EC_{10} values between the assays. Each line corresponds to a 10^n-fold deviation from the line of identity (n = ±1, ±2, etc.). Compounds with no observed effect in one or both systems were assigned a penalty (5× highest tested concentration) and shown as triangles; those with effects in both systems appear as circles. Unilateral detection is indicated by directional error bars**. B** Ratio plot displaying the ratio of effective concentrations of two cell systems on a decadic logarithmic scale. Only positive test results without penalties were compared. For substance with no observed effects, the highest tested concentration in M is listed below the ratio plot for each cell system. All data points and bars are colored in red, denoting hepatotoxicity.

Lipid droplet accumulation test

The lipid droplet accumulation assay yielded the fewest positive test results, resulting in only 8 to 10 compounds with comparable EC_{10} values across the cell systems.

Inter-system comparison of the Nile red readout in H4IIE and Zajdela cells

Figure 21 shows that a total of 8 substances tested positive for lipid droplet accumulation in both cell lines, with 17 positive results in the H4IIE and 18 in the Zajdelas. In the comparison between cell lines, Zajdela cells exhibited greater sensitivity than H4IIE cells for 5 out of 8 compounds. PFOS stands out, as it was detected more than 10 times lower in the Zajdela cells. When combining all positive results from both cell lines, 24 positive Nile red results are possible from the 40 compounds tested.

Inter-system comparison of the Nile red readout in H4IIE and primary rat hepatocytes

A comparison between the H4IIE cells and primary rat hepatocytes **Figure 22** reveals positive test results for lipid droplet accumulation in both cell systems for 10 substances. Notably, seven of these substances show greater sensitivity in the H4IIE cells. PFOS is detected in the H4IIE at a significantly higher level (×10), whereas TCAB and TRI exhibit more than 30 times lower levels in H4IIE compared to the primary hepatocytes. When combining the positive results from both cell systems, a total of 21 substances demonstrates positive Nile red outcomes.

Inter-system comparison of the Nile red readout in Zajdela and primary rat hepatocytes

The comparison of lipid droplet accumulation between the Zajdela cells and primary rat hepatocytes (**Figure 23**) shows 9 substances that tested positive in both cell systems. Seven of these results indicate greater sensitivity in the Zajdela cells. Overall, the Zajdela cells yield 18 positive test results, while the primary rat hepatocytes provide only 14. When combining all the positive results from both cell systems, lipid droplet accumulation can be observed in 22 compounds.

In summary, the cell lines generally yield more positive and sensitive results than the primary hepatocytes with Zajdela cells demonstrating the highest sensitivity in this assay. PFOS is detected at significantly higher levels in the H4IIE cells compared to the other cell systems. H4IIE cells also show the greatest concordance (10 substances) with the primary rat hepatocytes in terms of positive results. No positive results were observed for 12 substances in any of the cell systems (AFB1, APAP, CBD, DIX, EMO, GA, GFM, GST, IEG, MET, PCB126, and PYR).

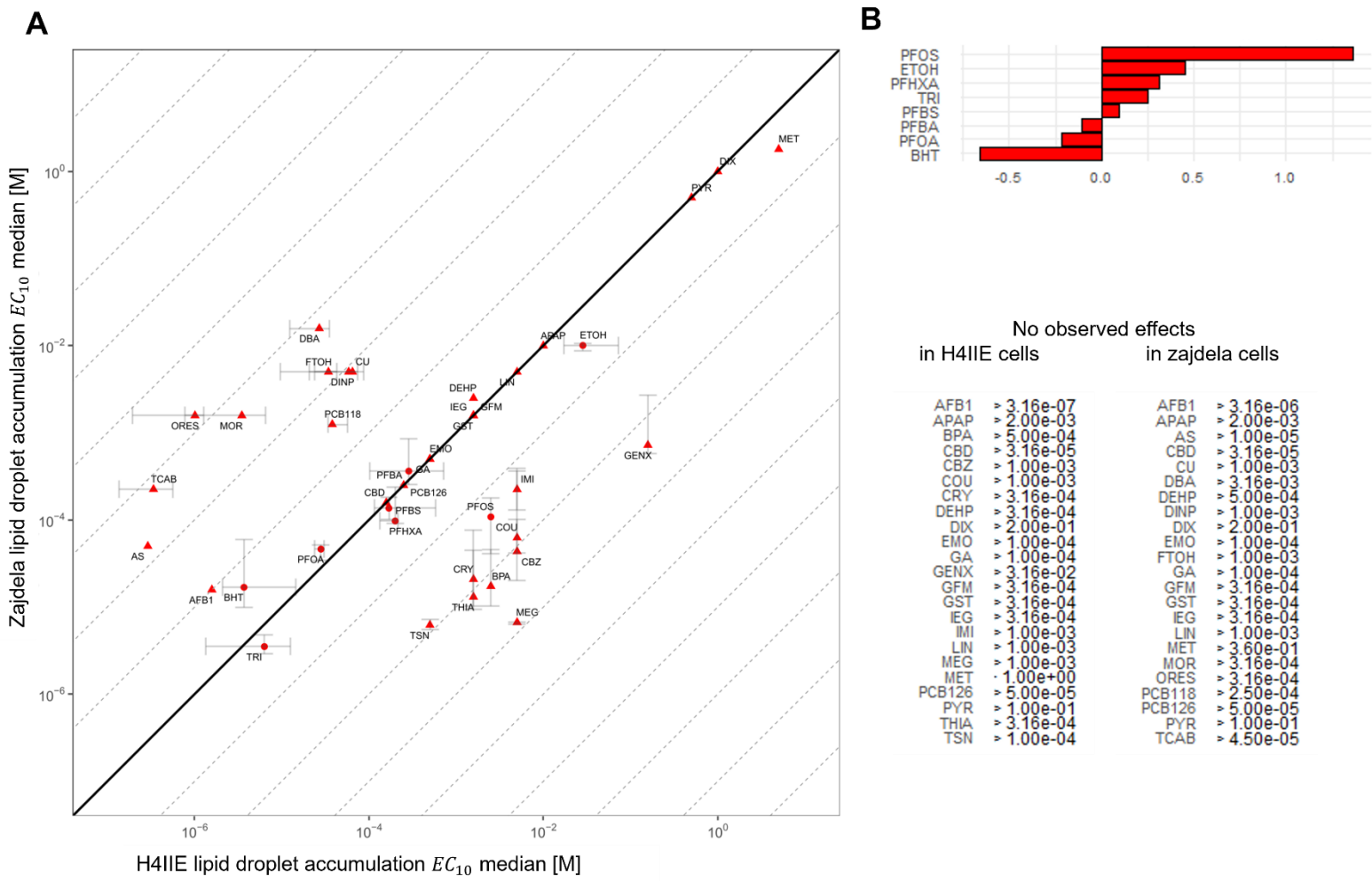

Figure 21 Comparison of the performance of H4IIE and Zajdela cells in the lipid droplet accumulation test

A Scatterplot of the median EC_{10} values (n = at least 3 independent experiments) for two cell systems with logarithmic scales on both axes. Error bars represent the minimum and maximum EC_{10} values. The black solid line represents the line of identity. Gray dashed lines mark constant factor differences (in decadic log scale) of the EC_{10} values between the assays. Each line corresponds to a 10^{n}-fold deviation from the line of identity (n = ±1, ±2, etc.). Compounds with no observed effect in one or both systems were assigned a penalty (5× highest tested concentration) and shown as triangles; those with effects in both systems appear as circles. Unilateral detection is indicated by directional error bars**. B** Ratio plot displaying the ratio of effective concentrations of two cell systems on a decadic logarithmic scale. Only positive test results without penalties were compared. For substance with no observed effects, the highest tested concentration in M is listed below the ratio plot for each cell system. All data points and bars are colored in red, denoting hepatotoxicity.

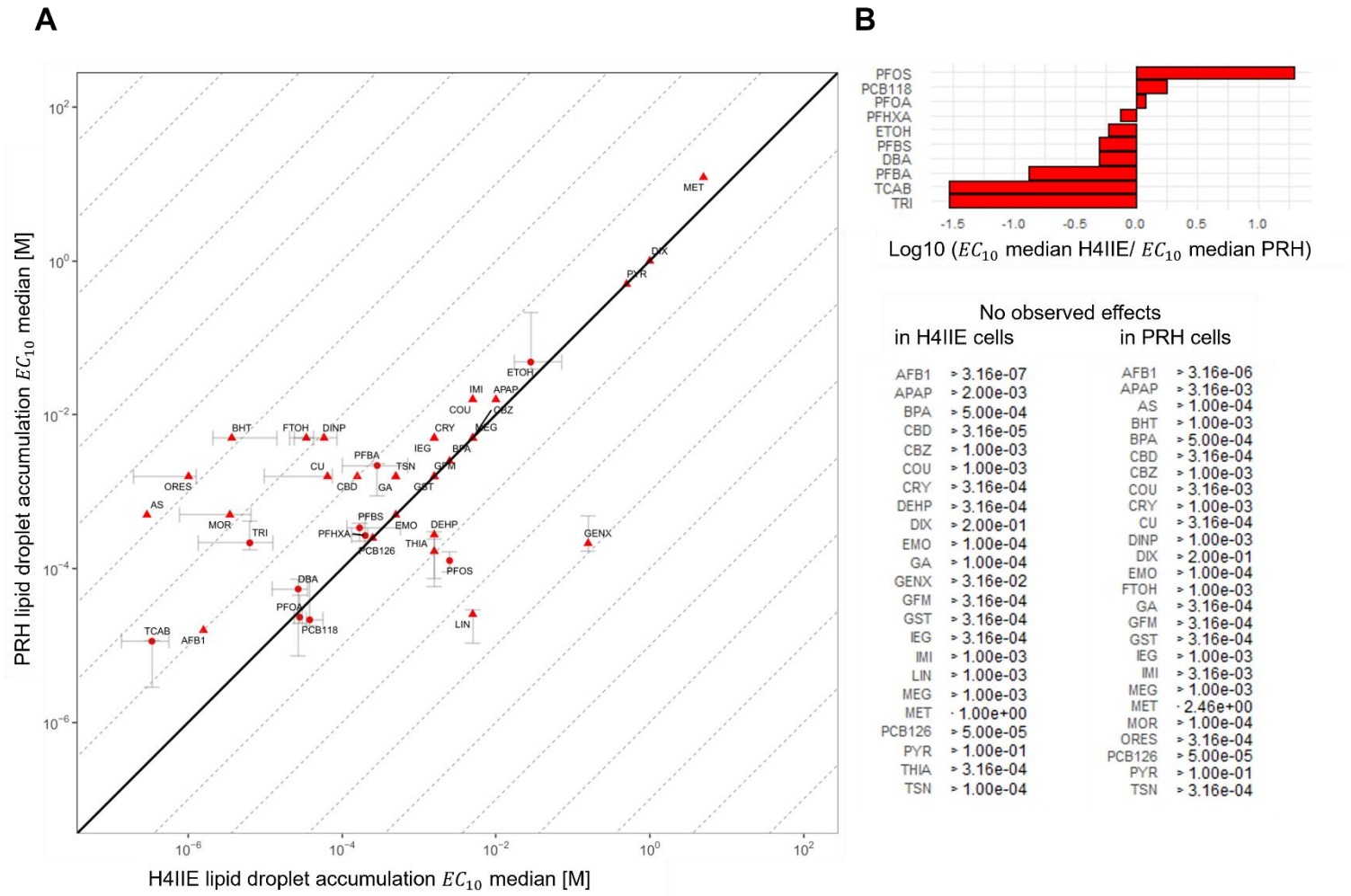

Figure 22 Comparison of the performance of H4IIE and primary hepatocytes in the lipid droplet accumulation test

A Scatterplot of the median EC_{10} values (n = at least 3 independent experiments) for two cell systems with logarithmic scales on both axes. Error bars represent the minimum and maximum EC_{10} values. The black solid line represents the line of identity. Gray dashed lines mark constant factor differences (in decadic log scale) of the EC_{10} values between the assays. Each line corresponds to a 10^n-fold deviation from the line of identity (n = ±1, ±2, etc.). Compounds with no observed effect in one or both systems were assigned a penalty (5× highest tested concentration) and shown as triangles; those with effects in both systems appear as circles. Unilateral detection is indicated by directional error bars**. B** Ratio plot displaying the ratio of effective concentrations of two cell systems on a decadic logarithmic scale. Only positive test results without penalties were compared. For substance with no observed effects, the highest tested concentration in M is listed below the ratio plot for each cell system. All data points and bars are colored in red, denoting hepatotoxicity.

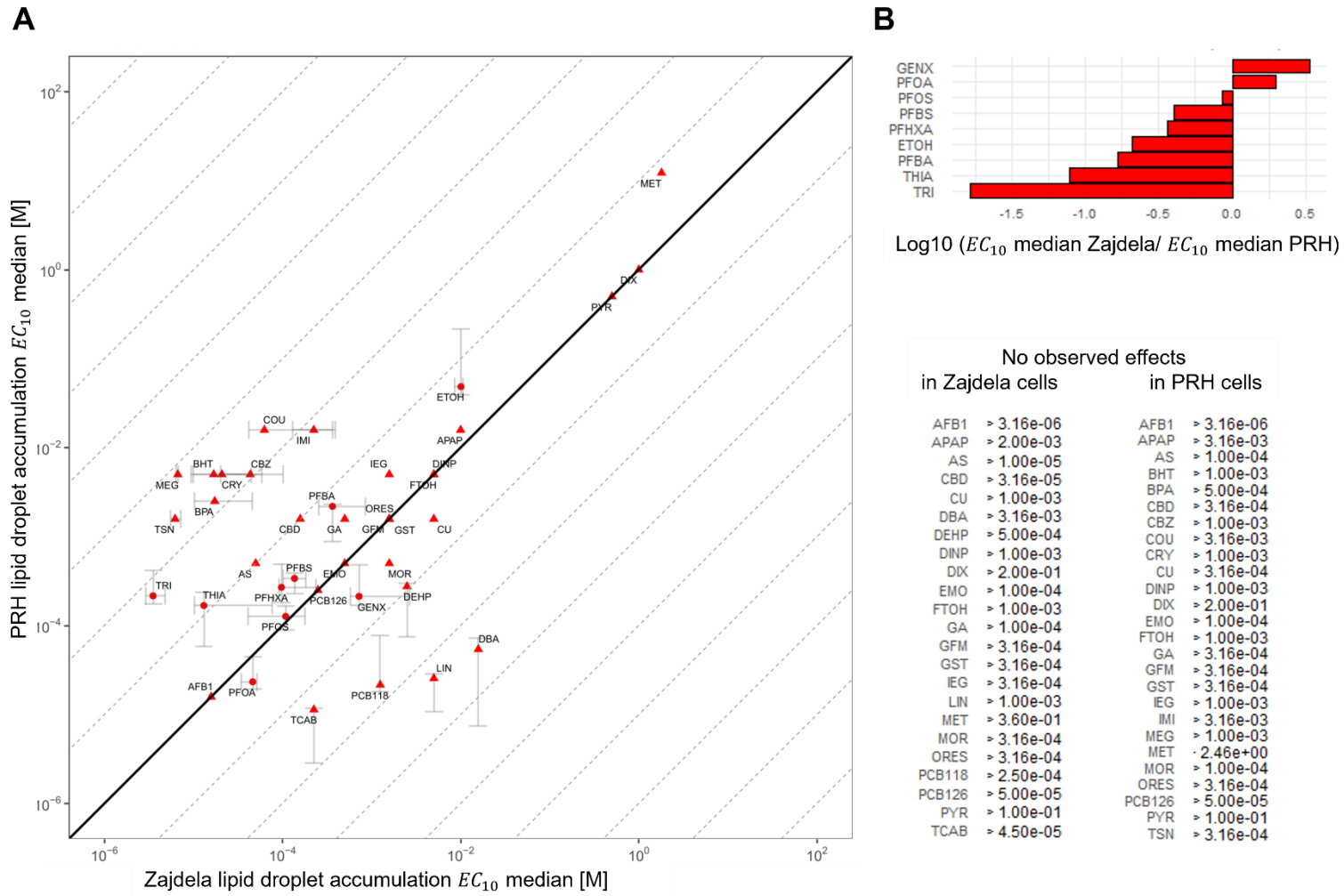

Figure 23 Comparison of the performance of Zajdela and primary hepatocytes in the lipid droplet accumulation test

A Scatterplot of the median EC_{10} values (n = at least 3 independent experiments) for two cell systems with logarithmic scales on both axes. Error bars represent the minimum and maximum EC_{10} values. The black solid line represents the line of identity. Gray dashed lines mark constant factor differences (in decadic log scale) of the EC_{10} values between the assays. Each line corresponds to a 10^{n}-fold deviation from the line of identity (n = ±1, ±2, etc.). Compounds with no observed effect in one or both systems were assigned a penalty (5× highest tested concentration) and shown as triangles; those with effects in both systems appear as circles. Unilateral detection is indicated by directional error bars**. B** Ratio plot displaying the ratio of effective concentrations of two cell systems on a decadic logarithmic scale. Only positive test results without penalties were compared. For substance with no observed effects, the highest tested concentration in M is listed below the ratio plot for each cell system. All data points and bars are colored in red, denoting hepatotoxicity.

Nuclear enumeration via Hoechst staining

The Hoechst readout, which stains and quantifies the nuclei of cells, allows for an assessment of cytotoxic effects by detecting changes in nuclear count. Compared to the Nile red assay, this readout yielded a considerably higher number of positive results across the tested compounds.

Inter-system comparison of the Hoechst readout in H4IIE and Zajdela cells

The comparison between the H4IIE and Zajdela cell lines (**Figure 24**) reveals a markedly higher sensitivity of the H4IIE cells. Overall, 35 positive test results were observed in the H4IIE cells, whereas only 28 were detected in the Zajdela cells. Among the 38 tested compounds, 27 were comparable between the two cell lines. Of these, 18 compounds were detected within a factor of 3.16, 3 compounds differed by a factor between 3.16 and 10, and 6 compounds showed differences exceeding a factor of 10. Notably, ORES, TCAB, and AFB1 were detected at significantly lower concentrations in the H4IIE cells, while PFHXA, DIX, and PCB118 were more sensitively detected in the Zajdela cells.

Inter-system comparison of the Hoechst readout in H4IIE and primary rat hepatocytes

When comparing H4IIE cells to primary rat hepatocytes (**Figure 25**), a distinct pattern becomes apparent: H4IIE cells are consistently more sensitive. Out of the tested substances, 19 compounds were directly comparable between the two systems. Among these, 7 compounds showed only minor differences, with sensitivity varying by less than a factor of 3.16. Another 8 compounds exhibited intermediate differences (between a factor of 3.16 and 10), while 4 compounds differed substantially, exceeding a factor of 10. The primary hepatocytes demonstrated slightly higher sensitivity to only two compounds—FTOH and IEG—yet even these differences remained within the lower range (below a factor of 3.16). In contrast, the H4IIE cells detected several substances with far greater sensitivity, including CBD, GFM, ORES, and AFB1, where differences exceeded a tenfold change.

Inter-system comparison of the Hoechst readout in Zajdela and primary rat hepatocytes

Figure 26 focuses on Zajdela cells in relation to primary rat hepatocytes, revealing a higher sensitivity in the Zajdela cell line. Zajdela cells produced 28 positive results compared to 21 in primary hepatocytes. Of 15 comparable compounds, 11 showed only minor differences in sensitivity (factor < 3.16), 2 ranged between factors of 3.16 and 10, and 2 exceeded a tenfold difference. GST and PFBS were detected more sensitively in Zajdela cells, while primary hepatocytes showed slightly higher sensitivity only for AFB1, with a difference below a factor of 3.16.

To sum up, H4IIE cells demonstrated the highest sensitivity overall in the Hoechst readout, identifying more positive compounds than both Zajdela cells and primary hepatocytes, with several substances—such as ORES, TCAB, and AFB1—detected at markedly lower

concentrations. Zajdela cells also outperformed primary hepatocytes in the Hoechst assay, with most inter-system differences remaining below a factor of 3.16, and only a few compounds showing substantial deviations (e.g., GST, PFBS).

Conclusion of inter-system comparison

In the following, the analyses of the inter-system comparison are concluded based on two criteria (deviation factor and the total number of comparable positive test results), which are summarized in **Table 23**. The deviation factor serves as a critical indicator of similarity between the cell systems. The percentage distribution of results across three categories: < 3.16, 3.16 - 10, and > 10 were analyzed. A lower deviation factor suggests a higher level of agreement between the cell systems.

These comparisons were aimed at identifying which cell systems are most similar in terms of test outcomes and to understand how each cell line performs in relation to primary rat hepatocytes.

Table 23 Overview of inter-system analysis

Comparison of cell systems within each assay, showing the percentage of compounds with deviation factors relative to the number of comparable positive test results (e.g., 75 % of compounds in the cytotoxicity assay for H4IIE vs. Zajdela deviate by less than a factor of 3.16).
PRH – primary rat hepatocytes

Deviation factor	**< 3.16** [%]	**3.16 - 10** [%]	**> 10** [%]	**Total no. of comparable pos. test results**
Cytotoxicity				
H4IIE vs. Zajdela	75.0	22.5	2.5	40
H4IIE vs. PRH	62.1	34.5	3.4	29
Zajdela vs. PRH	58.6	31.0	10.3	29
Lipid droplet accumulation				
H4IIE vs. Zajdela	75.0	12.5	12.5	8
H4IIE vs. PRH	60.0	10.0	30.0	10
Zajdela vs. PRH	44.4	33.3	22.2	9
Hoechst				
H4IIE vs. Zajdela	66.7	11.1	22.2	27
H4IIE vs. PRH	36.8	42.1	21.1	19
Zajdela vs. PRH	73.3	13.3	13.3	15

In the cytotoxicity assay, the two cell lines exhibit the highest agreement in the low deviation category, with 75 % of the results falling within this range. Additionally, there is minimal deviation with a factor >10, and the number of comparable positive results is maximized. In this assay, H4IIE cells show a closer resemblance to primary hepatocytes, particularly in terms of the lowest deviation (62.1 %).

When testing lipid droplet accumulation, both cell lines show significant similarity, but the number of comparable results is relatively low (only 8). While H4IIE cells display a stronger agreement with the primary hepatocytes in terms of low deviation, approximately one-third of the compounds deviate by more than a factor of 10, and only 10 comparable results were obtained.

In the Hoechst staining assay, Zajdela cells demonstrate the highest agreement with primary hepatocytes, with 73.3 % of the results falling within a deviation factor of under 3.16. The deviation factor higher 10 is also relatively low, and the number of comparable compounds is 15.

In summary, Zajdela cells and primary hepatocytes show the closest similarity in the Hoechst assay, while H4IIE cells are more like primary hepatocytes in the cytotoxicity assay. Both cell lines provide comparable results in cytotoxicity and lipid droplet accumulation assays.

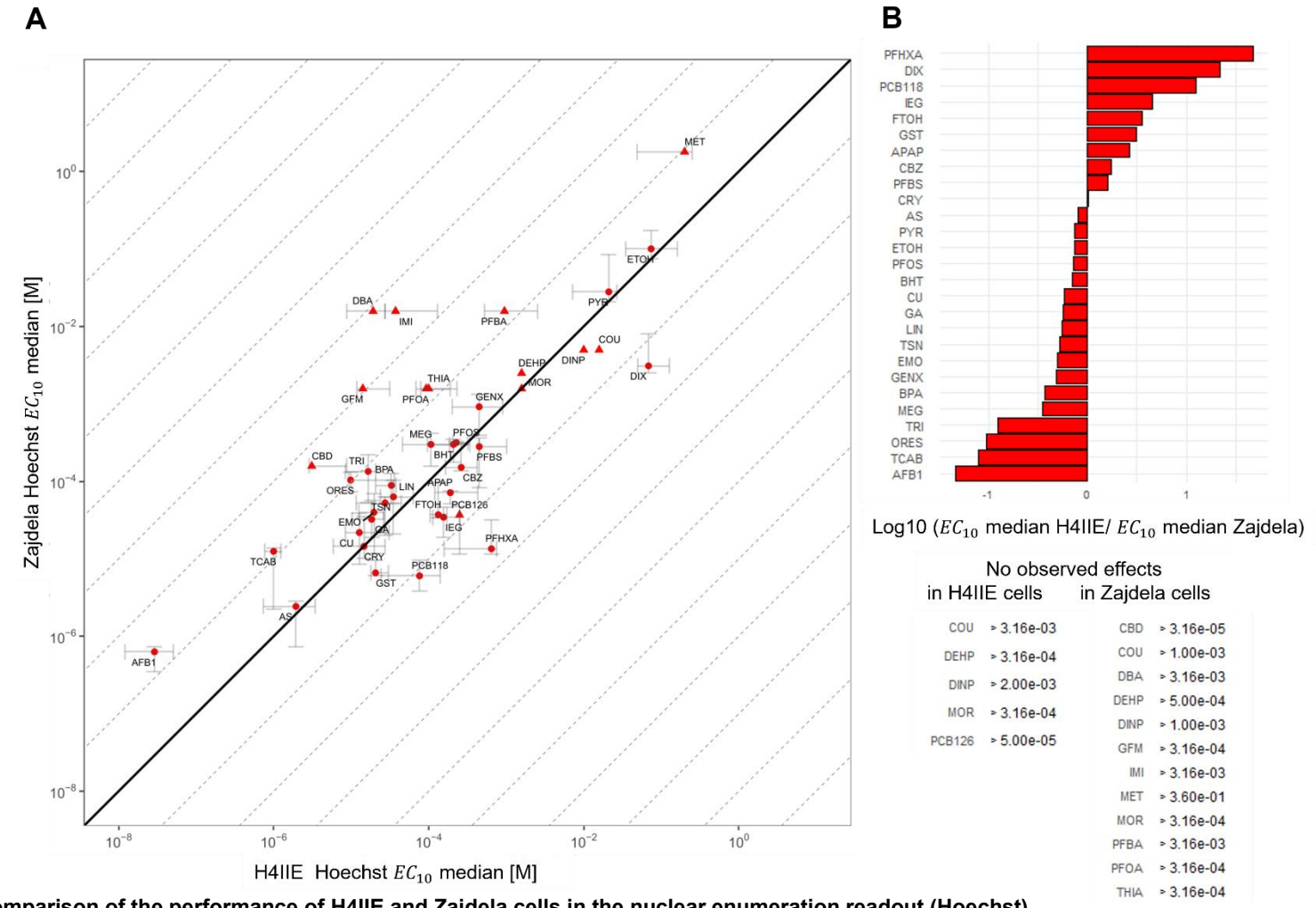

Figure 24 Comparison of the performance of H4IIE and Zajdela cells in the nuclear enumeration readout (Hoechst)

A Scatterplot of the median EC_{10} values (n = at least 3 independent experiments) for two cell systems with logarithmic scales on both axes. Error bars represent the minimum and maximum EC_{10} values. The black solid line represents the line of identity. Gray dashed lines mark constant factor differences (in decadic log scale) of the EC_{10} values between the assays. Each line corresponds to a 10^n-fold deviation from the line of identity (n = ±1, ±2, etc.). Compounds with no observed effect in one or both systems were assigned a penalty (5× highest tested concentration) and shown as triangles; those with effects in both systems appear as circles. Unilateral detection is indicated by directional error bars**. B** Ratio plot displaying the ratio of effective concentrations of two cell systems on a decadic logarithmic scale. Only positive test results without penalties were compared. For substance with no observed effects, the highest tested concentration in M is listed below the ratio plot for each cell system. All data points and bars are colored in red, denoting hepatotoxicity.

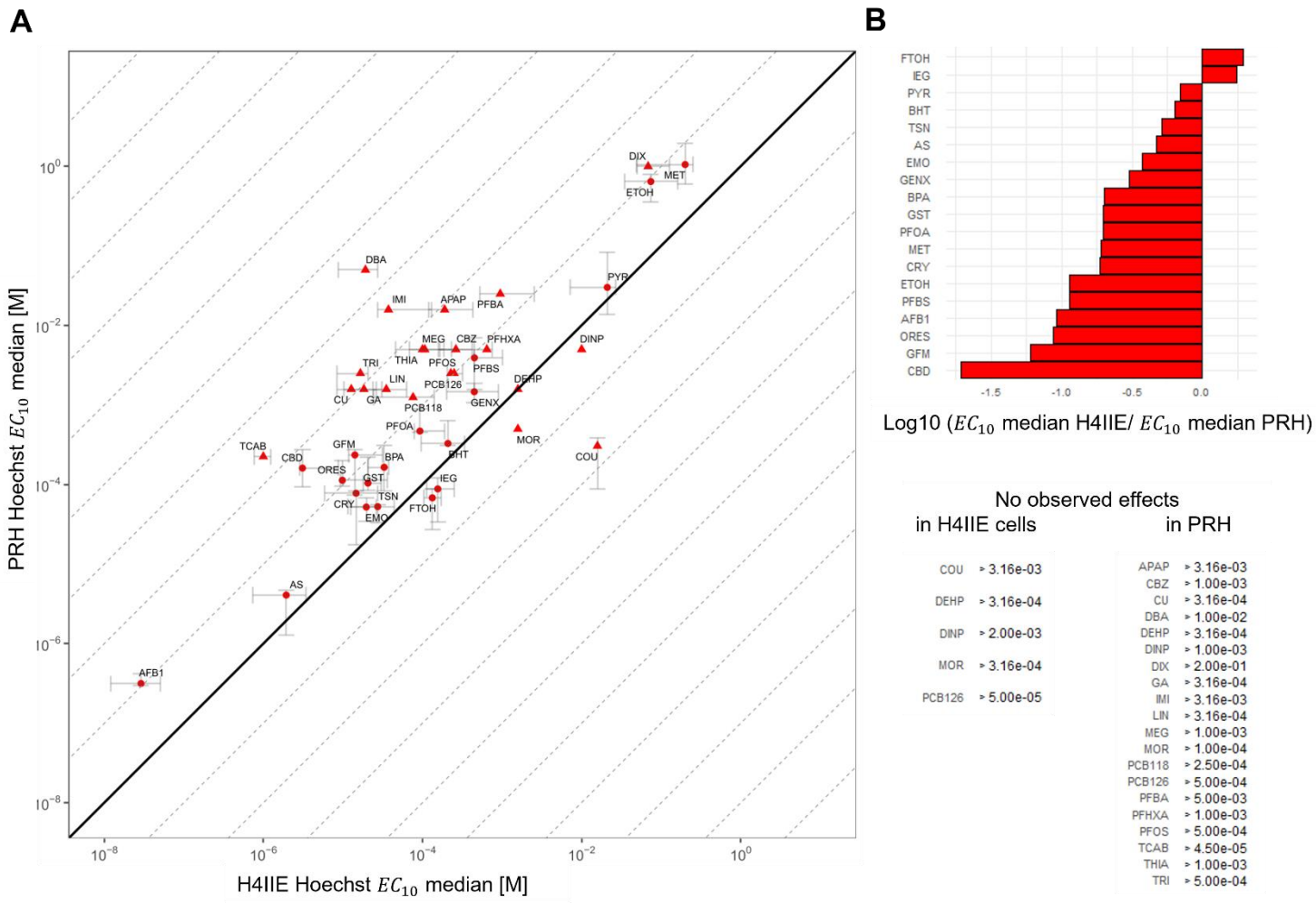

Figure 25 Comparison of the performance of H4IIE and primary rat hepatocytes in the nuclear enumeration readout (Hoechst)

A Scatterplot of the median EC_{10} values (n = at least 3 independent experiments) for two cell systems with logarithmic scales on both axes. Error bars represent the minimum and maximum EC_{10} values. The black solid line represents the line of identity. Gray dashed lines mark constant factor differences (in decadic log scale) of the EC_{10} values between the assays. Each line corresponds to a 10^{n}-fold deviation from the line of identity (n = ±1, ±2, etc.). Compounds with no observed effect in one or both systems were assigned a penalty (5× highest tested concentration) and shown as triangles; those with effects in both systems appear as circles. Unilateral detection is indicated by directional error bars**. B** Ratio plot displaying the ratio of effective concentrations of two cell systems on a decadic logarithmic scale. Only positive test results without penalties were compared. For substance with no observed effects, the highest tested concentration in M is listed below the ratio plot for each cell system. All data points and bars are colored in red, denoting hepatotoxicity.

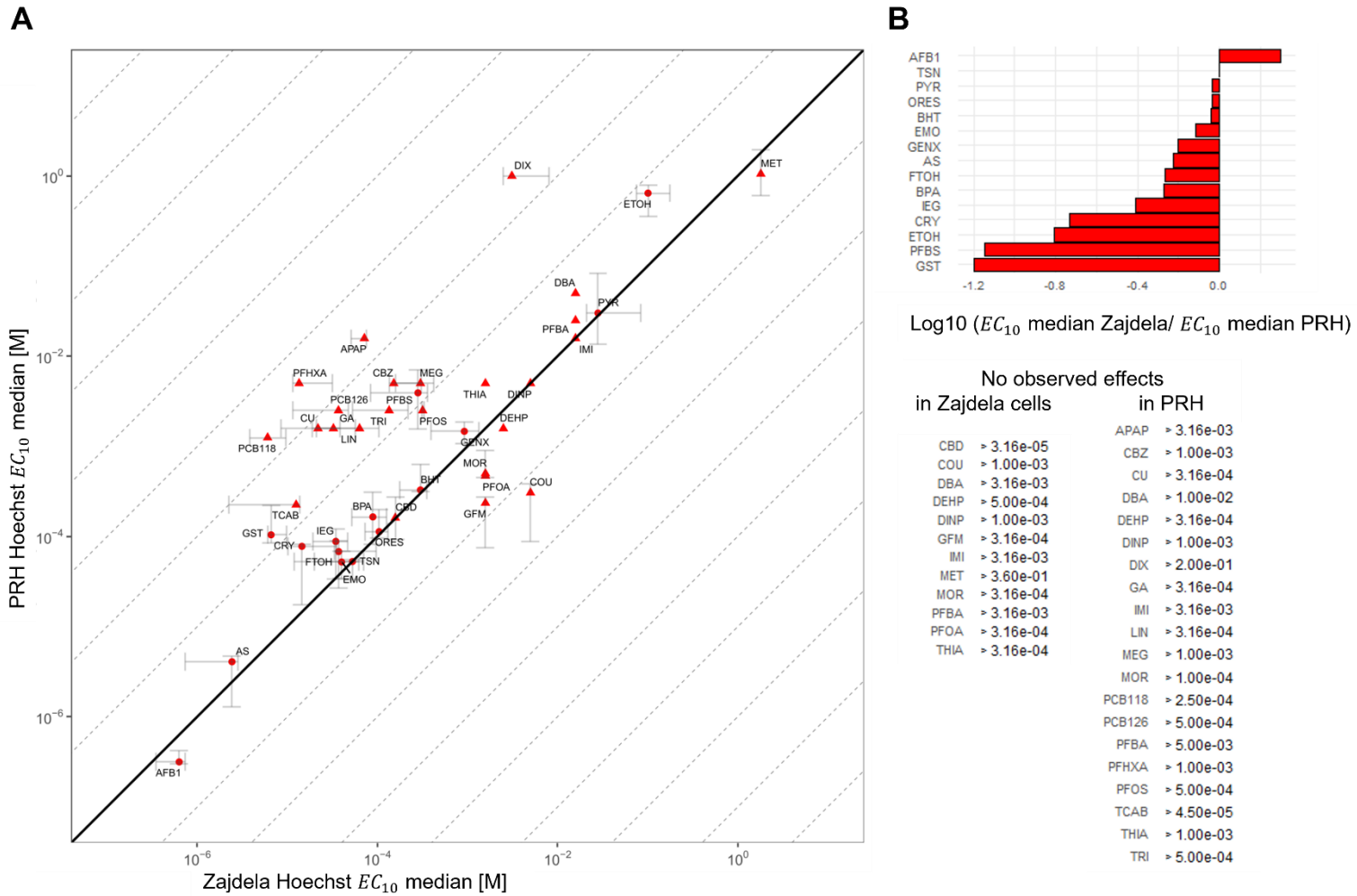

Figure 26 Comparison of the performance of Zajdela and primary rat hepatocytes in the nuclear enumeration readout (Hoechst)

A Scatterplot of the median EC_{10} values (n = at least 3 independent experiments) for two cell systems with logarithmic scales on both axes. Error bars represent the minimum and maximum EC_{10} values. The black solid line represents the line of identity. Gray dashed lines mark constant factor differences (in decadic log scale) of the EC_{10} values between the assays. Each line corresponds to a 10^{n}-fold deviation from the line of identity (n = ±1, ±2, etc.). Compounds with no observed effect in one or both systems were assigned a penalty (5× highest tested concentration) and shown as triangles; those with effects in both systems appear as circles. Unilateral detection is indicated by directional error bars**. B** Ratio plot displaying the ratio of effective concentrations of two cell systems on a decadic logarithmic scale. Only positive test results without penalties were compared. For substance with no observed effects, the highest tested concentration in M is listed below the ratio plot for each cell system. All data points and bars are colored in red, denoting hepatotoxicity.

3.3 *In vivo*

3.3.1 PBPK-based modeling of portal vein plasma concentrations

To estimate *in vivo* concentrations in the portal vein plasma, physiologically based pharmacokinetic (PBPK) modeling was applied. The models were based on experimental liver-specific LOAELs from repeated-dose toxicity studies in the rat, which served as hepatotoxic input doses for the simulations. From these doses, peak concentrations (C_{max}) in the portal vein plasma were derived for each compound, considering sex-specific differences when data were available. The portal vein was selected as the primary site of interest because it directly reflects the concentration reaching the liver after absorption, making it particularly relevant for assessing hepatic exposure and first-pass metabolism.

The resulting C_{max} values were subsequently used for further *in vitro–in vivo* comparisons (see Section 3.4). **Table 24** summarizes all compounds used for PBPK modeling, including the LOAEL input values, the predicted C_{max} in portal vein plasma, the sex associated with the LOAEL and validation dataset, and whether separate male and female models were available. A comprehensive overview of all input parameters used for the PBPK models can be found in **Supplement 4**.

A total of 52 pharmacokinetic models were developed based on 40 compounds, incorporating sex-specific parameters where available. Efforts were made to match the sex of the model parameters with those reported for the corresponding LOAEL data. However, the heterogeneity of the data across toxicological and pharmacokinetic studies often precluded this alignment. For 7 of the 40 compounds, it was possible to simulate sex-specific PK models separately; for the remaining compounds, available data were used regardless of sex specificity. The LOAELs across the compounds ranged from 550 ng/kg body weight (PCB126) to 3600 mg/kg body weight (ETOH). The corresponding peak plasma concentrations in the portal vein ranged from low nanomolar levels (PCB126, AFB1) to high millimolar concentrations (MET, ETOH). For the majority of compounds, however, peak concentrations were within the micromolar range. There is no statistical variability for the *in vivo* concentrations, as the models are based on data from a single rat rather than a population.

Table 24 Summary of input and output parameters of the pharmacokinetic models

In vivo concentrations and LOAELs with sex-specific parameters, where available. f – female, LOAEL – lowest observed adverse effect level, m – male, N.A. – no information available

Compound	Model Abbreviation	Input LOAEL [mg/kg bw]	Cmax portal vein plasma [M]	Sex (LOAEL)	Sex (PBPK validation data)	Separate models available?
Aflatoxin B1	AFB1	0.01	2.32E-08	male	male	no
Acetaminophen	APAP_f	1000	4.84E-03	female	female	no
Arsenic	AS	6	2.82E-05	male	female + male	no
Butylated hydroxy toluene	BHT	250	2.75E-04	male	male	no
Bisphenol - A	BPA	10	1.92E-07	male	female	no
Cannabidiol	CBD_f	140	2.71E-05	female	female + male	yes
Carbamazepine	CBZ	400	2.51E-04	female + male	male	no
Coumarin	COU	150	1.95E-04	female + male	male	no
Chrysin	CRY	1000	1.72E-06	female + male	male	no
Copper	CU	68.09	2.31E-04	female + male	male	no
Dibromoacetic acid	DBA_m	20	7.38E-05	male	female + male	no
Di(2-Ethylhexyl) Phthalate	DEHP_m	3000	4.30E-04	male	male	no
Di-isononylphthalate	DINP	152	3.81E-04	female + male	female + male	no
1,4-dioxane	DIX_f	1614	2.04E-03	female	male	no
1,4-dioxane	DIX_m	657	8.31E-04	male	male	no

Table 24 (continued) Summary of input and output parameters of the pharmacokinetic models

In vivo concentrations and LOAELs with sex-specific parameters, where available. C_{max} – peak concentration, f – female, LOAEL – lowest observed adverse effect level, m – male, N.A. – no information available

Compound	Model Abbreviation	Input LOAEL [mg/kg bw]	Cmax portal vein plasma [M]	Sex (LOAEL)	Sex (PBPK model)	Separate models available?
Emodin	EMO_f	340	3.31E-04	female	female	no
Emodin	EMO_m	170	1.65E-04	male	female	no
Ethanol	ETOH	3600	5.16E-02	female + male	male	no
8-2 fluorotelomer alcohol	FTOH_m	25	1.69E-05	male	male	no
Gallic acid	GA_f	70.5	4.10E-05	female	male	no
Gallic acid	GA_m	64.9	4.46E-05	male	male	no
2,3,3,3-tetrafluoro-2-(heptafluoropropoxy)propanoate	GENX_m	50	4.83E-04	female + male	male	no
Gemifloxacin mesylate	GFM_f	200	8.40E-05	female	male	no
Gemifloxacin mesylate	GFM_m	100	4.20E-05	male	male	no
Genistein	GST	500	1.01E-04	female + male	N.A.	no
Isoeugenol	IEG_f	300	1.83E-04	female	female	no
Imidacloprid	IMI	20	5.63E-05	female	male	no
Lindane	LIN_f	24	1.06E-05	female	male	no
Methyleugenol	MEG_f	100	9.54E-05	female	female	yes
Methyleugenol	MEG_m	100	1.13E-04	male	male	yes

Table 24 (continued) Summary of input and output parameters of the pharmacokinetic models

In vivo concentrations and LOAELs with sex-specific parameters, where available. C_{max} – peak concentration, f – female, LOAEL – lowest observed adverse effect level, m – male, N.A. – no information available

Compound	Model Abbreviation	Input LOAEL [mg/kg bw]	Cmax portal vein plasma [M]	Sex (LOAEL)	Sex (PBPK model)	Separate models available?
Methanol	MET	2500	1.72E-01	female + male	female	no
Morin	MOR	613	5.09E-05	female + male	male	no
Oxyresveratol	ORES	150	9.28E-05	female + male	male	no
2,3',4,4',5-pentachlorobiphenyl	PCB118_f	4.6	5.48E-07	female	male	no
3,3',4,4',5-pentachlorobiphenyl	PCB126_f	0.00055	3.02E-09	female	female	no
Perfluorobutanoic acid	PFBA_m	32.4	8.54E-04	male	female + male	yes
Perfluorobutane sulfonic acid	PFBS_f	250	1.75E-03	female	female	yes
Perfluorobutane sulfonic acid	PFBS_m	500	4.30E-03	male	male	yes
Perfluorohexanoic acid	PFHxA_f	500	2.86E-03	female	female	yes
Perfluorohexanoic acid	PFHxA_m	500	3.43E-03	male	male	yes
Perfluorooctanoic acid	PFOA_f	100	1.31E-03	female	female	yes
Perfluorooctanoic acid	PFOA_m	1.25	3.02E-04	male	male	yes
Perfluorooctanesulfonate	PFOS_m	1.25	3.97E-04	female	female	yes
Perfluorooctanesulfonate	PFOS_m	0.625	1.56E-04	male	male	yes

Table 24 (continued) Summary of input and output parameters of the pharmacokinetic models

In vivo concentrations and LOAELs with sex-specific parameters, where available. C_{max} – peak concentration, f – female, LOAEL – lowest observed adverse effect level, m – male, N.A. – no information available

Compound	Model Abbreviation	Input LOAEL [mg/kg bw]	Cmax portal vein plasma [M]	Sex (LOAEL)	Sex (PBPK model)	Separate models available?
Pyridine	PYR_f	90	1.11E-03	female	female + male	no
Pyridine	PYR_m	55	6.78E-04	male	female + male	no
3,3',4,4'-tetrachloroazobenzene	TCAB	3	2.75E-06	female + male	female	no
Thiabendazole	THIA_f	112	2.95E-04	female	male	no
Thiabendazole	THIA_m	90	2.37E-04	male	male	no
Triticonazole	TRI_f	22.3	2.91E-05	female	male	no
Triticonazole	TRI_m	1117	1.46E-03	male	male	no
Triclosan	TSN	750	3.31E-06	male	male	no

3.4 *In vitro–in vivo* analysis

In the final step of this study, the hepatotoxic concentrations of 40 food-relevant compounds obtained from *in vitro* analyses in hepatocyte models and the simulated *in vivo* C_{max} values at the LOAEL in portal vein plasma, are brought together. The objective is to assess the extent to which the two concentration datasets align and to determine which hepatocyte model and which assay provide the highest degree of overlap.

3.4.1 Assessment of *in vitro–in vivo* correlation using the Toxicity Iso-concentration Index (TII)

The Toxicity Iso-concentration index, which was described in detail in section 0, is a custom performance metric that quantifies the distance of a data point from the iso-concentration line in both directions. It serves as an indicator of how closely *in vitro* effective concentrations and *in vivo* plasma concentrations align. A TII value of 1 represents perfect alignment between the two datasets.

In the following, a systematic evaluation is performed: for each assay, an *in vitro–in vivo* extrapolation plot along with the corresponding ratio plot is generated. The analyses are conducted assay-wise across all cell systems. Finally, the lowest observed effect concentration (LOEC) across the three assays is identified for each cell system and benchmarked against the *in silico* C_{max} corresponding to the LAOEL in the portal vein plasma.

Color Scheme of Visualizations

In this chapter, colors reflect the assay type: cytotoxicity is shown in violet, Nile red in pink, and Hoechst nuclear staining in blue.

3.4.1.1 Cytotoxicity assay (CTB): *In vitro–in vivo* extrapolation

3.4.1.1.1 H4IIE

The *in vitro–in vivo* extrapolation of cytotoxicity data generated in H4IIE cells demonstrated a high agreement when compared to portal vein plasma C_{max} concentrations at the LOAEL, yielding an overall TII of 0.855 (**Figure 27**). Among 52 *in vitro–in vivo* pairs, 26 compounds (50 %) were predicted within a deviation factor of 3.16, indicating a strong concordance. An additional 12 compounds fell within a deviation factor between 3.16 and 10, while 12 compounds were within a factor between 10 and 100. Only two compounds, PCB 126 and PCB 118, exhibited deviations exceeding a factor of 100.

Notably, compounds at both toxicity extremes were well predicted, with low hepatotoxic substances such as MET, ETOH, and the highly hepatotoxic AFB1 all falling within a factor of

3.16. Among per- and polyfluoroalkyl substances (PFAS), all compounds were predicted within a factor of 10, with one exception of PFHxA_m, which deviated beyond this range.

A poorer alignment (deviation > factor 10) was observed for EMO, APAP, and DEHP. Additionally, TRI_m exhibited a greater deviation (> factor 10) compared to TRI_f (< factor 3.16). Further deviations greater than a factor of 10 were identified for CRY, DBA, DIX_f and DIX_m. BPA approached a deviation factor close to 100.

3.4.1.1.2 Zajdela

The comparison of cytotoxicity in Zajdela cells with the C_{max} at the LOAEL in portal vein plasma produced a TII of 0.847 (**Figure 28**).

Twenty-one of the 52 *in vitro–in vivo* pairs exhibiting a factor below 3.16. Eighteen pairs had a factor ranging from 3.16 to 10, and ten showed a factor between 10 and 100. Three compounds had a factor exceeding 100, including PCB 126, BPA, and PCB 118.

Among the compounds with a factor below 3.16, DEHP (showing better alignment than in H4IIE cells) stands out, along with several others such as PFOS, BHT, and TRI_f, which showed a very good agreement between *in vitro* and i*n vivo* data. Compounds falling between a factor of 3.16 and 10 include DINP, DIX_f (better than in H4IIE cells), MEG_f and MEG_m. For compounds with a factor greater than 10, notable examples include PFOA, GST, APAP, TRI_m DIX_m and IMI, which had a factor greater than 10 but below 100.

3.4.1.1.3 Primary rat hepatocytes

For the analysis of cytotoxicity in primary rat hepatocytes and portal vein plasma concentrations, a TII of 0.766 was calculated (**Figure 29**). In contrast to the other cell systems, the dataset here comprised only 38, not the complete 52 *in vitro–in vivo* pairs. Consequently, some substances that typically act as outliers, such as PCB126 and DEHP, were not included in the analysis due to a lack of available data.

Regarding the results, 24 of the *in vitro–in vivo* comparisons were within a factor of 3.16, 10 fell between a factor of 3.16 and 10, and 13 compounds showed deviations between a factor of 10 and 100. Only one compound, BPA, exhibited a deviation exceeding a factor of 100.

Compounds demonstrating particularly good alignment between *in vitro* and *in vivo* data included CBD, PFBAm, MOR, GFM (for both sexes), PFBS_m and GST (better than in Zajdela and H4IIE cells), and Arsenic. In contrast, poorly aligned compounds with deviations between a factor of 10 and 100 included PCB 118, DIX_f, DIX_m, FTOH_m, PYR_F, PYR_m, DBA_m, EMO, CU, PFOA, with BPA showing the greatest discrepancy exceeding a factor of 100.

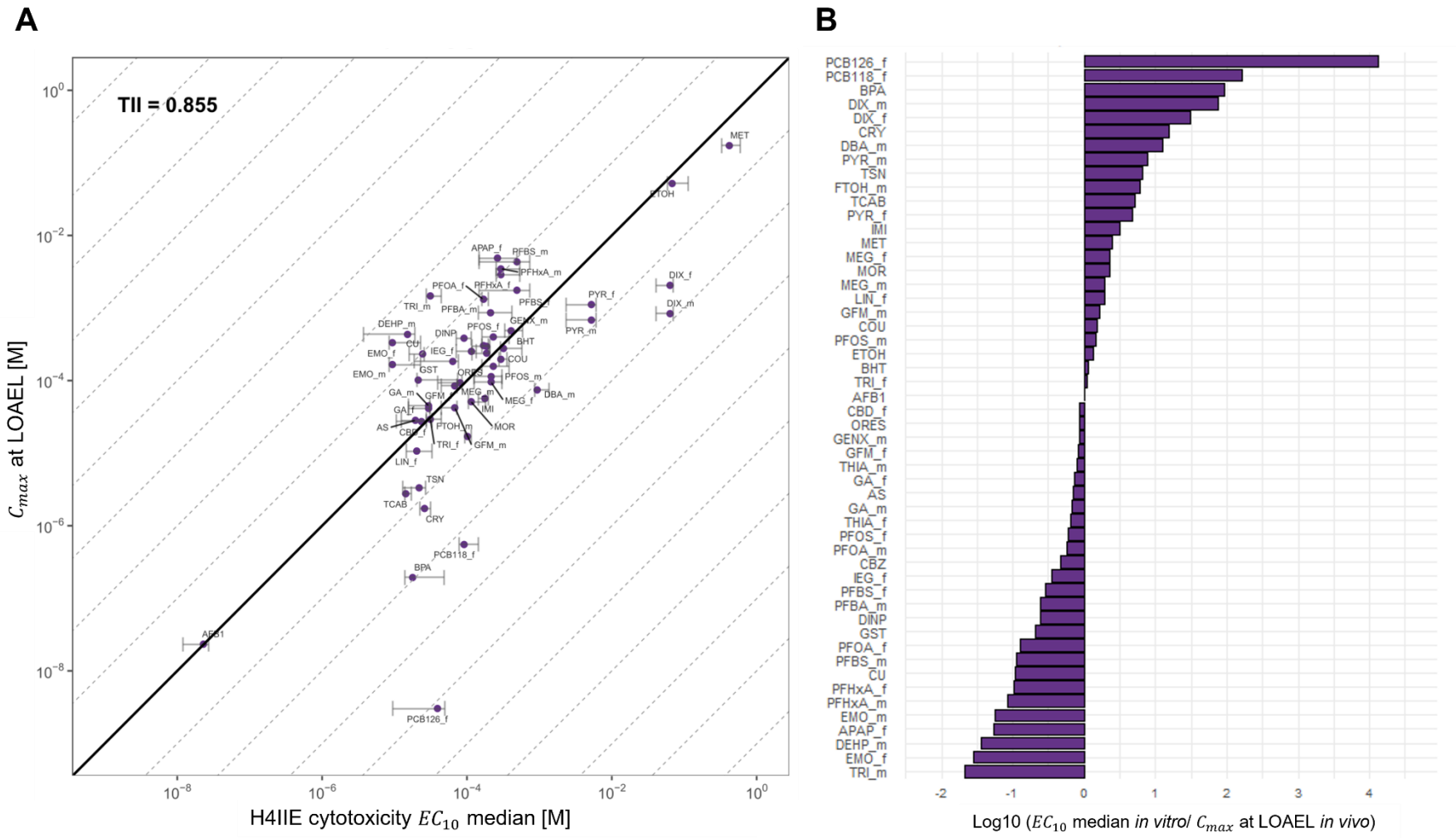

Figure 27 *In vitro–in vivo* extrapolation plot of H4IIE cytotoxicity and portal vein plasma concentrations

A Extrapolation plot of the median EC_{10} values (n = at least 3 independent experiments) and the modeled Cmax at LOAEL with logarithmic scales on both axes. Error bars represent the minimum and maximum EC_{10} values. The black solid line represents the line of identity. Gray dashed lines mark constant factor differences (in decadic log scale) of the EC_{10} and Cmax values. Each line corresponds to a 10^n-fold deviation from the line of identity (n = ±1, ±2, etc.). Compounds with no observed effect *in vitro* were assigned a penalty (5× highest tested concentration) and shown as triangles; those with effects appear as circles. **B** Ratio plot displaying the EC_{10}/Cmax ratios on a decadic logarithmic scale. Only positive test results without penalties were compared. All data points and bars are colored in violet, denoting the cytotoxicity assay.

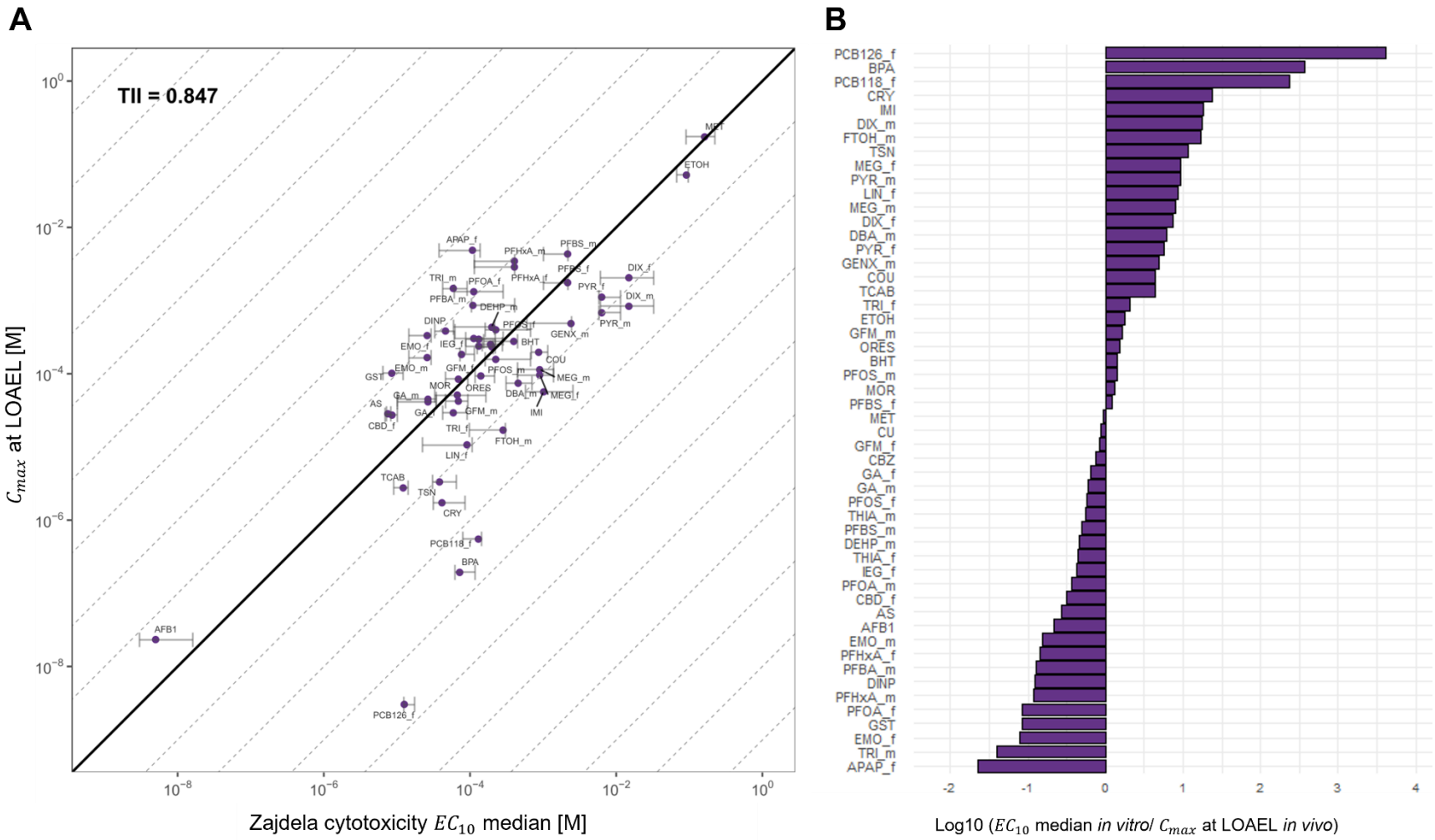

Figure 28 *In vitro–in vivo* extrapolation plot of Zajdela cytotoxicity and portal vein plasma concentrations

A Extrapolation plot of the median EC_{10} values (n = at least 3 independent experiments) and the modeled Cmax at LOAEL with logarithmic scales on both axes. Error bars represent the minimum and maximum EC_{10} values. The black solid line represents the line of identity. Gray dashed lines mark constant factor differences (in decadic log scale) of the EC_{10} and Cmax values. Each line corresponds to a 10^n-fold deviation from the line of identity (n = ±1, ±2, etc.). Compounds with no observed effect *in vitro* were assigned a penalty (5× highest tested concentration) and shown as triangles; those with effects appear as circles. **B** Ratio plot displaying the EC_{10}/Cmax ratios on a decadic logarithmic scale. Only positive test results without penalties were compared. All data points and bars are colored in violet, denoting the cytotoxicity assay.

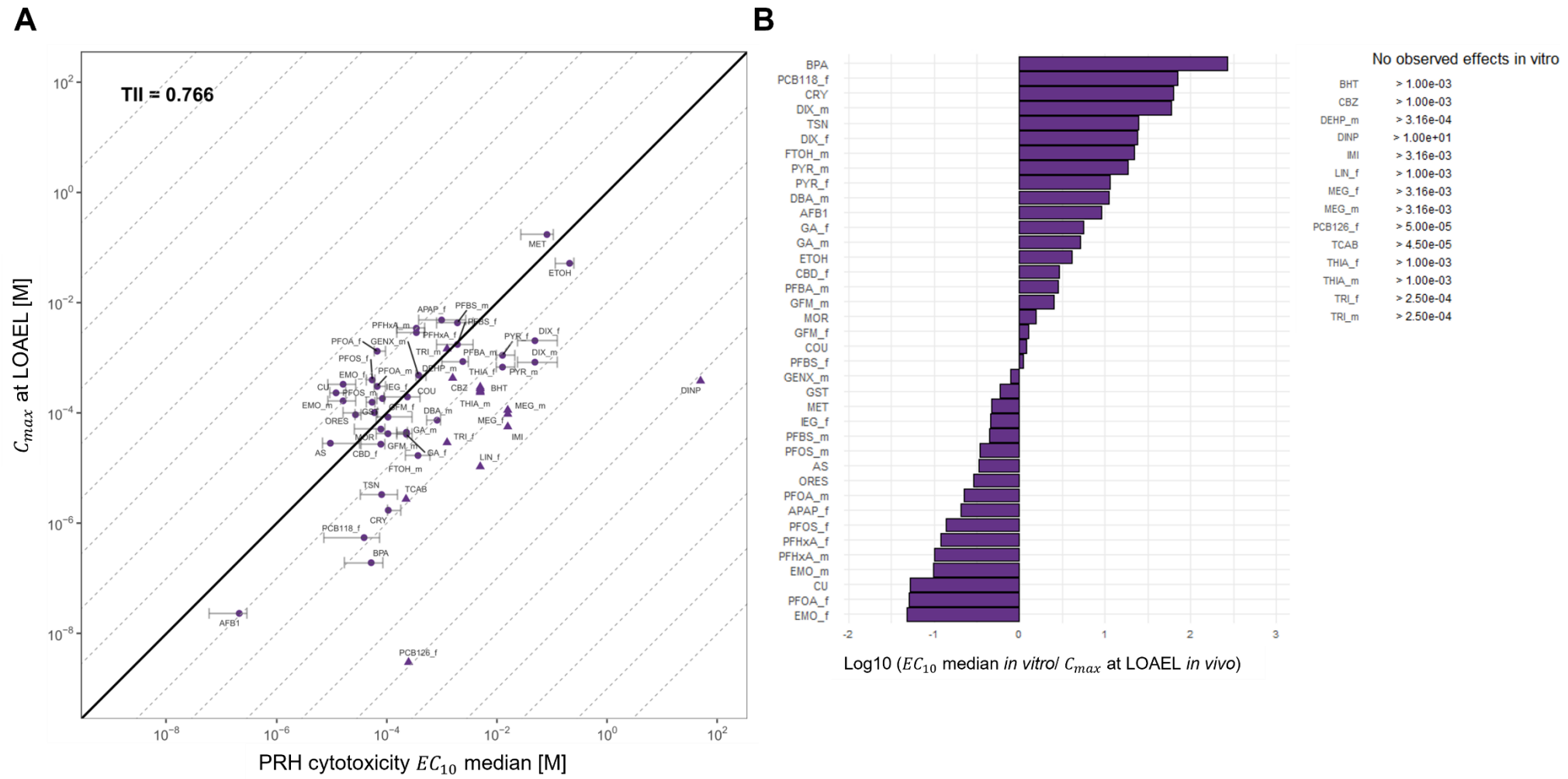

Figure 29 *In vitro–in vivo* extrapolation plot of primary rat hepatocytes cytotoxicity and portal vein plasma concentrations

A Extrapolation plot of the median EC_{10} values (n = at least 3 independent experiments) and the modeled Cmax at LOAEL with logarithmic scales on both axes. Error bars represent the minimum and maximum EC_{10} values. The black solid line represents the line of identity. Gray dashed lines mark constant factor differences (in decadic log scale) of the EC_{10} and Cmax values. Each line corresponds to a 10^n-fold deviation from the line of identity (n = ±1, ±2, etc.). Compounds with no observed effect *in vitro* were assigned a penalty (5× highest tested concentration) and shown as triangles; those with effects appear as circles. **B** Ratio plot displaying the EC_{10}/Cmax ratios on a decadic logarithmic scale. Only positive test results without penalties were compared. For substances with no observed effects, the highest tested concentration (in molarity, M) is listed beside the ratio plot. All data points and bars are colored in violet, denoting the cytotoxicity assay.

3.4.1.2 Lipid droplet accumulation assay: *In vitro–in vivo* extrapolation

3.4.1.2.1 H4IIE

In the H4IIE cell model, a TII of 0.7 was calculated based on the comparison between effective concentrations from lipid droplet accumulation readouts and portal vein plasma concentrations. Out of the 52 tested substances, only 20 yielded usable *in vitro–in vivo* pairs for this analysis (**Figure 30**). In 18 out of these 20 cases, the *in vitro* concentrations were lower than the corresponding *in vivo* concentrations; only for PCB118_f and FTOH_m were the in vivo concentrations lower than the *in vitro* estimates. Among these 20 pairs, only three—ETOH, FTOH_m, and PFBA—fall within a factor of 3.16. Several other substances, including CU, TRI_f, DBA, DINP, and TCAB, lie within a factor of 10. However, the majority of the substances showed larger discrepancies, particularly PFAS compounds, MOR, and AS, which exceeded a factor of 10. Strikingly, TRI_m and PCB118_f deviated by more than two orders of magnitude, suggesting major limitations in predictivity for these compounds.

3.4.1.2.2 Zajdela

The Zajdela cell system yielded a TII of 0.72 based on the comparison between *in vitro* lipid droplet accumulation and total portal vein plasma concentrations at the LOAEL. For this analysis, 24 compound pairs were available (**Figure 31**). Similar to the H4IIE results, the majority of *in vitro* concentrations were lower than their simulated *in vivo* values. Only five substances—BPA, CRY, IMI, TSN, and GENX—showed higher *in vitro* than *in vivo* concentrations. In terms of quantitative agreement, just five compounds fell within a 3.16-fold deviation between *in vitro* and *in vivo*, while another six substances deviated between 3.16- and 10-fold. Most of the compounds, however, showed discrepancies in the range of 10- to 100-fold. Notably, TRI_m showed the largest deviation, exceeding the factor of 100.

3.4.1.2.3 Primary rat hepatocytes

Only 20 usable *in vitro–in vivo* pairs were available for primary human hepatocytes (**Figure 32**). Again, *in vitro* concentrations tended to be lower than their *in vivo* counterparts, with only five compounds showing higher *in vivo* concentrations. However, compared to the cell lines, the primary hepatocytes exhibited notably better agreement: 50 % of all compound pairs showed a deviation of no more than 3.16-fold, with ETOH and PFOS_m being almost perfectly matched. No compound exceeded the 100-fold difference. The highest deviations were observed for PCB118_f and PFOA_f, along with several additional PFAS compounds, which were consistently underestimated *in vitro*.

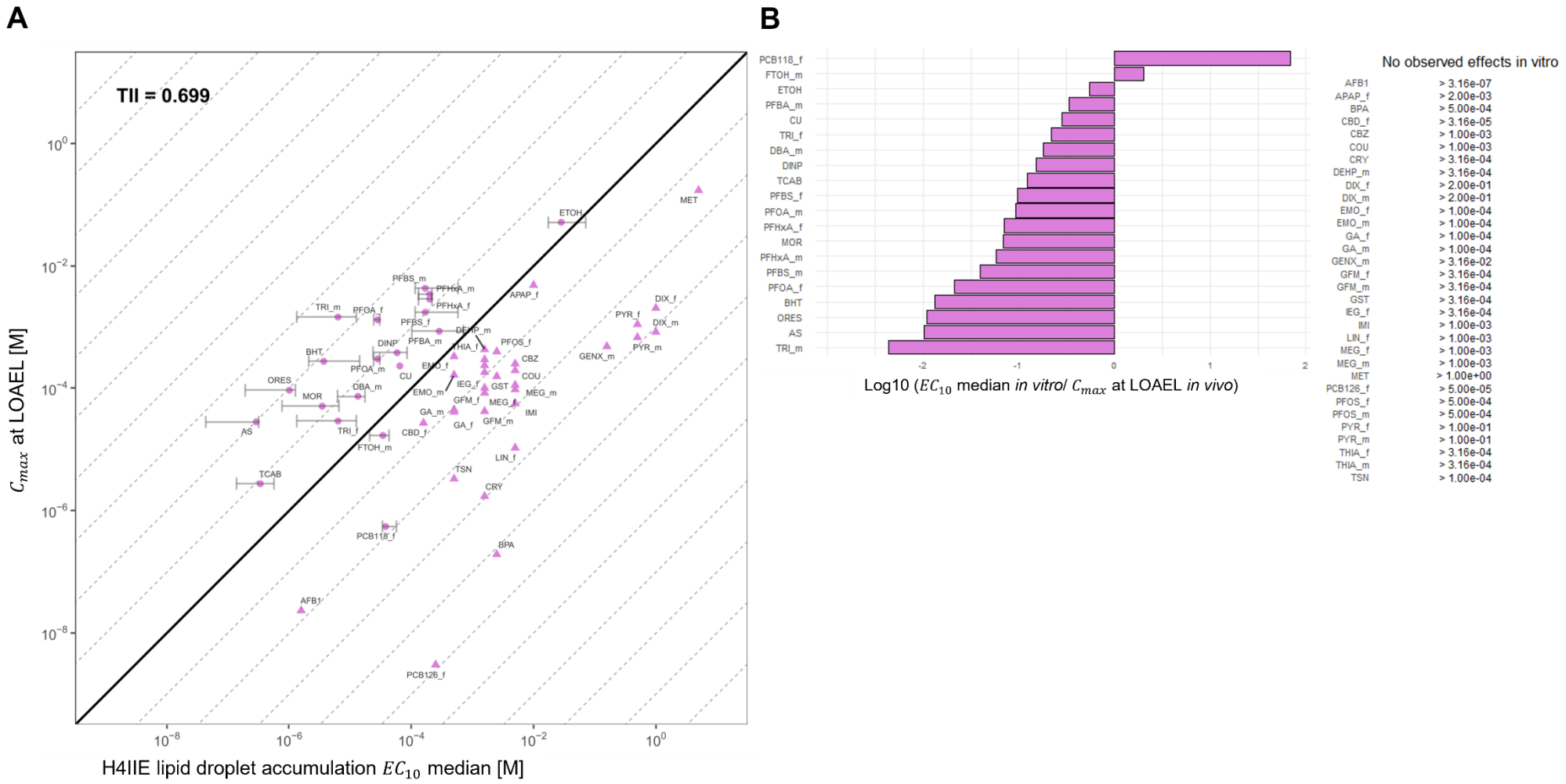

Figure 30 *In vitro–in vivo* extrapolation plot of H4IIE lipid droplet accumulation and portal vein plasma concentrations

A Extrapolation plot of the median EC_{10} values (n = at least 3 independent experiments) and the modeled Cmax at LOAEL with logarithmic scales on both axes. Error bars represent the minimum and maximum EC_{10} values. The black solid line represents the line of identity. Gray dashed lines mark constant factor differences (in decadic log scale) of the EC_{10} and Cmax values. Each line corresponds to a 10^n-fold deviation from the line of identity (n = ±1, ±2, etc.). Compounds with no observed effect *in vitro* were assigned a penalty (5× highest tested concentration) and shown as triangles; those with effects appear as circles. **B** Ratio plot displaying the EC_{10}/Cmax ratios on a decadic logarithmic scale. Only positive test results without penalties were compared. For substances with no observed effects, the highest tested concentration (in molarity, M) is listed beside the ratio plot. All data points and bars are colored in pink, denoting the lipid droplet accumulation assay.

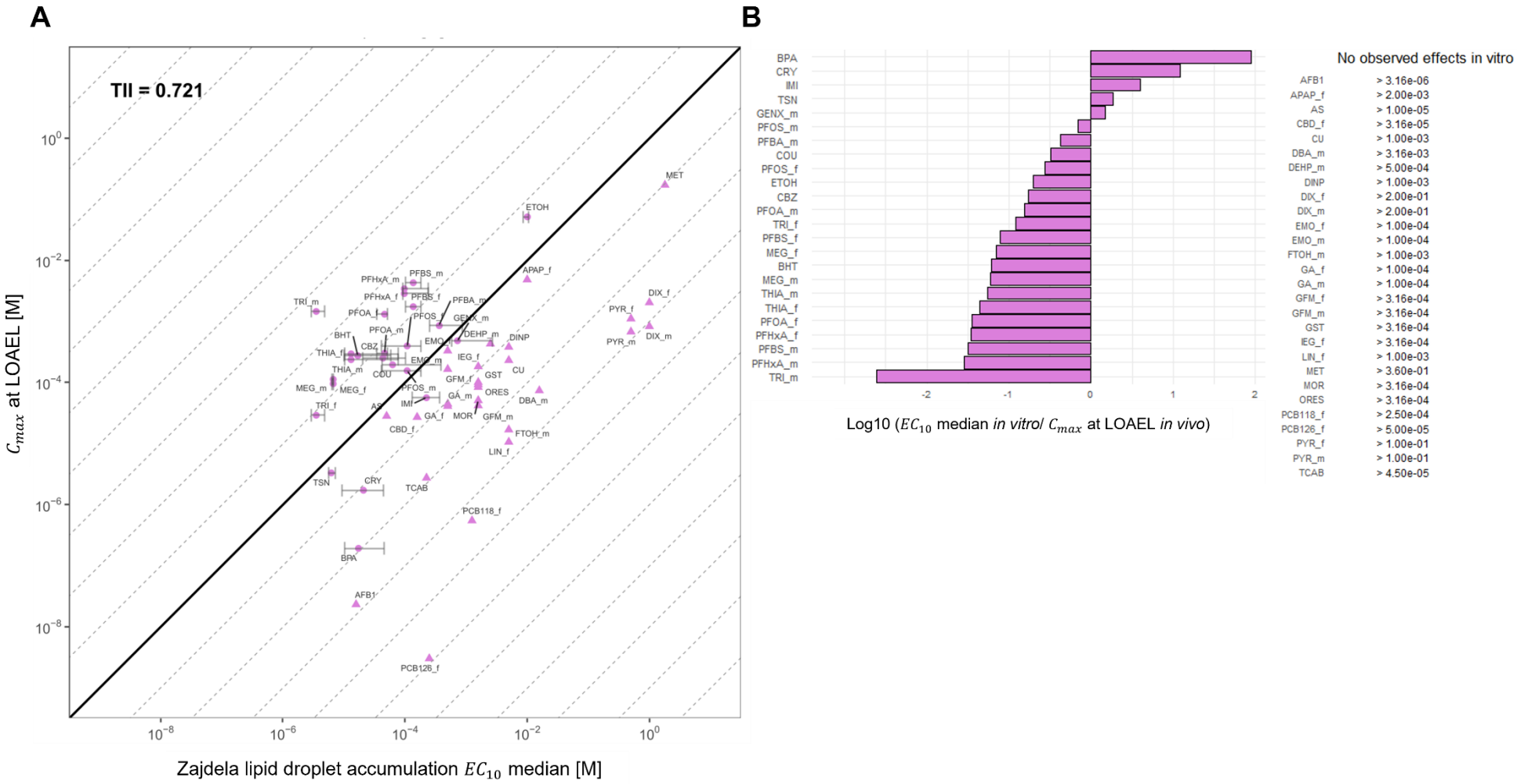

Figure 31 ***In vitro–in vivo*** **extrapolation plot of Zajdela lipid droplet accumulation and portal vein plasma concentrations**

A Extrapolation plot of the median EC_{10} values (n = at least 3 independent experiments) and the modeled Cmax at LOAEL with logarithmic scales on both axes. Error bars represent the minimum and maximum EC_{10} values. The black solid line represents the line of identity. Gray dashed lines mark constant factor differences (in decadic log scale) of the EC_{10} and Cmax values. Each line corresponds to a 10^n-fold deviation from the line of identity (n = ±1, ±2, etc.). Compounds with no observed effect *in vitro* were assigned a penalty (5× highest tested concentration) and shown as triangles; those with effects appear as circles. **B** Ratio plot displaying the EC_{10}/Cmax ratios on a decadic logarithmic scale. Only positive test results without penalties were compared. For substances with no observed effects, the highest tested concentration (in molarity, M) is listed beside the ratio plot. All data points and bars are colored in pink, denoting the lipid droplet accumulation assay.

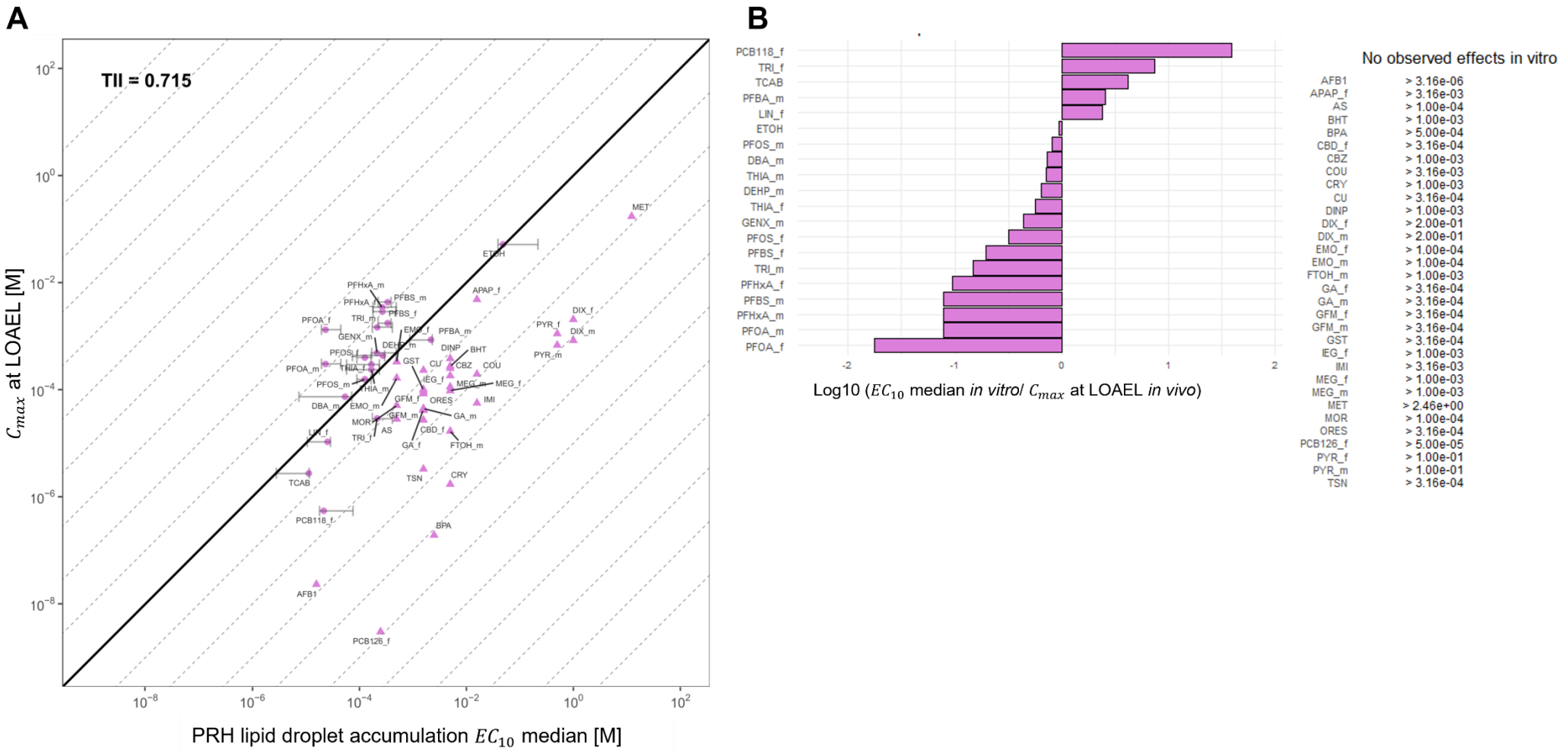

Figure 32 *In vitro–in vivo* extrapolation plot of primary rat hepatocytes lipid droplet accumulation and portal vein plasma concentrations

A Extrapolation plot of the median EC_{10} values (n=3 independent experiments) and the modeled Cmax at LOAEL with logarithmic scales on both axes. Error bars represent the minimum and maximum EC_{10} values. The black solid line represents the line of identity. Gray dashed lines mark constant factor differences (in decadic log scale) of the EC_{10} and Cmax values. Each line corresponds to a 10^n-fold deviation from the line of identity (n = ±1, ±2, etc.). Compounds with no observed effect *in vitro* were assigned a penalty (5× highest tested concentration) and shown as triangles; those with effects appear as circles. **B** Ratio plot displaying the EC_{10}/Cmax ratios on a decadic logarithmic scale. Only positive test results without penalties were compared. For substances with no observed effects, the highest tested concentration (in molarity, M) is listed beside the ratio plot. All data points and bars are colored in pink, denoting the lipid droplet accumulation assay.

3.4.1.3 Nuclear enumeration assay (Hoechst): *In vitro–in vivo* extrapolation

3.4.1.3.1 H4IIE

For the Hoechst assay in H4IIE cells (**Figure 33**), a total of 47 *in vitro–in vivo* pairs were available for comparison, resulting in a toxicity iso-concentration index of 0.83. In general, *in vitro* concentrations tended to be lower than *in vivo* concentrations; however, for 17 of the 47 pairs, the *in vivo* concentration was lower than the *in vitro* value. Most showed good agreement: 20 substances fell within a 3.16-fold deviation, including MEG, PFBA_m, CBZ, and GENX_m as particularly well-matched examples. An additional 15 pairs deviated between 3.16- and 10-fold, indicating that well over half of the compounds remained within a tenfold range. However, stronger deviations were observed for a few substances: BPA and PCB118_f exceeded a 100-fold difference, while DIX and PYR, APAP, and TRI_m also showed notable discrepancies, mostly in the 10- to 100-fold range.

3.4.1.3.2 Zajdela

The comparison of *in vitro* Hoechst assay results with portal vein plasma concentrations in Zajdela cells (**Figure 34**) yielded 37 usable compound pairs and resulted in a TII of 0.80. Interestingly, 21 of these pairs exhibited lower *in vivo* concentrations than their *in vitro* counterparts. One standout result is PCB126_f, which showed a lower level of over 10,000-fold lower *in vivo* concentration than *in vitro*. Similarly, BPA exhibited a significant discrepancy, with its *in vivo* concentration being more than 100-fold lower than the *in vitro* measurement. Other compounds such as PFHxA also showed large deviations, with *in vivo* concentrations more than 100-fold lower than *in vitro*. However, many compounds (more than 50 %) exhibited deviations of less than 10-fold. The remaining substances showed discrepancies between 10- and 100-fold. Notably, several substances were very well matched between *in vitro* and *in vivo* concentrations, particularly ORES, BHT, PFOS_f, DIX_f and GA which all fell within a 3.16-fold deviation.

3.4.1.3.3 Primary rat hepatocytes

In primary rat hepatocytes, a total of 25 *in vitro–in vivo* pairs were available for the Hoechst assay comparison, yielding a toxicity iso-concentration index of 0.76. In most cases, *in vivo* concentrations were lower than their *in vitro* counterparts, with BP) standing out by exhibiting an almost 1000-fold lower concentration *in vivo*. Many substances showed good agreement, with most falling within a 3.16-fold deviation. The best-matched compounds included GST, BHT, and PFBS_m. An additional eight compounds deviated by less than a factor of 10, while six substances (e.g., PYR, CRY) fell between a 10- and 100-fold deviation.

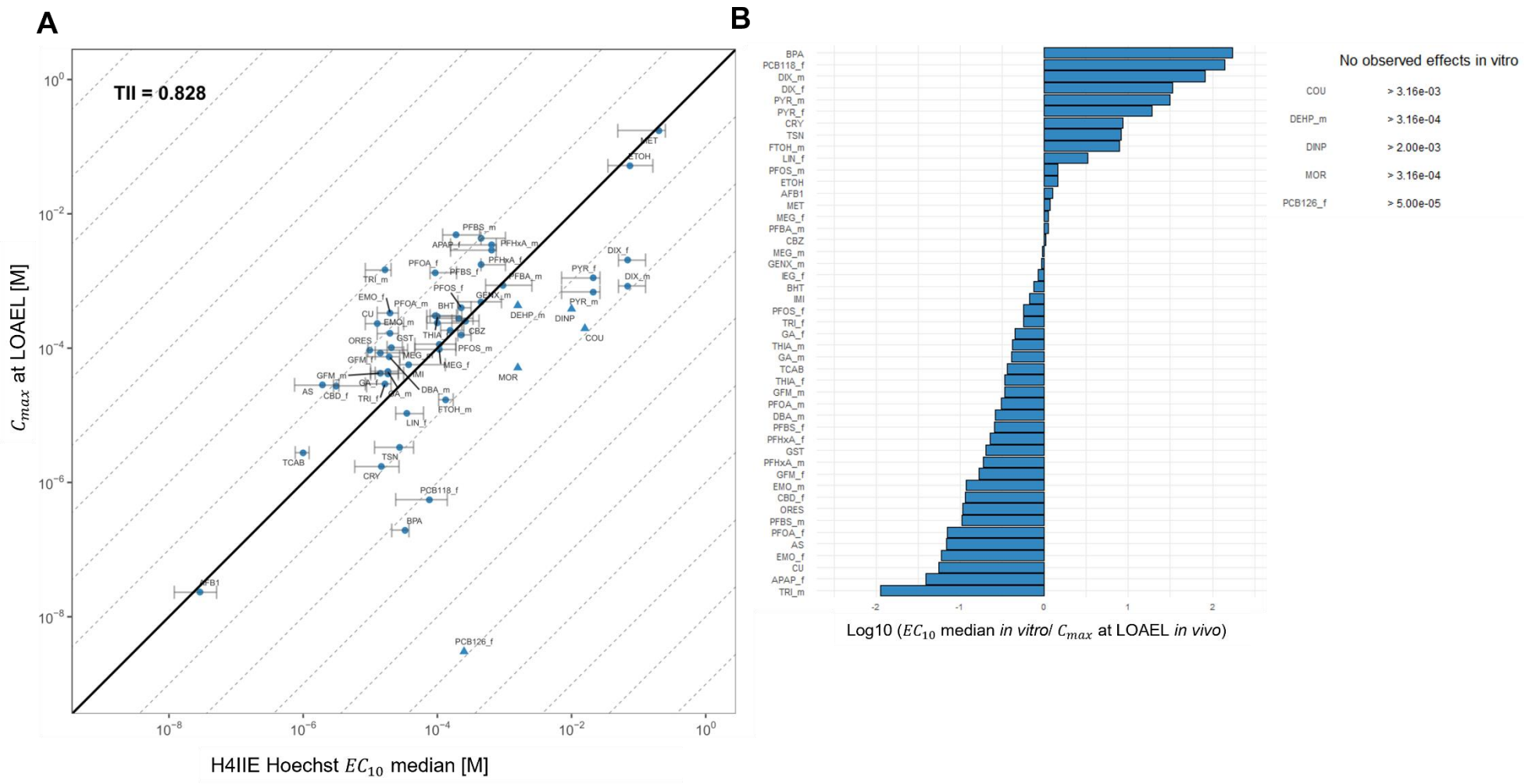

Figure 33 *In vitro–in vivo* extrapolation plot of H4IIE Hoechst and portal vein plasma concentrations

A Extrapolation plot of the median EC_{10} values (n = at least 3 independent experiments) and the modeled Cmax at LOAEL with logarithmic scales on both axes. Error bars represent the minimum and maximum EC_{10} values. The black solid line represents the line of identity. Gray dashed lines mark constant factor differences (in decadic log scale) of the EC_{10} and Cmax values. Each line corresponds to a 10^n-fold deviation from the line of identity (n = ±1, ±2, etc.). Compounds with no observed effect *in vitro* were assigned a penalty (5× highest tested concentration) and shown as triangles; those with effects appear as circles. **B** Ratio plot displaying the EC_{10}/Cmax ratios on a decadic logarithmic scale. Only positive test results without penalties were compared. For substances with no observed effects, the highest tested concentration (in molarity, M) is listed beside the ratio plot. All data points and bars are colored in blue, denoting the nuclear enumeration staining via Hoechst.

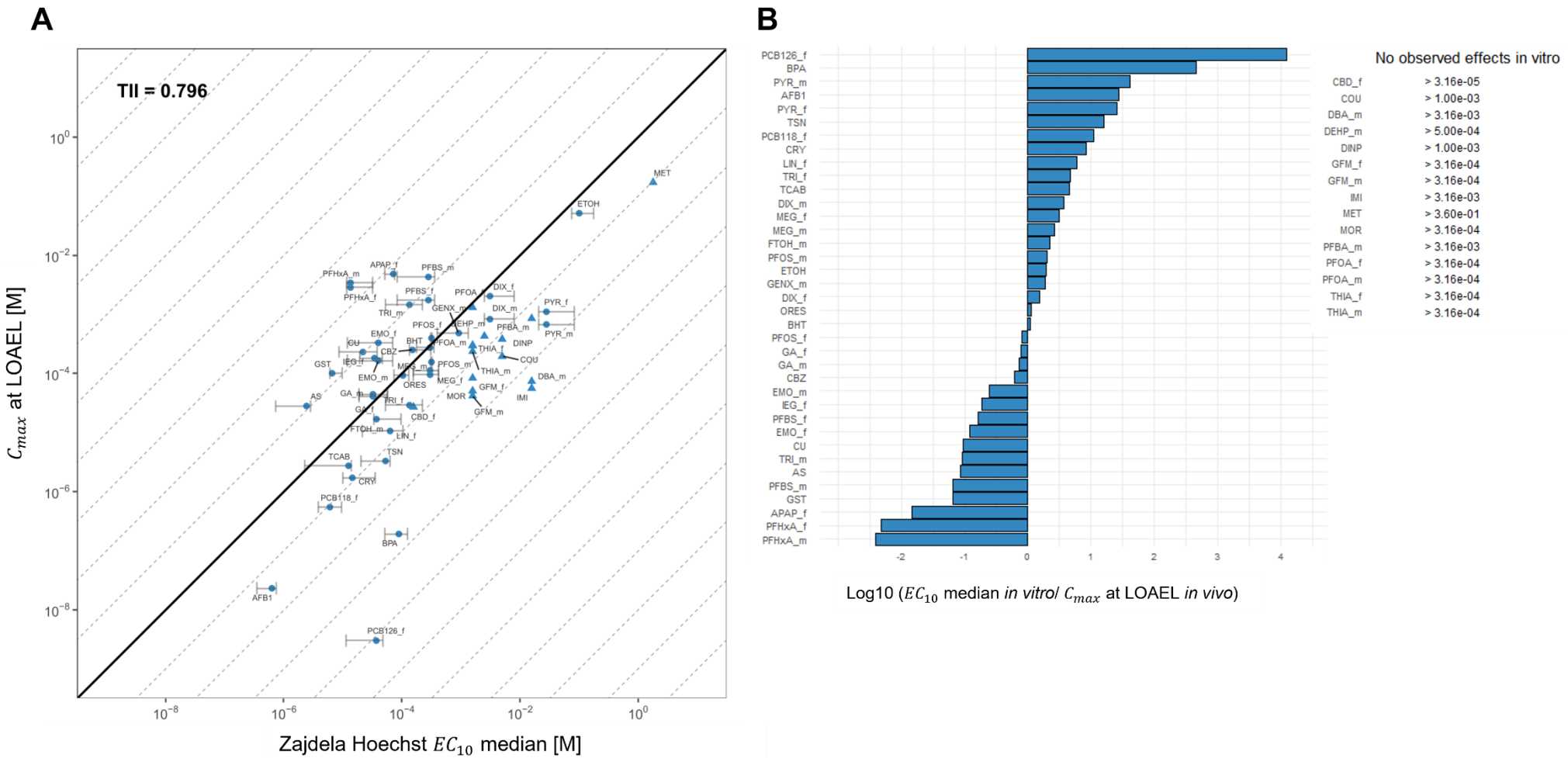

Figure 34 *In vitro–in vivo* extrapolation plot of Zajdela Hoechst and portal vein plasma concentrations

A Extrapolation plot of the median EC_{10} values (n = at least 3 independent experiments) and the modeled Cmax at LOAEL with logarithmic scales on both axes. Error bars represent the minimum and maximum EC_{10} values. The black solid line represents the line of identity. Gray dashed lines mark constant factor differences (in decadic log scale) of the EC_{10} and Cmax values. Each line corresponds to a 10^n-fold deviation from the line of identity (n = ±1, ±2, etc.). Compounds with no observed effect *in vitro* were assigned a penalty (5× highest tested concentration) and shown as triangles; those with effects appear as circles. **B** Ratio plot displaying the EC_{10}/Cmax ratios on a decadic logarithmic scale. Only positive test results without penalties were compared. For substances with no observed effects, the highest tested concentration (in molarity, M) is listed beside the ratio plot. All data points and bars are colored in blue, denoting the nuclear enumeration staining via Hoechst.

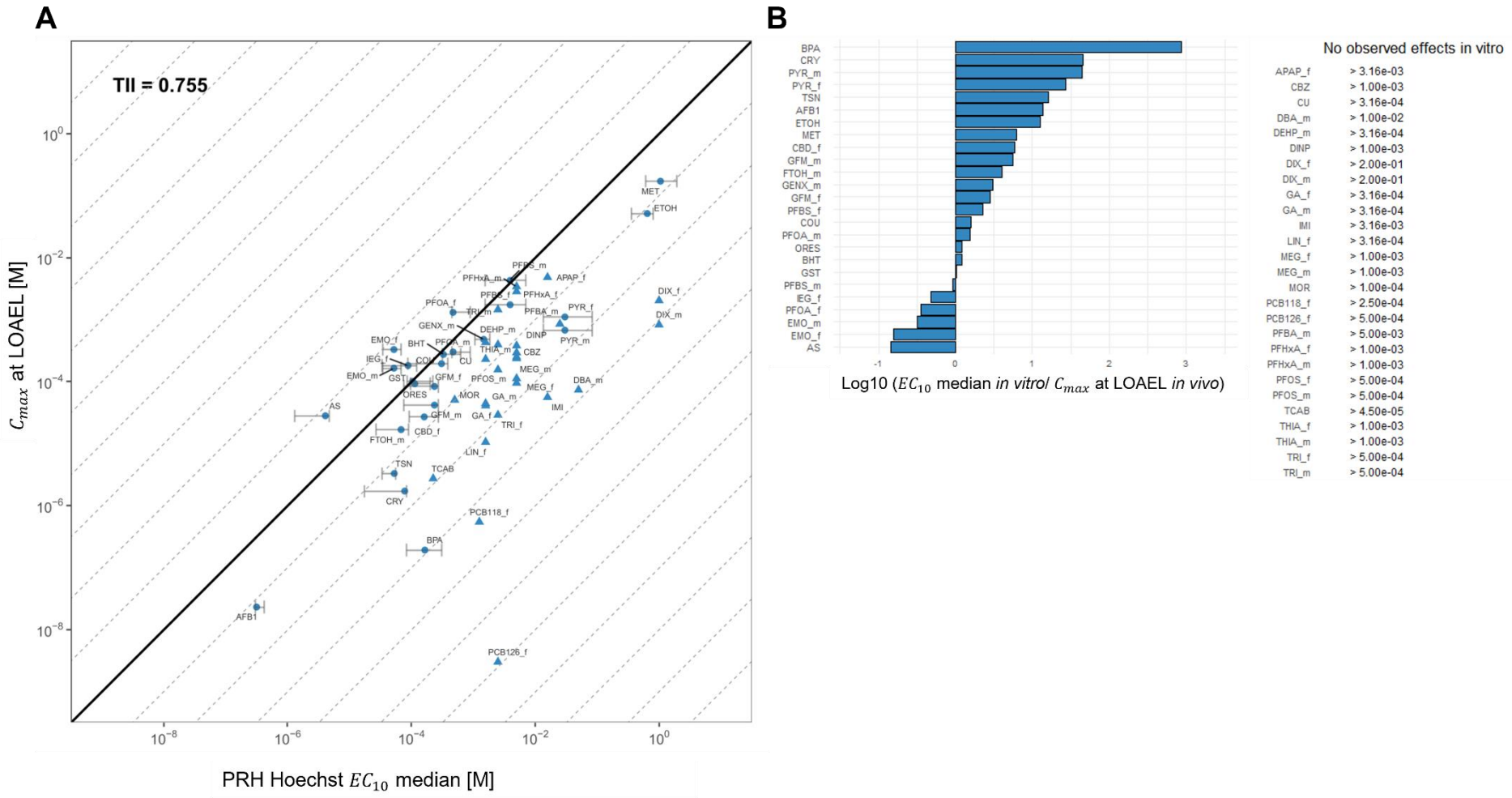

Figure 35 *In vitro–in vivo* extrapolation plot of primary rat hepatocytes Hoechst and portal vein plasma concentrations

A Extrapolation plot of the median EC_{10} values (n = at least 3 independent experiments) and the modeled Cmax at LOAEL with logarithmic scales on both axes. Error bars represent the minimum and maximum EC_{10} values. The black solid line represents the line of identity. Gray dashed lines mark constant factor differences (in decadic log scale) of the EC_{10} and Cmax values. Each line corresponds to a 10^n-fold deviation from the line of identity (n = ±1, ±2, etc.). Compounds with no observed effect *in vitro* were assigned a penalty (5× highest tested concentration) and shown as triangles; those with effects appear as circles. **B** Ratio plot displaying the EC_{10}/Cmax ratios on a decadic logarithmic scale. Only positive test results without penalties were compared. For substances with no observed effects, the highest tested concentration (in molarity, M) is listed beside the ratio plot. All data points and bars are colored in blue, denoting the nuclear enumeration staining via Hoechst.

3.4.1.4 Lowest observed effective concentration (LOEC) across assays: *In vitro–in vivo* extrapolation

The final analysis compares the lowest observed effective concentration for each compound across the three readouts (cytotoxicity, lipid droplet accumulation, and nuclear enumeration via Hoechst staining) in a cell system with the portal vein plasma concentration at the LOAEL. For this purpose, scatter- and ratio-plots were again prepared (**Figure 36** - **Figure 38**). The color of the dots/triangles and bars corresponds to the readout with the lowest effective concentration.

3.4.1.4.1 H4IIE

The analysis of the LOECs in H4IIE cells revealed a TII of 0.81 (**Figure 36**). Notably, *in vitro* concentrations tended to be lower than *in vivo* values. This trend was especially apparent for the Nile red assay, which contributed most of the lowest *in vitro* values. For example, TRI_m showed an over 100-fold lower *in vitro* concentration compared to *in vivo*. In contrast, cases where *in vivo* concentrations were lower were largely driven by the CTB assay, with PCB126_f exceeding a 10,000-fold difference and BPA approaching a 100-fold deviation. The Hoechst assay yielded more moderate results, with many compounds deviating by less than a factor of 3.16 and none surpassing 31.6. Interestingly, the Nile red assay's lowest *in vitro* values were predominantly observed for PFAS compounds.

3.4.1.4.2 Zajdela

In the Zajdela cell system, the analysis of minimum effective concentrations yielded a TII of 0.82 (**Figure 37**). Again *in vitro* concentrations were lower than *in vivo* concentrations. This pattern was predominantly observed in the Nile red assay, which contributed most of the lowest *in vitro* values. Some compounds showed substantial deviations, especially when the minimum concentration originated from the Hoechst assay e.g., APAP and PFHXA displayed deviations ranging from 31.6-fold to over 100-fold. As observed in previous analyses, PCB126_f stood out with the largest discrepancy, approaching almost 10,000-fold deviation. BPA also showed a pronounced deviation, nearing the 100-fold threshold. Notable best matches included ORES, MET, GFM, and PFOS_m.

3.4.1.4.3 Primary rat hepatocytes

The minimum effective concentrations observed in primary rat hepatocytes yielded a TII of 0.781 (**Figure 38**). Once again, *in vitro* concentrations tended to be lower than *in vivo* values. The lowest *in vitro* concentrations were predominantly associated with the Nile red assay. Notable deviations included BPA, which showed an over 100-fold lower concentration *in vivo* compared to *in vitro*, and DIX_f, with nearly a 100-fold discrepancy in the same direction. Conversely, substantial *in vitro* underestimations were observed for PFOA_f, nearing a 100-

fold deviation, and EMO_f, with a deviation between 10- and 31.6-fold. Strong matches included ETOH, BHT, COU, and GFM_f.

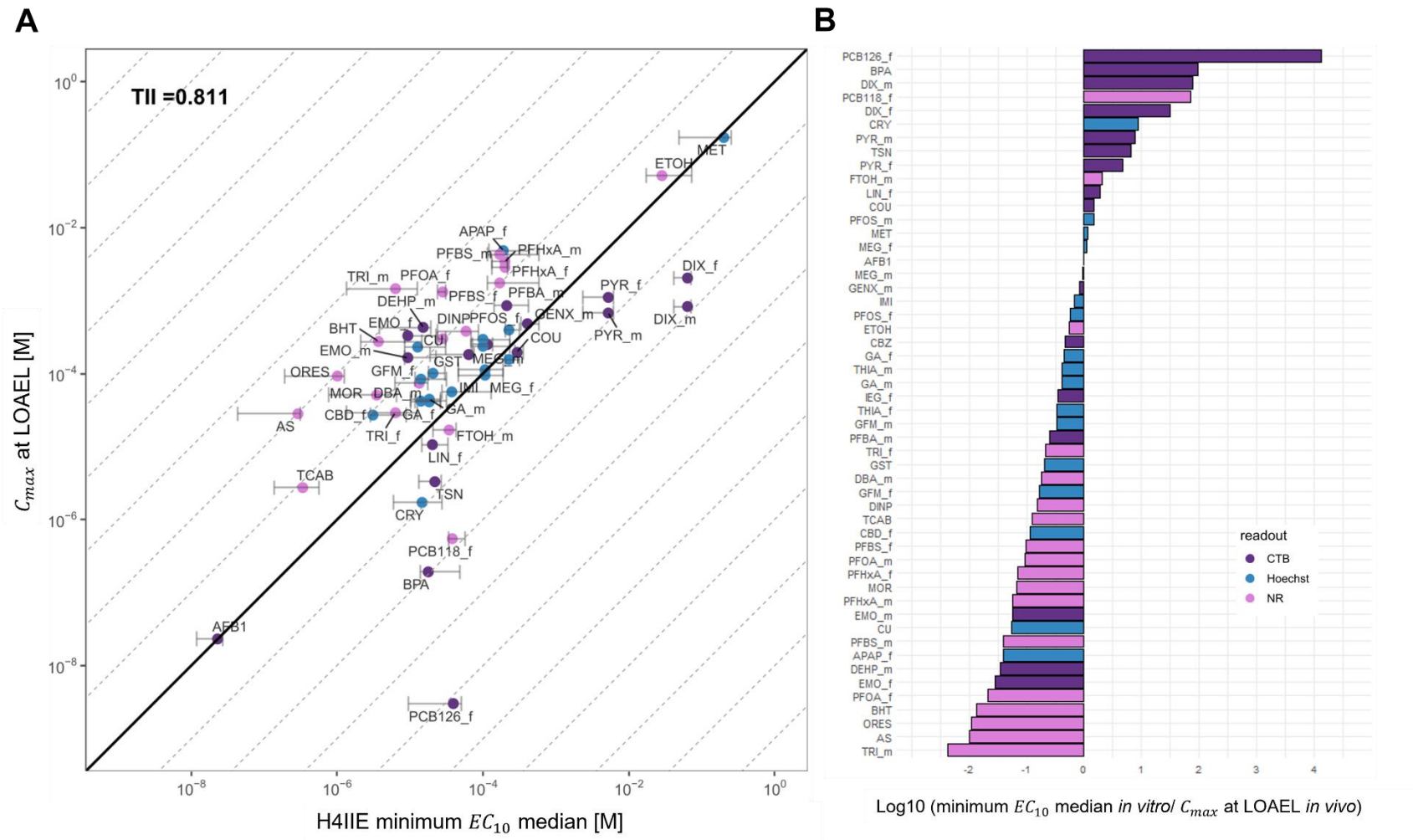

Figure 36 *In vitro–in vivo* extrapolation plot of minimum EC10 value across assays in H4IIE cells

A Extrapolation plot of the median EC_{10} values (n = at least 3 independent experiments) and the modeled Cmax at LOAEL with logarithmic scales on both axes. Error bars represent the minimum and maximum EC_{10} values. The black solid line represents the line of identity. Gray dashed lines mark constant factor differences (in decadic log scale) of the EC_{10} and Cmax values. Each line corresponds to a 10^n-fold deviation from the line of identity (n = ±1, ±2, etc.). Compounds with no observed effect *in vitro* were assigned a penalty (5× highest tested concentration) and shown as triangles; those with effects appear as circles. **B** Ratio plot displaying the EC_{10}/Cmax ratios on a decadic logarithmic scale. Only positive test results without penalties were compared. For substances with no observed effects, the highest tested concentration (in molarity, M) is listed beside the ratio plot.

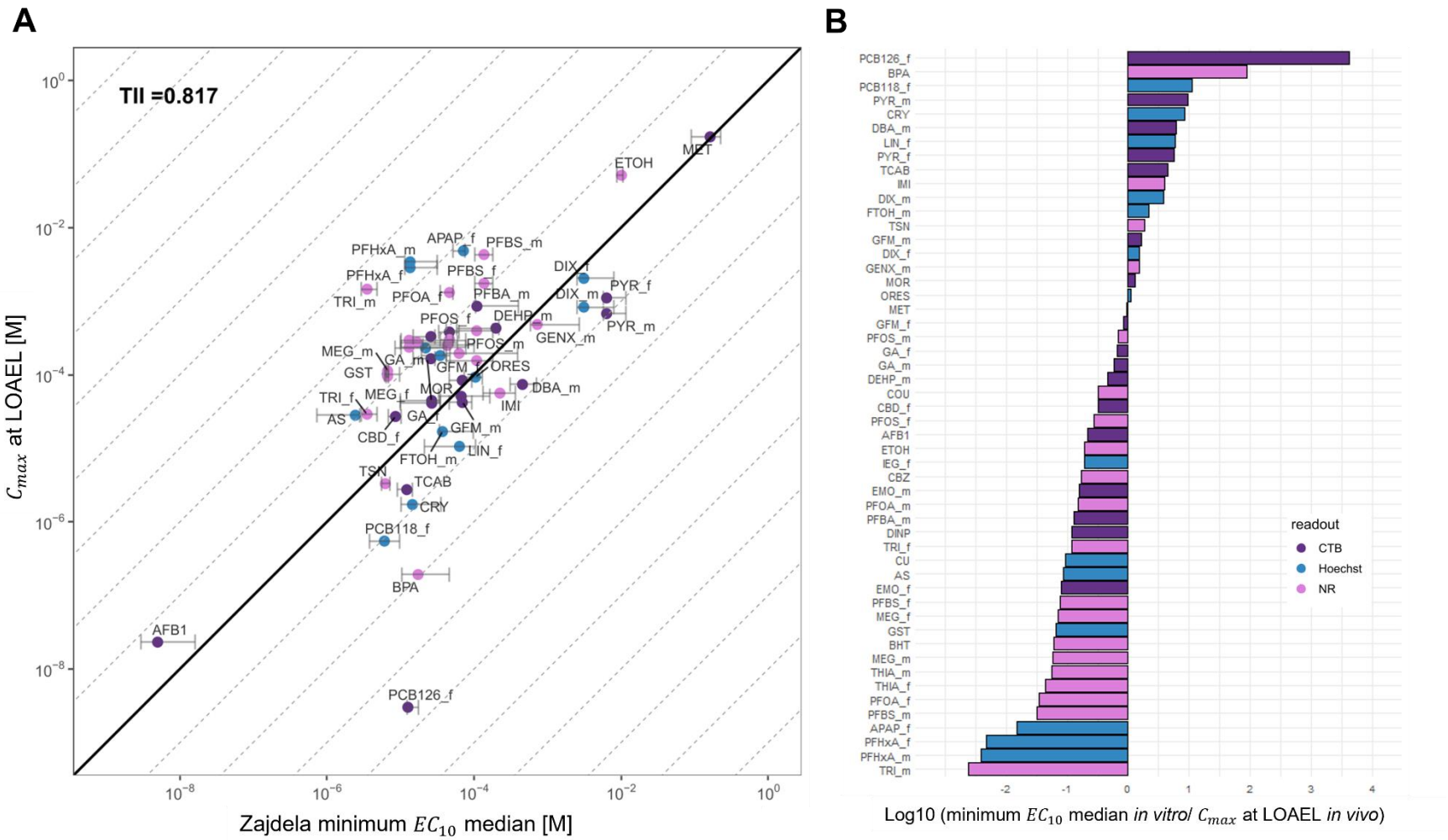

Figure 37 *In vitro–in vivo* extrapolation plot of minimum EC10 value across assays in Zajdela cells

A Extrapolation plot of the median EC_{10} values (n = at least 3 independent experiments) and the modeled Cmax at LOAEL with logarithmic scales on both axes. Error bars represent the minimum and maximum EC_{10} values. The black solid line represents the line of identity. Gray dashed lines mark constant factor differences (in decadic log scale) of the EC_{10} and Cmax values. Each line corresponds to a 10^n-fold deviation from the line of identity (n = ±1, ±2, etc.). Compounds with no observed effect *in vitro* were assigned a penalty (5× highest tested concentration) and shown as triangles; those with effects appear as circles. **B** Ratio plot displaying the EC_{10}/Cmax ratios on a decadic logarithmic scale. Only positive test results without penalties were compared. For substances with no observed effects, the highest tested concentration (in molarity, M) is listed beside the ratio plot.

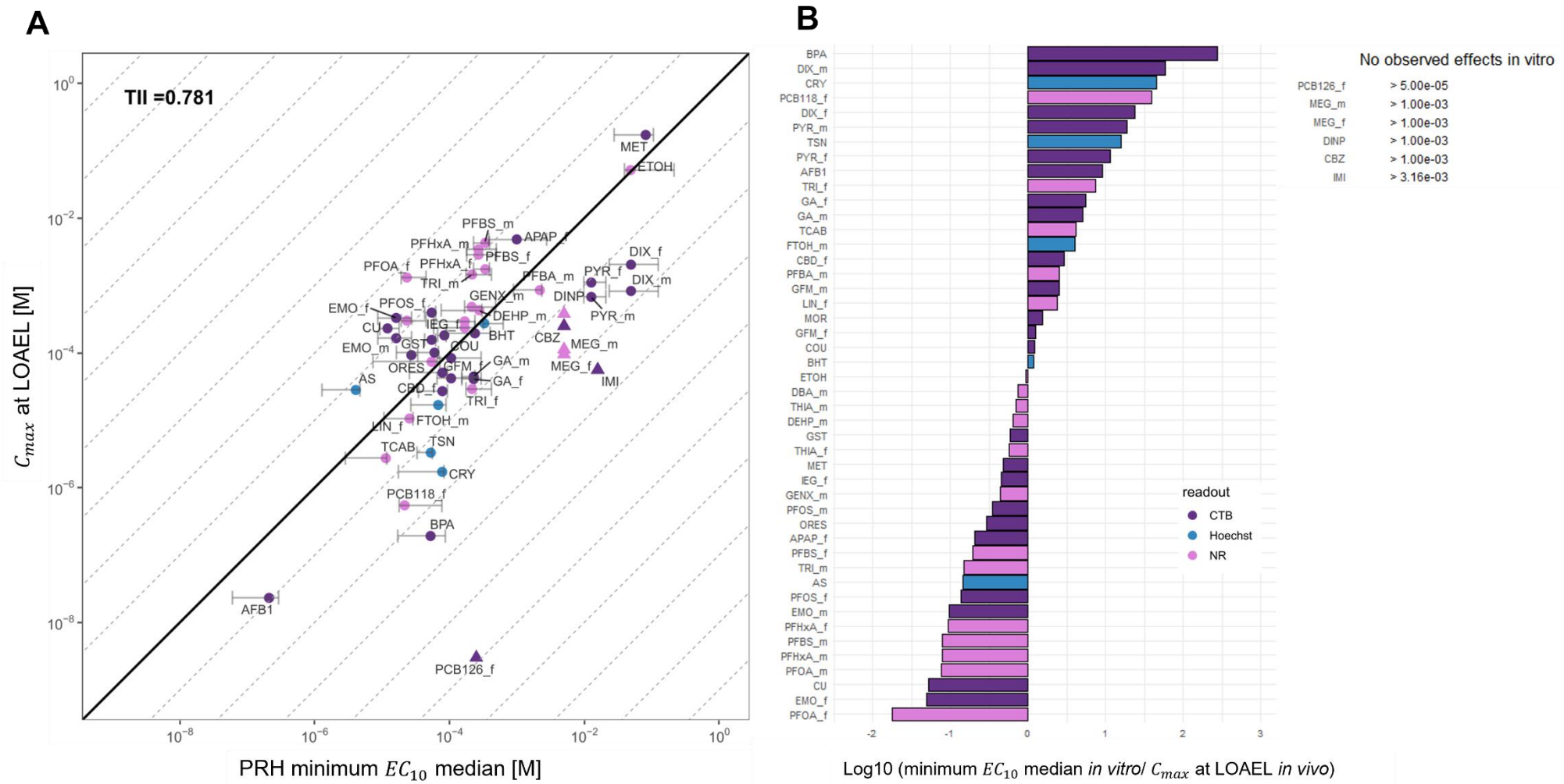

Figure 38 *In vitro–in vivo* extrapolation plot of minimum EC10 value across assays in primary rat hepatocytes

A Extrapolation plot of the median EC_{10} values (n = at least 3 independent experiments) and the modeled Cmax at LOAEL with logarithmic scales on both axes. Error bars represent the minimum and maximum EC_{10} values. The black solid line represents the line of identity. Gray dashed lines mark constant factor differences (in decadic log scale) of the EC_{10} and Cmax values. Each line corresponds to a 10^n-fold deviation from the line of identity (n = ±1, ±2, etc.). Compounds with no observed effect *in vitro* were assigned a penalty (5× highest tested concentration) and shown as triangles; those with effects appear as circles. **B** Ratio plot displaying the EC_{10}/Cmax ratios on a decadic logarithmic scale. Only positive test results without penalties were compared. For substances with no observed effects, the highest tested concentration (in molarity, M) is listed beside the ratio plot.

3.4.1.5 Conclusion of *in vitro–in vivo* analysis

Finally, the main results of the *in vitro–in vivo* analyses are summarized in **Table 25**. The table provides a summary of all TIIs and categorizes the *in vitro–in vivo* pairs according to deviation factors (< 3.16, 3.16-10, 10-100 and >100). In general, *in vitro* concentrations tend to be lower than their *in vivo* counterparts. The Nile red test often provides the lowest observed effect concentrations. This often leads to underestimation of certain compounds, especially PFAS (e.g. PFOA, PFBS, PFHxA, MEG, BHT, TRI_m). H4IIE cells showed the highest TII in cytotoxicity but the lowest in the lipid droplet accumulation assay, with no improvement when the readouts were combined. Zajdela cells showed a similar pattern, with the highest TII in cytotoxicity, but better performance in the lipid droplet accumulation assay (TII 0.72) and the Hoechst assay (TII 0.80), with no improvement from combining the readouts. For primary hepatocytes, the highest TII was found for the readout combination, while the lowest was found for the Nile red assay.

Table 25 Overview of toxicity iso-concentration indices and fold deviations

Percentages of fold deviations refer to the number of in *vitro–in vivo* pairs within the respective deviation range, normalized to the total number of pairs for each condition.
PRH – Primary rat hepatocytes, TII – Toxicity Iso-concentration Index

	TII	< 3.16 [%]	3.16 - 10 [%]	10 - 100 [%]	> 100 [%]	Total no. of *in vitro-in vivo* pairs
Cytotoxicity						
H4IIE	0.86	50.0	25.0	21.2	3.8	52
Zajdela	0.85	40.4	34.6	19.2	5.8	52
PRH	0.77	36.8	26.3	34.2	2.6	38
Lipid droplet accumulation						
H4IIE	0.70	15	25	55	5	20
Zajdela	0.72	20.8	25.0	50.0	4.2	24
PRH	0.72	50	20	30	0	20
Hoechst						
H4IIE	0.83	42.6	31.9	21.3	4.3	47
Zajdela	0.80	32.4	27.0	29.7	10.8	37
PRH	0.76	44	28	24	4	25
Readout minimum						
H4IIE	0.81	36.5	23.1	36.5	3.8	52
Zajdela	0.82	25	38.5	32.7	3.8	52
PRH	0.78	39.1	26.1	32.6	2.2	46

4 Discussion

4.1 A novel approach methodology (NAM) tailored to the organ-and species-specific evaluation of hepatotoxicity in the rat

In this thesis, a combined *in vitro–in silico* approach for simulating rat hepatotoxicity in relation to oral doses and peak concentrations in the portal vein at hepatotoxic LOAELs is presented. The strategy integrates an *in vitro* test battery covering hepatotoxicity-relevant endpoints, physiologically based pharmacokinetic modeling, and 40 well-defined hepatic LOAELs in rats, derived using a structured scoring system (SOS). A custom performance metric (TII) was developed to support system refinement and evaluate the concordance between datasets. In contrast to the correlation coefficient (R^2), which merely describes the direction and strength of a relationship, the TII provides a direct, log-scaled measure of the actual agreement between *in vitro* and *in vivo* concentrations.

For the best-performing cell system (H4IIE) and assay (cytotoxicity) (**Figure 27**), with a TII of 0.86, a geometric mean fold error (GMFE) of 5.3 (GSD: 5.5) was obtained, indicating a strong, albeit slightly variable agreement between *in vitro* and *in vivo* concentrations. This means, for these test substances, for this specific assay and cell system, the *in vivo* concentrations can be simulated within a 5.3-fold deviation (± 5.5-fold) from the *in vitro* concentrations, indicating that the *in vitro* measurements can predict *in vivo* levels within this range of variability. Of the 52 *in vitro–in vivo* pairs analyzed, 50 % showed deviations below a 3.16-fold difference, 25 % fell between 3.16- and 10-fold, 21 % between 10- and 100-fold, and only 3.8 % exceeded a 100-fold difference. This distribution falls within the range commonly reported for PBPK model performance in early drug development, where deviations within 2- to 3-fold are generally targeted and errors up to 10-fold are still considered acceptable in many contexts (Chang et al. 2022; Naga et al. 2022). The results demonstrate a high degree of predictability for many compounds, a characteristic drop-off across intermediate error ranges, and very few extreme outliers—indicating strong overall model performance. Given the large chemical space covered by this compound set, the outcome can be considered notably robust.

The resulting dataset provides species- and organ-specific concentration–effect data, which could enrich regulatory and public resources such as the European Chemicals Agency (ECHA), PubChem, or the CompTox Chemicals Dashboard. Additionally, this dataset could serve as a valuable training set for machine learning models designed to predict the hepatotoxicity of untested compounds, ultimately contributing to more efficient, animal-free chemical safety assessments.

4.2 From human to rat: adaptation of an *in vitro–in silico*-based hepatotoxicity evaluation strategy

The *in vitro–in silico* test strategy applied in this study was adapted from a previously published approach by Albrecht et al. (2019), which demonstrated promising predictive performance for human drug-induced liver injury (Brecklinghaus et al. 2022a,b; Albrecht et al. 2025). Unlike in humans, where hepatotoxic effects are often identified retrospectively based on clinical outcomes, frequently without precise knowledge of the corresponding doses or blood concentrations, rodent studies offer a more complete toxicological framework. In sub chronic *in vivo* studies, such as all-organ toxicity studies (e.g., OECD 408 (OECD 2018)), it is possible to derive liver-specific LOAELs that are experimentally defined and quantitatively linked to known oral doses. This availability of both thresholds and dosing information opens the opportunity to simulate peak concentrations in portal vein plasma at the lowest observed effect level (LOAEL) of hepatotoxicity. The simulated *in vivo* concentrations can then be directly compared to effective concentrations obtained from an *in vitro* test battery (including cytotoxicity testing, lipid droplet accumulation, nuclear enumeration via Hoechst staining) with hepatocyte models, allowing for a quantitative evaluation of concordance between the *in vivo* and *in vitro* concentrations. The portal vein was selected as the primary site of interest because it directly reflects the concentration reaching the liver after intestinal absorption. Among the various blood compartments that can be simulated with the modeling software (e.g., whole blood/plasma, systemic blood/plasma, or liver tissue) the portal vein offers the most physiologically relevant estimate for hepatic exposure and first-pass metabolism, as it represents the immediate influx of substances into the liver (Bonkovsky et al. 2012).

Based on this rationale, the present study addresses the following key questions (see **Figure 39**): (1) Can the human *in vitro–in silico* approach be transferred to a different species (rat) and substance set (food-relevant compounds)? (2) Can heterogeneous *in vivo* data be integrated into a consistent LOAEL estimate using systematic approaches? (3) Which cell system (cell lines vs. primary hepatocytes) provides the best *in vitro* to *in vivo* correlation? (4) Can combining multiple readouts improve the overall TII?

Aim: Simulation of an organ- and species-specific Cmax at the LOAEL in portal vein plasma using *in vitro–in silico* methods	
Transferability	Is the human *in vitro–in silico* approach of Albrecht et al. 2019 transferable to a different species and substance set ? *In vitro* hepatotoxicity screening with 3 rat hepatocyte models and 40 hepatotoxic test compounds All test compounds comply with Lipinski's rule of five and are considered drug-like The *in vitro–in silico* approach is transferable to both rat models and the food-relevant compounds
Data integration	Can heterogeneous *in vivo* data be integrated into a consistent LOAEL estimate? Introduction of the Score of Significane (SOS) Yes, the SOS allows for the consistent definition of liver-specific LOAELs
System performance	Which cell systems yields higher agreement between *in vitro* and *in vivo* data – cell lines or primary hepatocytes? TII comparison across cell systems Cell lines yielded higher agreement with *in vivo* data (TII > 0.8), primary hepatocytes showed lower TII values (< 0.8) Which test system-readout combination achieves the highest TII? TII comparison across cell systems The highest TII (0.86) was observed for cytotoxicity measured in the H4IIE cell line.
Readout combination	Can combining multiple readouts improve the overall TII? LOEC vs. simulated Cmax at LOAEL (portal vein) No improvement in cell lines; PRH showed a slight increase (although: TII < 0.8).
Conclusion: Simulation of Cmax at the LOAEL using effective *in vitro* concentrations in the rat for the test set was feasible.	

Figure 39 Overview of the test strategy
Cmax – peak concentration, LOEC – Lowest Observed Effect Concentration (*in vitro*), LOAEL – Lowest Observed Adverse Effect Level, PRH – Primary rat hepatocytes, SOS – Score of Significance, TII – Toxicity Iso-concentration Index

(1) Can the human in vitro–in silico approach be transferred to a different species (rat) and substance set (food-relevant compounds)?

The approach was successfully transferred to the rat context, utilizing three rat hepatocyte cell systems: two cancer cell lines (H4IIE and Zajdela) and primary rat hepatocytes. The *in vitro* test battery was adapted to the specific characteristics of each cell system. For all substances in the cell lines, reproducible results were obtained in at least three replicates, with maximum deviations of a factor of 5 for the EC_{10} median in the cell lines and a factor of 10 in primary hepatocytes. All compounds comply with the Lipinski's rule of five (Lipinski et al. 2001) according to the ChEMBL database (Zdrazil et al. 2024), with up to one permissible violation, primarily related to LogP deviations > 5 (see Supplement 1). Thus, the selected substances can be considered drug-like according to the rule of five, although no data was available for the elements As and Cu.

(2) Can heterogeneous in vivo data be integrated into a consistent LOAEL estimate using systematic approaches?

To address this, the Score of Significance (SOS) was introduced as a transparent system for deriving organ-specific LOAELs. The SOS was developed based on established criteria for hepatotoxicity determination, with effects categorized into primary and secondary according to their toxicological relevance (Ramaiah 2007; Singh et al. 2014; McInnes 2017; NTP Archives 2023). Primary effects are those that directly indicate liver damage, while secondary effects, such as changes in liver weight or total bilirubin, are not sufficient by themselves to define LOAELs. For instance, liver weight changes are considered secondary and only contribute to LOAEL determination when combined with primary effects. Total bilirubin levels are relevant only when differentiated into direct and indirect bilirubin, with only the direct form being indicative of liver injury. Hepatocyte hypertrophy is considered relevant for liver damage only when accompanied by increased cholesterol, triglycerides, or transaminases, or when localized in specific regions of the liver (periportal or panlobular) (The Food Safety Commisson of Japan 2017).

(3) Which cell system (cell lines vs. primary hepatocytes) provides the best in vitro to in vivo correlation? (4) Can combining multiple readouts improve the overall TII?

The cell lines not only yielded more positive results across the assays but also showed better performance in the *in vitro–in vivo* comparison. In the cytotoxicity assay, both cell lines achieved the highest TII values, with H4IIE slightly outperforming Zajdela (0.86 vs. 0.85), while primary hepatocytes reached only 0.77. Combining all readouts for LOEC derivation and comparison with *in vivo* concentrations did not further improve the TII for the cell lines. In contrast, a minor improvement was observed for primary hepatocytes (from 0.77 to 0.78). Notably, primary hepatocytes showed the highest number of positive results when combining

all readouts, yet five compounds (DINP, PCB126, MEG, CBZ, and IMI) showed no detectable effects in any assay. The decrease in performance upon readout combination in the cell lines was primarily due to the high sensitivity of the Nile red assay, which tends to underestimate *in vivo* concentrations and thus overestimate toxicity. Overall, the cell lines outperformed the primary hepatocytes, delivering at least one positive result (via CTB assay) for each compound.

4.3 Limitations of the *in vitro–in silico* approach

4.3.1 Outlier compounds

Despite the overall correlation between *in vitro* EC_{10} values and *in silico* simulated peak concentrations of the portal vein plasma, several limitations of this approach must be acknowledged. Notably, a few substances emerged as clear outliers, indicating that the method does not universally apply across all chemical classes.

One of the most striking outliers in the dataset is **PCB126**, for which the *in vitro* EC_{10} value is approximately 10,000-fold higher than the predicted *in vivo* concentration. This indicates a massive underestimation of toxicity in the *in vitro* system. Notably, PCB126 is the only compound in this study for which validated pharmacokinetic data are available that do not rely on blood concentrations but instead on tissue levels of lung, fat, and liver. This may inherently introduce a certain degree of discrepancy when compared to other compounds, which are typically modeled based on plasma concentrations. Moreover, the substantial deviation may be partially explained by the possibility that the selected *in vitro* readouts are not well suited for polychlorinated biphenyls (PCBs). Supporting this notion, PCB118 also deviates by more than two orders of magnitude from the *in vivo* concentrations. A potentially more sensitive biomarker for such substances could be CYP1A1 gene induction, measurable via qPCR. Indeed, previous work by Broccardo et al. (2005) demonstrated a clear transcriptional response of CYP1A1 in H4IIE cells after exposure to PCB126. Based on visual estimation from the data presented in Broccardo et al. (2005), the EC_{10} for PCB126, determined via CYP1A1 gene induction, appears to be approximately 2.5×10^{-11} M. These are several orders of magnitude lower than the cytotoxicity-based EC_{10} observed in H4IIE cells using the CTB assay (3.6×10^{-5} M), suggesting that the latter may significantly underestimate the compound's biological potency. The modeled *in vivo* peak concentration of PCB126 at the LOAEL in portal vein plasma is 3.02×10^{-9} M, which is closer to the gene induction-based value, further supporting the potential of more mechanism-specific readouts for improving *in vitro–in vivo* correlation.

Another outlier in the *in vitro–in vivo* correlation, where the *in vitro* EC_{10} value is higher than the modeled *in vivo* concentration and thus underestimates toxicity, is **1,4-dioxane**. One

possible explanation for this discrepancy could lie in the compound's metabolism. A study from Wang et al. 2024 indicates that metabolism—specifically via CYP2E1—plays a key role in the toxicity of 1,4-dioxane, as no adverse effects were observed in CYP2E1 knockout mice. This suggests that metabolic activation may occur to a greater extent *in vivo* than in standard *in vitro* cell systems.

Bisphenol A (BPA) is another compound with potentially underestimated hepatotoxicity *in vitro*, as the EC_{10} exceeds the modeled *in vivo* concentration by a factor of 100. One possible explanation lies in the PBPK model, which was validated using a low BPA dose (0.1 mg/kg bw), while the reported LOAEL is much higher (10 mg/kg bw). This discrepancy suggests potential non-linear kinetics at higher exposures. Moreover, the model was validated using data from female rats, whereas the LOAEL was derived from male rats. Sex-specific differences in hepatic UDP-glucuronosyltransferase (UGT) activity which are higher in females may explain lower BPA serum levels in females compared to males and thus contribute to the observed discrepancy (Takeuchi et al. 2004; Mazur et al. 2010). Additionally, intestinal glucuronidation could potentially play a role in influencing the concentration of BPA in the portal vein, which may help explain the observed discrepancy (Yang et al. 2017).

4.3.2 Experimental and data-related constraints

A key limitation of this study was the restricted solubility of several highly lipophilic compounds (e.g., usnic acid, cantaxanthin, lycopene), which narrowed the chemical space available for testing. Only substances that could be solubilized in standard culture media or organic solvents (e.g., DMSO, ethanol, methanol) were included in the experimental workflow. As a result, several compounds with known or suspected hepatotoxic potential could not be assessed. In addition, the heterogeneity and incompleteness of available toxicological and pharmacokinetic data posed significant challenges for the selection of suitable test compounds.

4.4 Comparison of selected studies on hepatotoxicity assessment in the rat

Several studies have investigated hepatotoxicity in rats using different *in vitro, in vivo* and *in silico* strategies, their objectives and methodologies vary notably. **Table 26** provides an overview of three selected studies, summarizing their methodological approaches, aims, key endpoints, and main findings. The present study uniquely compares *in vitro* EC_{10} values with PBPK-modeled *in vivo* C_{max} concentrations at a systematically defined hepatotoxic LOAEL.

Among the studies reviewed, Shah et al. (2021) share the most conceptual overlap with the present work, as both combine *in vitro* methods with PBPK modeling to evaluate hepatotoxicity in rats. However, key methodological differences limit direct comparability. Shah et al. (2021)

used high-content imaging to derive AC_{50} (concentration at 50 % maximal activity), while the current study relies on EC_{10} values from functional readouts. Moreover, their predictions are based on dose-level comparisons, whereas the present work focuses on concentration-based evaluation at the LOAEL.

Two other studies (Papa et al. 2018; Pannala et al. 2025), employed *in silico* methodologies for hepatotoxicity assessment in rats. However, these studies did not incorporate physiologically based pharmacokinetic (PBPK) modeling, making direct comparisons with the present work challenging. Nonetheless, they contribute valuable perspectives to the broader application of NAMs in evaluating hepatotoxicity in rats.

Pannala et al. (2025) utilized a rat-specific genome-scale metabolic model to integrate transcriptomic data, aiming to distinguish hepatotoxic from non-hepatotoxic food-related compounds. Papa et al. (2018) developed quantitative structure–activity relationship (QSAR) models based on molecular descriptors to predict hepatotoxicity in rats.

This study complements existing publications by providing concentration–response data for three different rat hepatocyte models and showing that the investigated cell lines exhibit superior performance compared to primary rat hepatocytes in toxicological evaluations. Furthermore, it highlights that a score-based, systematic derivation of organ-specific LOAELs is a meaningful approach to ensure data quality within the context of the underlying study.

4.5 Conclusions

The *in vitro–in silico* approach was feasible for simulating the C_{max} value in the portal vein at the LOAEL for the 40 compounds using *in vitro* methods, with 75 % of the *in vitro–in vivo* comparisons falling within a factor of 10, which can be considered acceptable. Forty LOAELs were systematically derived using a novel scoring system (SOS – Score of Significance). The data generated in this study, particularly the outstanding performance of the rat cell lines, significantly contributes to the field of hepatotoxicity assessment in rats. Combining multiple readouts (cytotoxicity, lipid droplet accumulation, and nuclear enumeration) did not improve the TII. However, further adjustments are necessary, particularly to address the outlier group of PCBs. This could potentially be accomplished by incorporating a readout that measures gene expression, such as CYP1A1 induction via qPCR, which might enhance the correlation for these specific compound groups. A further step in the future would be to develop a prediction model for hepatotoxic doses in rats based on this dataset, particularly for substances with known LOAELs, via reverse modeling.

Table 26 Comparative overview of *in vitro*, *in vivo* and *in silico* studies on rat hepatotoxicity
Cmax – Peak concentration, ER – Endoplasmic reticulum, HCI – High Content Imaging, k-NN – k-nearest neighbors algorithm, PBPK – Physiologically based Pharmacokinetics, QSAR – Quantitative Structure-Activity Relationship, TII – Toxicity Iso-concentration Index,

Study	Thesis: Gründler (2025)	Shah et al. (2021)	Pannala et al. (2025)	Papa et al. (2018)
No. of compounds	40	51	18	120+
Compound type	Food-relevant compounds, hepatotoxic	Pharmaceuticals and chemicals, hepatotoxic	Food-relavant compounds, hepatotoxic and non-hepatotoxic	Heterogeneous pharmaceuticals
Methods used	*In vitro* (hepatotoxicity assays in cell culture), *in silico* (PBPK modeling)	*In vitro* (rat primary hepatocytes with high-content imaging), *in silico* (toxicokinetic modeling)	*In vivo* (oral rat study), *in silico* (rat-specific genome-scale metabolic model)	*In silico* (QSAR modeling using molecular descriptors)
Species / cell line	Rat (primary hepatocytes, H4IIE, Zajdela)	Rat primary hepatocytes	Rat (5-day oral exposure)	Rat (based on *in vivo* training data)
Aim of the study	To simulate a Cmax at the LOAEL in the portal vein using effective concentrations measured *in vitro*	To estimate hepatotoxic doses using combined HCI data and PBPK modeling	To quantify liver toxicity using transcriptomics within a metabolic network model	To develop QSAR models for predicting rat hepatotoxicity based on molecular structure
Key endpoints	Cytotoxicity, lipid droplet accumulation, nuclear enumeration via Hoechst staining	Mitochondrial function, steatosis, ER stress, lysosomal mass, DNA texture, nuclear size, apoptosis, cell number	Transcriptomics, metabolic pathway shifts, ToxProfiler target genes	Binary hepatotoxicity classification using theoretical molecular descriptors
Main findings	Quantitave simulation feasable (TII = 0.86), cell lines outperform primary rat hepatoytes, cytotoxicity test identified as most suitable	Combined approach successfully predicted hepatotoxic doses; strong concordance with known *in vivo* data	Hepatotoxic compounds showed significant transcriptomic and metabolic alterations; separation from non-toxic compounds was achieved	k-NN QSAR model based on six descriptors, outperformed existing models, with better accuracy and fewer false negatives
Relevance for evaluation of hepatotoxicity in the rat	Supports combined *in vitro* and *in silico* methods for hepatotoxicity assessment	Supports the use of combined *in vitro* and *in silico* methods for hepatotoxicity assessment	Demonstrates the potential of a combined approach to distinguish toxic from non toxic chemicals	Highlights the potential of QSAR models as non-animal methods for predicting hepatotoxicity

5 References

Akaike H (2011) Akaike's Information Criterion. International Encyclopedia of Statistical Science 25–25. https://doi.org/10.1007/978-3-642-04898-2_110

Albrecht W, Brecklinghaus T, Stolte M, et al (2025) Improved identification of human hepatotoxic potential by summary variables of gene expression. ALTEX - Alternatives to animal experimentation. https://doi.org/10.14573/ALTEX.2403272

Albrecht W, Kappenberg F, Brecklinghaus T, et al (2019) Prediction of human drug-induced liver injury (DILI) in relation to oral doses and blood concentrations. Arch Toxicol 93:1609–1637. https://doi.org/10.1007/s00204-019-02492-9

Allison R, Guraka A, Shawa IT, et al (2023) Drug induced liver injury–a 2023 update. J Toxicol Environ Health B Crit Rev 26:442–467. https://doi.org/10.1080/10937404.2023.2261848

ATCC (2024) H-4-II-E - CRL-1548 | ATCC. https://www.atcc.org/products/crl-1548. Accessed 18 May 2025

aus der Beek T, Weber FA, Bergmann A, et al (2016) Pharmaceuticals in the environment--Global occurrences and perspectives. Environ Toxicol Chem 35:823–835. https://doi.org/10.1002/ETC.3339

Bonkovsky HL, Jones DP, Russo MW, Shedlofsky SI (2012) Drug-Induced Liver Injury. Zakim and Boyer's Hepatology 417–461. https://doi.org/10.1016/B978-1-4377-0881-3.00025-5

Brain P, Cousens R (1989) An equation to describe dose responses where there is stimulation of growth at low doses. Weed Res 29:93–96. https://doi.org/10.1111/J.1365-3180.1989.TB00845.X

Brecklinghaus T, Albrecht W, Duda J, et al (2022a) In vitro/in silico prediction of drug induced steatosis in relation to oral doses and blood concentrations by the Nile Red assay. Toxicol Lett 368:33–46. https://doi.org/10.1016/j.toxlet.2022.08.006

Brecklinghaus T, Albrecht W, Kappenberg F, et al (2022b) The hepatocyte export carrier inhibition assay improves the separation of hepatotoxic from non-hepatotoxic compounds. Chem Biol Interact 351:109728. https://doi.org/10.1016/j.cbi.2021.109728

Bretz F, Pinheiro JC, Branson M (2005) Combining Multiple Comparisons and Modeling Techniques in Dose-Response Studies. Biometrics 61:738–748. https://doi.org/10.1111/J.1541-0420.2005.00344.X

Broccardo CJ, Billings RE, Andersen ME, Hanneman WH (2005) Probing the control elements of the CYP1A1 switching module in H4IIE hepatoma cells. Toxicological Sciences 88:82–94. https://doi.org/10.1093/toxsci/kfi271

Chang X, Tan Y-M, Allen DG, et al (2022) IVIVE: Facilitating the Use of In Vitro Toxicity Data in Risk Assessment and Decision Making. Toxics 10:232. https://doi.org/10.3390/toxics10050232

Cytion (2025) Zajdela-Hepatoma Cells ZH-CLS. https://www.cytion.com/Zajdela-Hepatoma-Cells/500306. Accessed 18 May 2025

DeepL GmbH (2025) DeepL Translator [Machine Translation Software]. https://www.deepl.com/de/translator. Accessed 12 May 2025

Devarbhavi H, Bonkovsky HL, Russo M, Chalasani N (2018) Drug-Induced Liver Injury. In: Sanyal AJ, Boyer TD, Terrault N, Lindor KD (eds) Zakim and Boyer's Hepatology: A Textbook of Liver Disease, 7th edn. pp 844–890

Donohoe T, Garnett K, Lansink AO, et al (2018) Emerging risks identification on food and feed – EFSA. EFSA Journal 16:e05359. https://doi.org/10.2903/J.EFSA.2018.5359

EFSA (2024) Chemical contaminants in food and feed | EFSA. https://www.efsa.europa.eu/en/topics/topic/chemical-contaminants-food-feed. Accessed 6 May 2025

European Commission (2023) Roadmap towards phasing out animal testing. https://single-market-economy.ec.europa.eu/sectors/chemicals/reach/roadmap-towards-phasing-out-animal-testing_en. Accessed 6 May 2025

Giknis M, Clifford C (2006) Clinical laboratory parameters for Crl:CD (SD) rats. Wilmington

Gómez-Lechón MJ, Tolosa L, Donato MT (2016) Metabolic activation and drug-induced liver injury: in vitro approaches for the safety risk assessment of new drugs. Journal of Applied Toxicology 36:752–768. https://doi.org/10.1002/JAT.3277

Gu X, Manautou JE (2012) Molecular mechanisms underlying chemical liver injury. Expert Rev Mol Med 14:e4. https://doi.org/10.1017/S1462399411002110

Kim S, Chen J, Cheng T, et al (2023) PubChem 2023 update. Nucleic Acids Res 51:D1373–D1380. https://doi.org/10.1093/NAR/GKAC956

Kolaric TO, Nincevic V, Kuna L, et al (2021) Drug-induced Fatty Liver Disease: Pathogenesis and Treatment. J Clin Transl Hepatol 9:731–737. https://doi.org/10.14218/JCTH.2020.00091

Lee S, Lee IH, Kim HJ, et al (2002) The PreADME Approach: Web-based program for rapid prediction of physico-chemical, drug absorption and drug-like properties. euro QSAR 2002 - Designing Drugs and Crop Protectants: Processes Problems and Solutions 418–420

Lipinski CA, Lombardo F, Dominy BW, Feeney PJ (2001) Experimental and computational approaches to estimate solubility and permeability in drug discovery and development settings. Adv Drug Deliv Rev 46:3–26. https://doi.org/10.1016/S0169-409X(00)00129-0

Mazur CS, Kenneke JF, Hess-Wilson JK, Lipscomb JC (2010) Differences between Human and Rat Intestinal and Hepatic Bisphenol A Glucuronidation and the Influence of Alamethicin on In Vitro Kinetic Measurements. Drug Metabolism and Disposition 38:2232–2238. https://doi.org/10.1124/dmd.110.034819

McGill MR, Jaeschke H (2019) Biomarkers of drug-induced liver injury. Adv Pharmacol 85:221–239. https://doi.org/10.1016/BS.APHA.2019.02.001

McInnes EF. (2017) Pathology for toxicologists : principles and practices of laboratory animal pathology for study personnel. Wiley Blackwell

Naga D, Parrott N, Ecker GF, Olivares-Morales A (2022) Evaluation of the Success of High-Throughput Physiologically Based Pharmacokinetic (HT-PBPK) Modeling Predictions to

Inform Early Drug Discovery. Mol Pharm 19:2203–2216. https://doi.org/10.1021/acs.molpharmaceut.2c00040

NTP Archives (2023) Hepatobiliary System- Nonneoplastic Lesion Atlas. https://ntp.niehs.nih.gov/atlas/nnl/hepatobiliary-system. Accessed 3 May 2025

OECD (1998) Test No. 408: Repeated Dose 90-day Oral Toxicity Study in Rodents. OECD Guidelines for the Testing of Chemicals, Section 4, OECD Publishing, Paris 1–10

OECD (2018) Test No. 408: Repeated Dose 90-Day Oral Toxicity Study in Rodents, OECD Guidelines for the Testing of Chemicals. OECD Publishing, Paris

OpenAI (2025) ChatGPT. Version GPT-4 [Conversational AI]. https://openai.com/. Accessed 12 May 2025

Pannala VR, Hari A, Abdulhameed MDM, et al (2025) Quantifying liver-toxic responses from dose-dependent chemical exposures using a rat genome-scale metabolic model. Toxicological Sciences 204:154–168. https://doi.org/10.1093/TOXSCI/KFAF005

Papa E, Sangion A, Taboureau O, Gramatica P (2018) Quantitative Prediction of Rat Hepatotoxicity by Molecular Structure. International Journal of Quantitative Structure-Property Relationships (IJQSPR) 3:49–60. https://doi.org/10.4018/IJQSPR.2018070104

Pires DE V., Blundell TL, Ascher DB (2015) pkCSM: Predicting Small-Molecule Pharmacokinetic and Toxicity Properties Using Graph-Based Signatures. J Med Chem 58:4066–4072. https://doi.org/10.1021/acs.jmedchem.5b00104

Ramaiah SK (2007) A toxicologist guide to the diagnostic interpretation of hepatic biochemical parameters. Food and Chemical Toxicology 45:1551–1557. https://doi.org/10.1016/j.fct.2007.06.007

Rietjens IMCM, Pascale M, Pellegrino G, et al (2025) The definition of chemical contaminants in food: Ambiguity and consequences. Regulatory Toxicology and Pharmacology 155:105739. https://doi.org/10.1016/J.YRTPH.2024.105739

Ritz C, Baty F, Streibig JC, Gerhard D (2015) Dose-Response Analysis Using R. PLoS One 10:e0146021. https://doi.org/10.1371/journal.pone.0146021

Roth RA, Jaeschke H, Luyendyk JP (2019) Toxic Responses of the Liver. In: Klaassen CD (ed) Casarett & Doull’s Toxicology: The Basic Science of Poisons, 9th edition. McGraw-Hill Education, New York, NY

Russel W, Burch R (1959) The Principles of Humane Experimental Technique. Methuen, London

Schrenk D, Bignami M, Bodin L, et al (2020) Risk assessment of aflatoxins in food. EFSA Journal 18:e06040. https://doi.org/10.2903/J.EFSA.2020.6040

Shah I, Antonijevic T, Chambers B, et al (2021) Estimating Hepatotoxic Doses Using High-Content Imaging in Primary Hepatocytes. Toxicological Sciences 183:285–301. https://doi.org/10.1093/TOXSCI/KFAB091

Singh A, Bhat TK, Sharma Om P (2014) Clinical Biochemistry of Hepatotoxicity. J Clin Toxicol S4:001. https://doi.org/10.4172/2161-0495.S4-001

Takeuchi T, Tsutsumi O, Nakamura N, et al (2004) Gender difference in serum bisphenol A levels may be caused by liver UDP-glucuronosyltransferase activity in rats. Biochem Biophys Res Commun 325:549–554. https://doi.org/10.1016/J.BBRC.2004.10.073

Technische Universität Dortmund (2025) Campus AI [Artificial Intelligence Platform]. https://campus-ki.tu-dortmund.de. Accessed 12 May 2025

The Food Safety Commisson of Japan (2017) Interpretation of the liver hypertrophy in the toxicological evaluation of veterinary medicinal products and feed additives

Tian H, Ketkar R, Tao P (2022) ADMETboost: a web server for accurate ADMET prediction. J Mol Model 28:408. https://doi.org/10.1007/s00894-022-05373-8

Van Renswoude AJBM, Westenberg P, Scherphof GL (1979) In vitro interaction of Zajdela acites hepatoma cells with lipid vesicles. Biochim Biophys Acta 558:22–40

Wang Y, Charkoftaki G, Orlicky DJ, et al (2024) CYP2E1 in 1,4-dioxane metabolism and liver toxicity: insights from CYP2E1 knockout mice study. Arch Toxicol 98:3241–3257. https://doi.org/10.1007/s00204-024-03811-5

Wild CP, Gong YY (2010) Mycotoxins and human disease: a largely ignored global health issue. Carcinogenesis 31:71–82. https://doi.org/10.1093/CARCIN/BGP264

Williams AJ, Grulke CM, Edwards J, et al (2017) The CompTox Chemistry Dashboard: a community data resource for environmental chemistry. J Cheminform 9:61. https://doi.org/10.1186/s13321-017-0247-6

Xiong G, Wu Z, Yi J, et al (2021) ADMETlab 2.0: An integrated online platform for accurate and comprehensive predictions of ADMET properties. Nucleic Acids Res 49:W5–W14. https://doi.org/10.1093/nar/gkab255

Yang G, Ge S, Singh R, et al (2017) Glucuronidation: driving factors and their impact on glucuronide disposition. Drug Metab Rev 49:105–138. https://doi.org/10.1080/03602532.2017.1293682

Yang Y, Wang Y, Zeng W, et al (2024) Physiologically-based pharmacokinetic/pharmacodynamic modeling of meropenem in critically ill patients. Sci Rep 14:19269. https://doi.org/10.1038/s41598-024-64223-0

Zdrazil B, Felix E, Hunter F, et al (2024) The ChEMBL Database in 2023: a drug discovery platform spanning multiple bioactivity data types and time periods. Nucleic Acids Res 52:D1180–D1192. https://doi.org/10.1093/nar/gkad1004

6 Appendix

Supplement 1: Compound information

Supplement 2: Raw and processed *in vitro* data

Supplement 3: LOAEL data

Supplement 4: Pharmacokinetic data

Supplement 5: Concentration-response curves

6.1 References for LOAEL data

Abdo KM, Cunningham ML, Snell ML, et al (2001) 14-Week toxicity and cell proliferation of methyleugenol administered by gavage to F344 rats and B6C3F1 mice. Food and Chemical Toxicology 39:303–316. https://doi.org/10.1016/S0278-6915(00)00143-5

Alam N, Najnin H, Islam M, et al (2023) Biochemical and histopathological analysis after sub-chronic administration of oxyresveratrol in Wistar rats. Drug Chem Toxicol 46:166–175. https://doi.org/10.1080/01480545.2021.2015243

Amyes SJ (1990) Lindane: Combined oncogenicity and toxicity study by dietary administration to Wistar rats for 104 weeks. Unpublished report LSR No. 90/CIL002/0839

ATSDR (2007) Toxicological profile for arsenic. https://doi.org/10.15620/cdc:11481

Bhardwaj S, Srivastava MK, Kapoor U, Srivastava LP (2010) A 90 days oral toxicity of imidacloprid in female rats: Morphological, biochemical and histopathological evaluations. Food and Chemical Toxicology 48:1185–1190. https://doi.org/10.1016/j.fct.2010.02.009

Butenhoff JL, Bjork JA, Chang SC, et al (2012) Toxicological evaluation of ammonium perfluorobutyrate in rats: Twenty-eight-day and ninety-day oral gavage studies. Reproductive Toxicology 33:513–530. https://doi.org/10.1016/J.REPROTOX.2011.08.004

Cho YM, Onodera H, Ueda M, et al (2006) A 13-week subchronic toxicity study of dietary administered morin in F344 rats. Food and Chemical Toxicology 44:891–897. https://doi.org/10.1016/j.fct.2005.12.002

Ena L, Lim JS, Son JY, et al (2018) Evaluation of subchronic exposure to triclosan on hepatorenal and reproductive toxicities in prepubertal male rats. J Toxicol Environ Health A 81:421–431. https://doi.org/10.1080/15287394.2018.1451188

Fowler BA, Woods JS, Schiller CM (1977) Ultrastructural and biochemical effects of prolonged oral arsenic exposure on liver mitochondria of rats. Environ Health Perspect 19:197–204. https://doi.org/10.1289/ehp.7719197

Fujii T, Mikuriya H, Sasaki M (1991) Chronic oral toxicity and carcinogenicity study of thiabendazole in rats. Food and Chemical Toxicology 29:771–775. https://doi.org/10.1016/0278-6915(91)90186-B

Hassan ZK, Elobeid MA, Virk P, et al (2012) Bisphenol A Induces Hepatotoxicity through Oxidative Stress in Rat Model. Oxid Med Cell Longev 2012:1–6. https://doi.org/10.1155/2012/194829

Henderson RG, Lefever TW, Heintz MM, et al (2023) Oral toxicity evaluation of cannabidiol. Food and Chemical Toxicology 176:113778. https://doi.org/10.1016/j.fct.2023.113778

Kano H, Umeda Y, Saito M, et al (2008) Thirteen-week oral toxicity of 1,4-dioxane in rats and mice. J Toxicol Sci 33:141–153. https://doi.org/10.2131/jts.33.141

Ladics GS, Kennedy GL, O'Connor J, et al (2008) 90-Day oral gavage toxicity study of 8-2 fluorotelomer alcohol in rats. Drug Chem Toxicol 31:189–216. https://doi.org/10.1080/01480540701873103

Lington AW, Bird MG, Plutnik RT, et al (1997) Chronic Toxicity and Carcinogenic Evaluation of Diisononyl Phthalate in Rats. Toxicological Sciences 36:79–89. https://doi.org/10.1093/toxsci/36.1.79

McClain RM, Wolz E, Davidovich A, et al (2006) Acute, subchronic and chronic safety studies with genistein in rats. Food and Chemical Toxicology 44:56–80. https://doi.org/10.1016/j.fct.2005.05.021

National Toxicology Program (1993a) TR-394: Acetaminophen (CASRN 103-90-2) in F344 Rats and B6C3F1Mice (Feed Studies) | Enhanced Reader. Natl Toxicol Program Tech Rep Ser 394:1–274

National Toxicology Program (1993b) Toxicology and Carcinogenesis Studies of Coumarin (CAS No. 91-64-5) in F344/N Rats and B6C3F1 Mice (Gavage Studies). Natl Toxicol Program Tech Rep Ser 422:1–340

National Toxicology Program (1993c) NTP technical report on the toxicity studies of Cupric Sulfate (CAS No. 7758-99-8) Administered in Drinking Water and Feed to F344/N Rats and B6C3F1 Mice - PubMed. Natl Toxicol Program Tech Rep Ser

National Toxicology Program (2007) TR-537: Toxicology and Carcinogenesis Studies of Dibromoacetic Acid (CASRN 631-64-1) in F344/N Rats and B6C3F1 Mice (Drinking Water Studies) | Enhanced Reader. Natl Toxicol Program Tech Rep Ser

National Toxicology Program (2001) TR-493: Emodin (CAS No. 518-82-1) in F344/N rats and B6C3F1 mice (feed studies). Natl Toxicol Program Tech Rep Ser

National Toxicology Program (2010a) TR-551: Toxicology and Carcinogenesis Studies of Isoeugenol (CASRN 97-54-1) in F344/N Rats and B6C3F1 Mice (Gavage studies) | Enhanced Reader. Natl Toxicol Program Tech Rep Ser

National Toxicology Program (2010b) TR-559: 2,3',4,4',5-Pentachlorobiphenyl (PCB 118) (CASRN 31508-00-6) in Female Harlan Sprague-Dawley Rats (Gavage Studies) | Enhanced Reader. Natl Toxicol Program Tech Rep Ser

National Toxicology Program (2006) TR-520: 3,3',4,4',5-Pentachlorobiphenyl (PCB 126) (CASRN 57465-28-8) in Female Harlan Sprague-Dawley Rats (Gavage Studies) | Enhanced Reader. Natl Toxicol Program Tech Rep Ser

National Toxicology Program (2019a) Toxicity studies of perfluoroalkyl sulfonates administered by gavage to Sprague Dawley (Hsd:Sprague Dawley SD) rats (revised). Toxic Rep Ser. https://doi.org/10.22427/NTP-TOX-96

National Toxicology Program (2019b) Toxicity studies of perfluoroalkyl carboxylates administered by gavage to Sprague Dawley (Hsd:Sprague Dawley SD) Rats. Toxic Rep Ser. https://doi.org/10.22427/NTP-TOX-97

National Toxicology Program (1993d) TR-404: 5,5-Diphenylhydantoin (CASRN 57-41-0) (Phenytoin) in F344/N Rats and B6C3F1Mice (Feed Studies) | Enhanced Reader. Natl Toxicol Program Tech Rep Ser

National Toxicology Program (2000) TR-470: Toxicology and Carcinogenesis Studies of Pyridine (CASRN 110-86-1) in F344/N Rats, Wistar Rats, and B6C3F1 Mice (Drinking Water Studies) | Enhanced Reader. National Toxicology Program

National Toxicology Program (2010c) TR-558: 3,3',4,4'-Tetrachloroazobenzene (TCAB) (CASRN 14047-09-7) in Harlan Sprague Dawley Rats and B6C3F1 Mice (Gavage Studies) | Enhanced Reader. Natl Toxicol Program Tech Rep Ser

Niho N, Shibutani M, Tamura T, et al (2001) Subchronic toxicity study of gallic acid by oral administration in F344 rats. Food and Chemical Toxicology 39:1063–1070. https://doi.org/10.1016/S0278-6915(01)00054-0

OECD (2004) OECD SIDS Ethanol UNEP publications SIDS Initial Assessment Report. 64–81

Perkins RG, Butenhoff JL, Kennedy GL, Palazzolo MJ (2004) 13-Week Dietary Toxicity Study of Ammonium Perfluorooctanoate (APFO) in Male Rats. Drug Chem Toxicol 27:361–378. https://doi.org/10.1081/DCT-200039773

Powell CJ, Connelly JC, Jones SM, et al (1986) Hepatic responses to the administration of high doses of BHT to the rat: Their relevance to hepatocarcinogenicity. Food and Chemical Toxicology 24:1131–1143. https://doi.org/10.1016/0278-6915(86)90299-1

Qian G, Wang F, Tang L, et al (2013) Integrative Toxicopathological Evaluation of Aflatoxin B1 Exposure in F344 Rats. Toxicol Pathol 41:1093–1105. https://doi.org/10.1177/0192623313477256

Rae JMC, Craig L, Slone TW, et al (2015) Evaluation of chronic toxicity and carcinogenicity of ammonium 2,3,3,3-tetrafluoro-2-(heptafluoropropoxy)-propanoate in Sprague-Dawley rats. Toxicol Rep 2:939–949. https://doi.org/10.1016/j.toxrep.2015.06.001

Roy B, Sarkar AK, Sengupta P, et al (2010) Twenty-eight days repeated oral dose toxicity study of gemifloxacin in Wistar albino rats. Regulatory Toxicology and Pharmacology 58:196–207. https://doi.org/10.1016/J.YRTPH.2010.05.008

Okafor S, Akunne T, Igweze Z, et al (2017) Toxicological Profile of Carbamazepine and Levetiracetam on Some Biochemical and Haematological Parameters in Rats.

Pharmaceutical and Biosciences Journal 5:30–37. https://doi.org/10.20510/ukjpb/5/i4/155974

TRL Toxicity Research Laboratories (1986) Rat oral subchronic toxicity study with methanol. Muskegon, MI

US EPA (2013) IRIS Toxicological Review of Methanol (Noncancer) (Revised External Review Draft). U.S. Environmental Protection Agency, Washington, DC, EPA/635/R-11/001Ba-b

US EPA (2000) US EPA-Pesticides; Triticonazole (RPA400727)

Venkatesan PS, Deecaraman M, Vijayalakshmi M, Sakthivelan SM (2014) Sub-acute Toxicity Studies of Acetaminophen in Sprague Dawley Rats. Biol Pharm Bull 37:1184–1190. https://doi.org/10.1248/bpb.b14-00066

Wang G, Chen Q, Tian P, et al (2020) Gut microbiota dysbiosis might be responsible to different toxicity caused by Di-(2-ethylhexyl) phthalate exposure in murine rodents. Environmental Pollution 261:114164. https://doi.org/10.1016/j.envpol.2020.114164

Yao W, Cheng J, Kandhare AD, et al (2021) Toxicological evaluation of a flavonoid, chrysin: morphological, behavioral, biochemical and histopathological assessments in rats. Drug Chem Toxicol 44:601–612. https://doi.org/10.1080/01480545.2019.1687510

6.2 References for pharmacokinetic data

Bachmann K, Pardoe D, White D (1996) Scaling basic toxicokinetic parameters from rat to man. Environ Health Perspect 104:400–407. https://doi.org/10.1289/ehp.96104400

Batterman SA, Chernyak S, Su F-C (2016) Measurement and Comparison of Organic Compound Concentrations in Plasma, Whole Blood, and Dried Blood Spot Samples. Front Genet 7:189866. https://doi.org/10.3389/fgene.2016.00064

Born SL, Api AM, Ford RA, et al (2003) Comparative metabolism and kinetics of coumarin in mice and rats. Food and Chemical Toxicology 41:247–258. https://doi.org/10.1016/S0278-6915(02)00227-2

Caldwell GW, Masucci JA, Yan Z, Hageman W (2004) Allometric scaling of pharmacokinetic parameters in drug discovery: Can human CL, Vss and t1/2 be predicted fromin-vivo rat data? Eur J Drug Metab Pharmacokinet 29:133–143. https://doi.org/10.1007/BF03190588

CEBS (2016) Toxicokinetic Evaluation (C55301B) of Pyridine (110-86-1) in F344/N Rats and B6C3F1 Mice Exposed via Gavage or Intravenous Injection | Chemical Effects in Biological Systems. https://cebs.niehs.nih.gov/cebs/study/002-02756-0031-0000-6. Accessed 18 May 2025

CEBS (2006) Toxicokinetic Evaluation (S0624) of 3,3’,4,4’,5-pentachlorobiphenyl (DTXSID3032179) in Rat | Chemical Effects in Biological Systems. https://cebs.niehs.nih.gov/cebs/study/002-02863-0008-0000-9. Accessed 18 May 2025

Chang SC, Das K, Ehresman DJ, et al (2008) Comparative pharmacokinetics of perfluorobutyrate in rats, mice, monkeys, and humans and relevance to human exposure via drinking water. Toxicol Sci 104:40–53. https://doi.org/10.1093/TOXSCI/KFN057

Chang-Liao WL, Hou ML, Chang LW, et al (2013) Determination and pharmacokinetics of Di-(2-ethylhexyl) phthalate in rats by ultra performance liquid chromatography with tandem mass spectrometry. Molecules 18:11452–11466. https://doi.org/10.3390/MOLECULES180911452

ChEMBL (2000) ChEMBL - database of bioactive molecules with drug-like properties. https://www.ebi.ac.uk/chembl/. Accessed 18 May 2025

Chen M, Liu X, Yang S, et al (2022) HPLC–MS/MS method for the simultaneous determination of aflatoxins in blood: toxicokinetics of aflatoxin B1 and aflatoxin M1 in rats. J Anal Sci Technol 13:27. https://doi.org/10.1186/s40543-022-00336-3

Child RB, Tallon MJ (2022) Cannabidiol (CBD) Dosing: Plasma Pharmacokinetics and Effects on Accumulation in Skeletal Muscle, Liver and Adipose Tissue. Nutrients 14:2101. https://doi.org/10.3390/nu14102101

Chou WC, Lin Z (2019) Bayesian evaluation of a physiologically based pharmacokinetic (PBPK) model for perfluorooctane sulfonate (PFOS) to characterize the interspecies uncertainty between mice, rats, monkeys, and humans: Development and performance verification. Environ Int 129:408–422. https://doi.org/10.1016/J.ENVINT.2019.03.058

Davis JA (2021) IRIS Toxicological Review of Perfluorobutanoic Acid (PFBA) and Related Salts (Public Comment and External Review Draft, 2021)

Di Martino MT, Arbitrio M, Fonsi M, et al (2019) Allometric Scaling Approaches for Predicting Human Pharmacokinetic of a Locked Nucleic Acid Oligonucleotide Targeting Cancer-Associated miR-221. Cancers (Basel) 12:27. https://doi.org/10.3390/cancers12010027

Di X, Wang X, Liu Y (2015) Effect of piperine on the bioavailability and pharmacokinetics of emodin in rats. J Pharm Biomed Anal 115:144–149. https://doi.org/10.1016/J.JPBA.2015.06.027

Doerge DR, Twaddle NC, Vanlandingham M, Fisher JW (2010) Pharmacokinetics of bisphenol A in neonatal and adult Sprague-Dawley rats. Toxicol Appl Pharmacol 247:158–165. https://doi.org/10.1016/J.TAAP.2010.06.008

Dong D, Quan E, Yuan X, et al (2017) Sodium Oleate-Based Nanoemulsion Enhances Oral Absorption of Chrysin through Inhibition of UGT-Mediated Metabolism. Mol Pharm 14:2864–2874. https://doi.org/10.1021/ACS.MOLPHARMACEUT.6B00851

Dupont (2009) DuPont-24281: Memo Report - HFPO Dimer Acid Ammonium Salt - Biopersistence and pharmacokinetic screen in the rat

Dzierlenga AL, Robinson VG, Waidyanatha S, et al (2020) Toxicokinetics of perfluorohexanoic acid (PFHxA), perfluorooctanoic acid (PFOA) and perfluorodecanoic acid (PFDA) in male and female Hsd:Sprague dawley SD rats following intravenous or gavage administration. Xenobiotica 50:722–732. https://doi.org/10.1080/00498254.2019.1683776

Fda Prescribing Information Factive ® (gemifloxacin mesylate) Tablets

Fitzpatrick G, Huang Y, Qiu F, et al (2024) Entry of cannabidiol into the fetal, postnatal and adult rat brain. Cell Tissue Res 396:177–195. https://doi.org/10.1007/S00441-024-03867-W

Garcia-Lopez P, Perez-Urizar J, Ibarra A, et al (1996) Comparison between Sprague-Dawley and Wistar rats as an experimental model of pharmacokinetic alterations induced by spinal cord injury. Arch Med Res 27:453–457

García-Martínez BA, Montes S, Tristán-López L, et al (2021) Copper biodistribution after acute systemic administration of copper gluconate to rats. Biometals 34:687–700. https://doi.org/10.1007/S10534-021-00304-1

Gardner I, Wakazono H, Bergin P, et al (1997) Cytochrome P450 mediated bioactivation of methyleugenol to 1'-hydroxymethyleugenol in Fischer 344 rat and human liver microsomes. Carcinogenesis 18:1775–1783. https://doi.org/10.1093/CARCIN/18.9.1775

Gilbert-Sandoval I, Wesseling S, Rietjens IMCM (2020) Predicting the Acute Liver Toxicity of Aflatoxin B1 in Rats and Humans by an In Vitro–In Silico Testing Strategy. Mol Nutr Food Res 64:e2000063. https://doi.org/10.1002/mnfr.202000063

Hong SP, Fuciarelli AF, Johnson JD, et al (2013) Toxicokinetics of methyleugenol in F344 rats and B6C3F$_1$ mice. Xenobiotica 43:293–302. https://doi.org/10.3109/00498254.2012.711496

Hou ML, Chang LW, Chiang CJ, et al (2013) Pharmacokinetics of di-isononyl phthalate in freely moving rats by UPLC-MS/MS. Int J Pharm 450:36–43. https://doi.org/10.1016/J.IJPHARM.2013.04.033

Huang MC, Dzierlenga AL, Robinson VG, et al (2019a) Toxicokinetics of perfluorobutane sulfonate (PFBS), perfluorohexane-1-sulphonic acid (PFHxS), and perfluorooctane sulfonic acid (PFOS) in male and female Hsd:Sprague Dawley SD rats after intravenous and gavage administration. Toxicol Rep 6:645–655. https://doi.org/10.1016/J.TOXREP.2019.06.016

Huang MC, Robinson VG, Waidyanatha S, et al (2019b) Toxicokinetics of 8:2 fluorotelomer alcohol (8:2-FTOH) in male and female Hsd:Sprague Dawley SD rats after intravenous and gavage administration. Toxicol Rep 6:924–932. https://doi.org/10.1016/J.TOXREP.2019.08.009

Junqueira VBC, Koch OR, Arisi ACM, et al (1997) Regression of morphological alterations and oxidative stress-related parameters after acute lindane-induced hepatotoxicity in rats. Toxicology 117:199–205. https://doi.org/10.1016/S0300-483X(96)03580-9

Junsaeng D, Anukunwithaya T, Songvut P, et al (2019) Comparative pharmacokinetics of oxyresveratrol alone and in combination with piperine as a bioenhancer in rats. BMC Complement Altern Med 19:235. https://doi.org/10.1186/s12906-019-2653-y

Kurebayashi H (2003) Disposition of a Low Dose of 14C-Bisphenol A in Male Rats and Its Main Biliary Excretion as BPA Glucuronide. Toxicological Sciences 73:17–25. https://doi.org/10.1093/toxsci/kfg040

Lee EW, Gamer CD, Terzo TS (1994) Animal model for the study of methanol toxicity: comparison of folate-reduced rat responses with published monkey data. J Toxicol Environ Health 41:71–82. https://doi.org/10.1080/15287399409531827

Li J, Yang Y, Ning E, et al (2018) Mechanisms of poor oral bioavailability of flavonoid Morin in rats: From physicochemical to biopharmaceutical evaluations. Eur J Pharm Sci 128:290–298. https://doi.org/10.1016/J.EJPS.2018.12.011

Liu W, Wang B, Zhao Y, et al (2021) Pharmacokinetic Characteristics, Tissue Bioaccumulation and Toxicity Profiles of Oral Arsenic Trioxide in Rats: Implications for the Treatment and Risk Assessment of Acute Promyelocytic Leukemia Tissue Bioaccumulation and Toxicity Profiles of Oral Arsenic Trioxide in Rats: Implications for the Treatment and Risk Assessment of Acute. Front Pharmacol 12:647687. https://doi.org/10.3389/fphar.2021.647687

Lombardo F, Berellini G, Obach RS (2018) Trend Analysis of a Database of Intravenous Pharmacokinetic Parameters in Humans for 1352 Drug Compounds. Drug Metab Dispos 46:1466–1477. https://doi.org/10.1124/DMD.118.082966

Mamada H, Iwamoto K, Nomura Y, Uesawa Y (2021) Predicting blood-to-plasma concentration ratios of drugs from chemical structures and volumes of distribution in humans. 25:1261–1270. https://doi.org/10.1007/s11030-021-10186-7

National Toxicology Program (2010a) TR-551: Toxicology and Carcinogenesis Studies of Isoeugenol in F344/N Rats and B6C3F1 Mice (Gavage Studies)

National Toxicology Program (2000) TR-491: Toxicology and Carcinogenesis Studies of Methyleugenol in F344/N Rats and B6C3F1 Mice (Gavage Studies)

National Toxicology Program (2007) TR-537: Toxicology and Carcinogenesis Studies of Dibromoacetic Acid (CASRN 631-64-1) in F344/N Rats and B6C3F1 Mice (Drinking Water Studies) | Enhanced Reader. Natl Toxicol Program Tech Rep Ser

National Toxicology Program (2010b) TR-558: 3,3’,4,4’-Tetrachloroazobenzene (TCAB) (CASRN 14047-09-7) in Harlan Sprague Dawley Rats and B6C3F1 Mice (Gavage Studies) | Enhanced Reader. Natl Toxicol Program Tech Rep Ser

Nie J, Yaro P, He K, Zeng S (2019) Development of a novel LC-MS/MS method for quantitation of triticonazole enantiomers in rat plasma and tissues and application to study on toxicokinetics and tissue distribution. J Pharm Biomed Anal 172:78–85. https://doi.org/10.1016/J.JPBA.2019.04.004

Ohmori K, Kudo N, Katayama K, Kawashima Y (2003) Comparison of the toxicokinetics between perfluorocarboxylic acids with different carbon chain length. Toxicology 184:135–140. https://doi.org/10.1016/S0300-483X(02)00573-5

Owen CA, Hazelrig J (1968) Copper deficiency and copper toxicity in the rat. American Journal of Physiology-Legacy Content 215:334–338. https://doi.org/10.1152/ajplegacy.1968.215.2.334

Pearce RG, Setzer RW, Strope CL, et al (2017) httk : R Package for High-Throughput Toxicokinetics. J Stat Softw 79:1–26. https://doi.org/10.18637/jss.v079.i04

Pu X, Lee LS, Galinsky RE, Carlson GP (2006) Bioavailability of 2,3′,4,4′,5-pentachlorobiphenyl (PCB118) and 2,2′,5,5′-tetrachlorobiphenyl (PCB52) from soils using a rat model and a physiologically based extraction test. Toxicology 217:14–21. https://doi.org/10.1016/J.TOX.2005.08.012

Ramji J V., Austin NE, Boyle GW, et al (2001) The Disposition of Gemifloxacin, a New Fluoroquinolone Antibiotic, in Rats and Dogs. Drug Metabolism and Disposition 29:435–442

Roine RP, Gentry RT, Lim RT, et al (1991) Effect of concentration of ingested ethanol on blood alcohol levels. Alcohol Clin Exp Res 15:734–738. https://doi.org/10.1111/J.1530-0277.1991.TB00589.X

Saunders LJ, Diaz-Blanco G, Lee Y-S, et al (2020) Hepatic Clearance Binding Terms of Hydrophobic Organic Chemicals in Rainbow Trout: Application of a Streamlined Sorbent-Phase Dosing Method. Environ Sci Technol Lett 7:672–676. https://doi.org/10.1021/acs.estlett.0c00518

Schultz IR, Merdink JL, Gonzalez-Leon A, Bull RJ (1999) Comparative toxicokinetics of chlorinated and brominated haloacetates in F344 rats. Toxicol Appl Pharmacol 158:103–114. https://doi.org/10.1006/TAAP.1999.8698

Schwope DM, Karschner EL, Gorelick DA, Huestis MA (2011) Identification of recent cannabis use: whole-blood and plasma free and glucuronidated cannabinoid pharmacokinetics following controlled smoked cannabis administration. Clin Chem 57:1406–1414. https://doi.org/10.1373/CLINCHEM.2011.171777

Shi Y, Li J, Ren Y, et al (2015) Pharmacokinetics and tissue distribution of emodin loaded nanoemulsion in rats. J Drug Deliv Sci Technol 30:242–249. https://doi.org/10.1016/J.JDDST.2015.10.019

Takano R, Murayama N, Horiuchi K, et al (2010) Blood concentrations of 1,4-dioxane in humans after oral administration extrapolated from In Vivo rat pharmacokinetics, In Vitro human metabolism, and physiologically based pharmacokinetic modeling. Journal of Health Science 56:557–565. https://doi.org/10.1248/JHS.56.557

Tusell JM, Suñol C, Gelpí E, Rodríguez-Farré E (1987) Relationship between lindane concentration in blood and brain and convulsant response in rats after oral or intraperitoneal administration. Arch Toxicol 60:432–437. https://doi.org/10.1007/BF00302386

Uchimura T, Kato M, Saito T, Kinoshita H (2010) Prediction of Human Blood-to-Plasma Drug Concentration Ratio. Biopharm Drug Dispos 31:286–297. https://doi.org/10.1002/bdd.711

Verhagen H, Beckers HHG, Comuth PAWV, et al (1989) Disposition of single oral doses of butylated hydroxytoluene in man and rat. Food Chem Toxicol 27:765–772. https://doi.org/10.1016/0278-6915(89)90105-1

Wambaugh JF, Hughes MF, Ring CL, et al (2018) Evaluating in vitro-in vivo extrapolation of toxicokinetics. Toxicological Sciences 163:152–169. https://doi.org/10.1093/TOXSCI/KFY020

Ward KW, Perkins RA, Kawagoe JL, Pollack GM (1995) Comparative Toxicokinetics of Methanol in the Female Mouse and Rat. Fundamental and Applied Toxicology 26:258–264. https://doi.org/10.1006/faat.1995.1096

Wilson CG, Parke D V., Green J, Cawthorne MA (1979) Inhibition of thiabendazole metabolism in the rat. Xenobiotica 9:343–351. https://doi.org/10.3109/00498257909038738

Wu J, Yue H, Cai Z (2009) Investigation on metabolism and pharmacokinetics of triclosan in rat plasma by using UPLC-triple quadrupole MS. Chinese Journal of Chromatography 27:724–730

Xiong G, Wu Z, Yi J, et al (2021) ADMETlab 2.0: An integrated online platform for accurate and comprehensive predictions of ADMET properties. Nucleic Acids Res 49:W5–W14. https://doi.org/10.1093/nar/gkab255

Yu Z, Song F, Jin YC, et al (2018) Comparative Pharmacokinetics of Gallic Acid After Oral Administration of Gallic Acid Monohydrate in Normal and Isoproterenol-Induced Myocardial Infarcted Rats. Front Pharmacol 9:328. https://doi.org/10.3389/FPHAR.2018.00328

Zhang Q, Hu S, Dai W, et al (2023) The partitioning and distribution of neonicotinoid insecticides in human blood. Environmental Pollution 320:121082. https://doi.org/10.1016/J.ENVPOL.2023.121082

Zhou S, Hu Y, Zhang B, et al (2008) Dose-dependent absorption, metabolism, and excretion of genistein in rats. J Agric Food Chem 56:8354–8359. https://doi.org/10.1021/JF801051D

6.3 References for online databases and prediction tools

Marvin sketch 22.7 Marvin - Chemical Drawing Software. https://chemaxon.com/marvin. Accessed 18 May 2025

pkCSM predicting small-molecule. https://biosig.lab.uq.edu.au/pkcsm/prediction. Accessed 18 May 2025

PreADMET | Prediction of ADME/Tox – Just another BMDRC Sites site. https://preadmet.webservice.bmdrc.org/. Accessed 18 May 2025

PubChem. https://pubchem.ncbi.nlm.nih.gov/. Accessed 18 May 2025

SwissADME. http://www.swissadme.ch/. Accessed 18 May 2025

CompTox Chemicals Dashboard. https://comptox.epa.gov/dashboard/. Accessed 18 May 2025

WebPlotDigitizer automeris.io: Computer vision assisted data extraction from charts using WebPlotDigitizer. https://automeris.io/. Accessed 18 May 2025

Deep-PK Deep-PK | Home. https://biosig.lab.uq.edu.au/deeppk/. Accessed 18 May 2025

DrugBank DrugBank Online | Database for Drug and Drug Target Info. https://go.drugbank.com/. Accessed 18 May 2025

ChemSpider ChemSpider: Search and Share Chemistry - Homepage. https://www.chemspider.com/. Accessed 27 Mar 2025

Chemaxon. https://chemaxon.com/. Accessed 27 Mar 2025

Admetlab 3.0 ADMETlab 3.0 -Pharmacokinetic prediction tool. https://admetlab3.scbdd.com/. Accessed 28 Mar 2025

6.4 List of Figures

6.5 List of Tables

6.6 Acknowledgement

First, I would like to thank Prof. Dr. Hengstler for making this project possible and for his continuous support, as well as for granting me the scientific freedom to pursue my own ideas.

Dr. Wiebke Albrecht, who closely supervised this project, developed every pharmacokinetic model, and significantly shaped its conceptual framework. Her guidance and the many discussions – especially those at the Schultenhof – were essential throughout.

I also thank Dr. Tim Brecklinghaus, who was always ready to help with challenging experiments and contributed many creative ideas. Many thanks to Dr. Iain Gardner, who carefully reviewed each model and generously shared his expertise whenever needed.

I would like to thank the research group of Prof. Dr. Jörg Rahnenführer from the department of statistics at TU Dortmund – in particular Dr. Franziska Kappenberg and Dr. Julia Duda – for their statistical support, and Prof. Dr. Jörg Rahnenführer for serving as the second reviewer of this thesis.

I am especially grateful to Dr. Birgit Arnold-Schulz-Gahmen, whose support extended far beyond science – from last-minute presentation rehearsals to reviewing posters, tables, and medical school applications. Her keen eye and unexpected flair for color theory brought clarity and harmony to more than one figure.

Many thanks to the perfusion team – Sara Bauer, Dr. Philipp Gabrys, Katharina Grgas, and Georgia Günther – for their great commitment in learning and teaching new techniques that were essential to this work. Thanks to Prof. Dr. Gisela Degen for providing methyleugenol, and to my lab colleagues – Karolina Zajac, Arianna Borgers, Lea Drescher, Nuwin Mohamad, Josefine Reiser, Dr. Zhwan Mahmoud, and Janina Winken – who made long pipetting days a bit more enjoyable.

To Marc – thank you for your patience and for vacuuming less so I could concentrate on writing. To Christiane, whose perfectly timed spaghetti kept me going, and to Paul, who taught me to appreciate the true magic of the PNG format.

Finally, to Susanne, Eleftheria, and Leyla – thank you for going through every high and low with me and for encouraging me to keep going. And Leyla: without you, I would never have had the courage to apply in the first place.

Thank you.

Note on the use of AI

This thesis was prepared with the assistance of AI-supported tools (OpenAI, DeepL, TU Dortmund Campus AI) for support in text phrasing, language optimization, and R code development. All AI-generated suggestions were critically reviewed, extensively revised or partly discarded. The responsibility for content, structure, and scientific reasoning remains with the author.

Eidesstattliche Versicherung (Affidavit)

Gründler, Lisa — 238249

Name, Vorname
(Surname, first name)

Matrikel-Nr.
(Enrolment number)

Belehrung:

Wer vorsätzlich gegen eine die Täuschung über Prüfungsleistungen betreffende Regelung einer Hochschulprüfungsordnung verstößt, handelt ordnungswidrig. Die Ordnungswidrigkeit kann mit einer Geldbuße von bis zu 50.000,00 € geahndet werden. Zuständige Verwaltungsbehörde für die Verfolgung und Ahndung von Ordnungswidrigkeiten ist der Kanzler/die Kanzlerin der Technischen Universität Dortmund. Im Falle eines mehrfachen oder sonstigen schwerwiegenden Täuschungsversuches kann der Prüfling zudem exmatrikuliert werden, § 63 Abs. 5 Hochschulgesetz NRW.

Die Abgabe einer falschen Versicherung an Eides statt ist strafbar.

Wer vorsätzlich eine falsche Versicherung an Eides statt abgibt, kann mit einer Freiheitsstrafe bis zu drei Jahren oder mit Geldstrafe bestraft werden, § 156 StGB. Die fahrlässige Abgabe einer falschen Versicherung an Eides statt kann mit einer Freiheitsstrafe bis zu einem Jahr oder Geldstrafe bestraft werden, § 161 StGB.

Die oben stehende Belehrung habe ich zur Kenntnis genommen:

Official notification:

Any person who intentionally breaches any regulation of university examination regulations relating to deception in examination performance is acting improperly. This offence can be punished with a fine of up to EUR 50,000.00. The competent administrative authority for the pursuit and prosecution of offences of this type is the chancellor of the TU Dortmund University. In the case of multiple or other serious attempts at deception, the candidate can also be unenrolled, Section 63, paragraph 5 of the Universities Act of North Rhine-Westphalia.

The submission of a false affidavit is punishable.

Any person who intentionally submits a false affidavit can be punished with a prison sentence of up to three years or a fine, Section 156 of the Criminal Code. The negligent submission of a false affidavit can be punished with a prison sentence of up to one year or a fine, Section 161 of the Criminal Code.

I have taken note of the above official notification.

Dortmund, 2.10.2025

Ort, Datum
(Place, date)

Unterschrift
(Signature)

Titel der Dissertation:
(Title of the thesis):

In vitro–in vivo extrapolation of hepatotoxicity for food-relevant compounds in the rat

Ich versichere hiermit an Eides statt, dass ich die vorliegende Dissertation mit dem Titel selbstständig und ohne unzulässige fremde Hilfe angefertigt habe. Ich habe keine anderen als die angegebenen Quellen und Hilfsmittel benutzt sowie wörtliche und sinngemäße Zitate kenntlich gemacht.
Die Arbeit hat in gegenwärtiger oder in einer anderen Fassung weder der TU Dortmund noch einer anderen Hochschule im Zusammenhang mit einer staatlichen oder akademischen Prüfung vorgelegen.

I hereby swear that I have completed the present dissertation independently and without inadmissible external support. I have not used any sources or tools other than those indicated and have identified literal and analogous quotations.

The thesis in its current version or another version has not been presented to the TU Dortmund University or another university in connection with a state or academic examination.*

*Please be aware that solely the German version of the affidavit ("Eidesstattliche Versicherung") for the PhD thesis is the official and legally binding version.

Dortmund, 2.10.2025

Ort, Datum
(Place, date)

Unterschrift
(Signature)